NASA CR-160236
ERIM 132400-10-R

NASA

Technical Memorandum

UNIFORM COLOR SPACE ANALYSIS OF LACIE IMAGE PRODUCTS

R. J. BALON and R. C. CICONE

MAY 1979

Prepared for

NATIONAL AERONAUTICS AND SPACE ADMINISTRATION

Johnson Space Center
Earth Observations Division
Houston, Texas 77058
Contract No. NAS9-15476
Technical Monitor: I. Dale Browne/SF3

ENVIRONMENTAL
RESEARCH INSTITUTE OF MICHIGAN
FORMERLY WILLOW RUN LABORATORIES THE UNIVERSITY OF MICHIGAN
BOX 8618 • ANN ARBOR • MICHIGAN 48107

NOTICES

Sponsorship. The work reported herein was conducted by the Environmental Research Institute of Michigan under Contract NAS9-15476 for the National Aeronautics & Space Administration, Johnson Space Center, Houston, Texas 77058. I. Dale Browne was Technical Monitor for NASA. Contracts and grants to the Institute for the support of sponsored research are administered through the Office of Contracts Administration.

Availability Notice. Request for copies of this memorandum should be referred to:

National Aeronautics & Space Administration
Scientific & Technical Information Facility
P. O. Box 33
College Park, Maryland 20740

TECHNICAL REPORT STANDARD TITLE PAGE

1. Report No.	2. Government Accession No.	3. Recipient's Catalog No.
132400-10-F		

4. Title and Subtitle	5. Report Date
Uniform Color Space Analysis of LACIE Image Products	May 1979
	6. Performing Organization Code

7. Author(s)	8. Performing Organization Report No.
R. J. Balon and R. C. Cicone	132400-10-F

9. Performing Organization Name and Address	10. Work Unit No.
Environmental Research Institute of Michigan Infrared and Optics Division P. O. Box 8618 Ann Arbor, Michigan 48107	11. Contract or Grant No. NAS9-15476
	13. Type of Report and Period Covered Technical Memorandum Nov. 15, 1977 - June 14, 1978
12. Sponsoring Agency Name and Address National Aeronautics & Space Administration Johnson Space Center Houston, Texas 77058	14. Sponsoring Agency Code

15. Supplementary Notes

The work was performed for the Earth Observations Division.
Mr. I. Dale Browne (SF3) was the Technical Monitor.
The ERIM Principal Investigator was Richard F. Nalepka.

16. Abstract

This working paper presents an in-depth technical description of research, conducted in a six-month period, related to the analysis of false-color images. This report is directed to researchers active in this area.

False-color imagery is the primary display form for Landsat data utilized by LACIE Analyst-Interpreters engaged in crop labeling. The fidelity of presentation of the digital data through LACIE image products is the primary issue and concern of this report. An analytic description and evaluation of the data-to-image conversion process has been sought and the results are reported herein.

Models of LACIE imagery generation which account for the large scale physical considerations of film production and the psychological considerations of human color perception are described. The models are employed to investigate performance of image products which use a scaled and biased data channel to control each color primary. A technique is presented for displaying the sensitivity of an image to differential motion in the data. This technique was used to evaluate the characteristics of LACIE Product One imagery and the Kraus Product. An experiment is presented which utilizes probability of misclassification analysis to assess, in an overall manner, how well crop class information carries over into image format. Causes of information loss and their relative significance are interpreted from the results.

17. Key Words	18. Distribution Statement
False Color Image Products Uniform Color Space Image Sensitivity Analysis Multispectral Remote Sensing Landsat LACIE	Initial distribution is listed at the end of this document.

19. Security Classif. (of this report)	20. Security Classif. (of this page)	21. No. of Pages	22. Price
Unclassified	Unclassified	xi + 139	

PREFACE

This technical memorandum describes part of a comprehensive and continuing program of research in multispectral remote sensing from aircraft and satellites, and the supporting effort of researchers in coordinating and analyzing the data gathered by these means. The objective of this program is to improve the utility of remote sensing as a tool for providing decision makers with timely and economical information from large geographical areas. The feasibility of using remote sensing techniques to detect and discriminate between objects or conditions at or near the surface of the earth has previously been demonstrated. Applications in agriculture, urban planning, water quality control, forest management, and other areas have been developed. The thrust of this program is directed toward the development of advanced remote sensing systems and includes activities in system design, data collection, processing and analysis.

The specific focus of the work reported here was understanding the properties of false color image products generated from Landsat digital, multispectral scanner data for the purpose of aiding an analyst interpreter in identifying crops in Landsat data from an agricultural scene. This memorandum is addressed to those researchers active in this area. A psycho-physical model has been established for this data-to-perception conversion process. The model is employed to investigate the sensitivity of film products used by the Large Area Crop Inventory Experiment. Subsequent research by the authors has begun to probe the possibilities for improved image products and this work will be documented in forthcoming reports.

The research covered in this memorandum was performed under NASA Contract NAS9-15476. The research was carried out in ERIM's Infrared and Optics Division directed by R. R. Legault. The Project Manager was Q. A. Holmes, Head of the Information Systems and Analysis Department, and R. F. Nalepka, Head of the Multispectral Analysis Section was the Principal Investigator through the period reported.

CONTENTS

CONTENTS (CONT'D)

CONTENTS (CONT'D)

FIGURES

FIGURES (CONT'D)

TABLES

SUMMARY

False color image products are the primary form of display of Landsat digital data utilized by Analyst-Interpreters engaged in crop labeling for LACIE. The properties of the imagery used, with regard to the accuracy of portrayal of the data, has not heretofore been addressed on a fully analytic basis. The fidelity of the presentation of Landsat data through LACIE image products is the primary issue and concern of this report. An analytic description of the data-to-image conversion process has been developed and significant progress has now been made in understanding the characteristics of false color image products. Development of a model which characterizes the conversion of Landsat data into false color imagery by the Production Film Converter (PFC) at NASA/Lyndon B. Johnson Space Center is described. This model is then employed to analyze characteristics of film products currently used in LACIE.

The PFC is modeled using mathematical principles of color science and photography. The effective primary colors of the PFC are established along with the manner in which each primary is quantitatively activated by the input channel assigned to it. In order to account for the non-uniform human perception of color differences, colors are specified in coordinates designed to make distance between points reliably indicate the perceptible difference between colors represented by those points.

The model is employed to investigate within-image characteristics and performance of image products which use a single, scaled and biased, data channel to activate each individual color primary. A technique is presented for displaying the sensitivity of an image to differential motion in the data (perceptual distance in UCS* units/data space

*Uniform Color Space

distance) at any point in data space. The technique is used to display image sensitivity of LACIE PFC "Product One" and "Product Three", also known as the Kraus Product, for a typical set of acquisitions that span the growing cycle of wheat.

It was determined that the images do not preserve, in color, the spectral distance relationships present in the raw digital data. In other words, the images present a distorted view of the data to the eye. Also, the images do not generally resolve the data, i.e., a significant difference in data levels may not be converted to a perceptible difference in color. An experiment is presented which uses probability of misclassification analysis to assess how well information relevant to crop separability carries over into image form. The experiment shows that information is lost in the data-to-image conversion and points to causes.

Ongoing research includes the analysis of image-to-image (i.e., between image) color characteristics as related to crop canopy cover, as well as the development of image products which take advantage of the understanding of color production characteristics of the PFC to avoid the shortcomings of current products.

2 INTRODUCTION

2.1 BACKGROUND

Development of the potential of satellite remote sensing for purposes of crop production estimation has proceeded under the sponsorship of the National Aeronautics and Space Administration, the U.S. Department of Agriculture and the National Oceanic and Atmospheric Administration. The work began under a pilot project (CITARS) [1] under NASA/JSC which led to the Large Area Crop Inventory project (LACIE) [2]. LACIE was concerned solely with wheat production forecasting. The work is currently transitioning to the inventorying of multiple crops.

In order to conduct crop inventories in remote areas, LACIE is operationally required to estimate crop production in the absence of ground truth. Hence, manual identification of crop types using Landsat imagery is integral to the LACIE approach to crop inventory. There has been an acknowledgement of the importance of providing the Analyst-Interpreter with as accurate and complete a presentation of the available information as possible in that continuing research has been directed into analysis and improvement of AI aids and keys. This memorandum documents research carried out by ERIM in part of the 1978 contract year on false color image products, the primary form of data presentation that analysts interpret.

2.2 THE PROBLEM OF ASSESSING IMAGE SENSITIVITY

At the time the present method of film generation on the PFC developed, consideration was not given to the extent to which resulting imagery would portray the information present in the digital data fully and without distortions. In the course of operational use, the developed method of film generation proved to have certain shortcomings. Because of this, research has been directed upon the basic method of film generation [3,4,5,6,7,8]. What has been needed by researchers is an accurate model of the color production characteristics of the PFC.

Such a model, coupled with a model describing the psychological process of color perception by a human interpreter has been developed and is herein described.

Utilizing the model, the authors developed a graphical approach to display of image sensitivity to the data information content. Presentation of this approach and interpretation of the implications for film generation are the major items reported on in this technical memorandum.

Section 4 of this memorandum presents the model which has been developed of the physics of image generation using the PFC. A model accounting for human perception of color differences is discussed in Section 5. Sensitivity analysis of image products is presented in Section 6. We conclude with an analysis of the sources of information loss in the data-to-image conversion process (Section 7), followed by Conclusions and Recommendations (Section 8).

3
OBJECTIVE AND APPROACH

3.1 OBJECTIVE

The objective of the work reported herein is the determination of the adequacy of currently used film products in portraying the information content of Landsat digital data. From our analysis we seek to define the manner and extent to which imagery can be improved.

3.2 APPROACH

The essence of our approach was the implementation of a mathematical model of the data-to-image conversion process. Properly speaking, this model is a psychophysical model. It must take account of not only the physical properties of film generation, but also the psychological properties of color perception by a human being. With a model in hand we assess image performance by 1) graphic display of image sensitivity throughout the range of the data and 2) comparing the discriminability of crops in image format to the discriminability inherent in the original data.

4

MODELING THE COLOR PRODUCTION CHARACTERISTICS OF THE PRODUCTION FILM CONVERTER (PFC)

In order to investigate image product sensitivity, one must first acquire an understanding of the color production characteristics of the PFC. Hence a mathematical model of the film generation process which at least accounts for the larger scale color characteristics of the process is required. In this section we describe a model of the PFC, developed by Richard Juday of NASA/JSC, based on principles of color science and technical measurements of PFC test images. In this section we present a description of the model sufficient for understanding subsequent references to it. Readers interested in knowing further details should examine either Appendix I or Juday's memos [9,10].

4.1 BASIC DESCRIPTION OF THE PFC

The Production Film Converter (PFC) generates false color images from multispectral scanner data. The apparatus essentially consists of a scanning cathode-ray tube and three color filters. The filter colors are blue, green and red. To produce an image a color negative is exposed three times, once through each filter. Each exposure is controlled by signal levels of a separate channel of data on a picture element by picture element (pixel by pixel) basis [11].*

To prepare a data channel for use in exposure control, a linear transformation is applied to the channel. This consists of expansion by a "scale factor" followed by translation by a "bias factor". Call the

*It should be noted that the technique of controlling each primary with one data channel is not the only conceivable method of using the PFC. In general, the primaries could be controlled by functions on all channels: $f_B(x_1, x_2, x_3, x_4)$, $f_G(x_1, x_2, x_3, x_4)$, $f_R(x_1, x_2, x_3, x_4)$.

exposure control channel counts C_B, C_G, and C_R to correspond to the blue, green and red filtered exposures, respectively. We may write the control channels in terms of Landsat data channels 1, 2, and 4, which we denote x_1, x_2, and x_4, and the assigned scale factor, A_i, and bias factor B_i:*

$$\begin{aligned} C_B &= A_1 x_1 + B_1 \\ C_G &= A_2 x_2 + B_2 \\ C_R &= A_4 x_4 + B_4 \end{aligned} \qquad (1)$$

The purpose of the transformation is to make the dynamic range of the data more appropriate to the range of values which span the exposure control levels. The scale and bias factors may be determined in any manner and several methods have been proposed [3,6,7,8]. Each method amounts to selecting an interval of digital values out of the range of the three data channels. This interval is then mapped, by choice of the linear transformation factors A and B, to the range of exposure control values which is the interval 0 to 255.

In principle, one is overlapping three images of a given scene with each mono-color image portraying one band of the multispectral scanner. Viewing the complete image, one's perception of the color of each pixel is determined in part by each of the three images. Thus spectral information from these data channels is packed into one image. How well this method of packing retains the original amount of information present in the data is one of the primary questions to be addressed in this memo.

*This assignment of channels to colors is specified by the algorithm which produces the "Product One" image. It is the same order of assignment specified by the Kraus Product (Product 3) and all proposed alternatives to Product One. Product Two employs the channels 2, 3, and 4.

The color production characteristics of the PFC are described by two specifications: (1) a technical specification of the color of the three effective primaries (Section 4.2), and (2) the activation of each primary as a function of the counts on the control channels input to the PFC device (Section 4.3). Knowing the color of the primaries, one can predict the color which results from their combination at a specified level of activation for each. Specifying the primaries and how their activation is controlled gives a complete description of the color production characteristics of the PFC.

4.2 TECHNICAL SPECIFICATION OF THE PRIMARIES

We present here a brief description of how colors may be specified in a numerical system of coordinates. Appendix I presents a detailed description of the derivation of the primaries for the PFC photographic system for the reader who is interested.

The perceived color of a light stimulus upon the retina is determined by the spectral distribution of the light. Let the spectral irradiance on the retina be $E(\lambda)$. Values may be extracted from the distribution which characterize its shape and hence the color perception it will stimulate. These values are of the form

$$X = \int E(\lambda)\ x(\lambda)\ d\lambda \qquad (2)$$

where $x(\lambda)$ is a weighting function and the integral is over all visible wavelengths. It has been found empirically that three values are required to specify a color uniquely. A standard set of tristimulus values to be used in color specification was set down in 1931 by the International Commission on Illumination (Commission Internationale de l'Eclairage or CIE). The three standard vectors are called X, Y and Z and define what is called the 1931 CIE Standard Color Space [12,13].

To determine the Standard Color Space tristimulus values of the PFC primaries it is necessary to find $E(\lambda)$ for each. For a film transparency being viewed with the aid of a given light source, $E(\lambda)$ may be broken down into two parts thus:

$$E(\lambda) = \tau(\lambda)L(\lambda) \cdot \text{constant} \tag{3}$$

Here $L(\lambda)$ is the spectral radiance of the light source at a given wavelength and $\tau(\lambda)$is the spectral transmittance of the film to that wavelength of light. The product is proportional to the spectral irradiance on the retina. In generating the model, the spectral radiance of the light source, $L(\lambda)$, was taken to be that of cool white fluorescent light bulbs. This is the type of bulb in the light tables used to view the standard LACIE film product. The spectral energy distribution specified by the industry was employed. The transmittance, $\tau(\lambda)$, for each primary was measured from test products produced on the PFC. The X, Y, Z tristimulus values here after refered to as the color coordinates of the PFC primaries were then found by numerical integration. For example, the red primary tristimulus values were found from the following integrations:

$$\begin{aligned} X_R &= \int L(\lambda)\ \tau_R(\lambda)\ x(\lambda)\ d\lambda \cdot \text{constant} \\ Y_R &= \int L(\lambda)\ \tau_R(\lambda)\ y(\lambda)\ d\lambda \cdot \text{constant} \\ Z_R &= \int L(\lambda)\ \tau_R(\lambda)\ z(\lambda)\ d\lambda \cdot \text{constant} \end{aligned} \tag{4}$$

4.3 RELATIONSHIP OF DIGITAL COUNTS ON INPUT CHANNEL TO RESULTING ACTIVATION OF A PRIMARY

We will define "activation of a primary" and describe how the color of a given combination of the primaries may be specified. We will then examine how primary activation is controlled by counts on the input channel.

Colors expressed in tristimulus values (color coordinates in Standard Color Space) add as vectors. If one has three primary colors which can be combined in controlled amounts, the color coordinates of the combination may be found by adding together the vector contribution from each primary. We call the fractional amount of primary used the "activation" of the primary. Suppose our primaries are a red color, $\vec{r}$, a green color, $\vec{g}$, and a blue color, $\vec{b}$, with the following standard color space coordinates:

$$\begin{aligned} \vec{r} &= (X_r, Y_r, Z_r) \\ \vec{g} &= (X_g, Y_g, Z_g) \\ \vec{b} &= (X_b, Y_b, Z_b) \end{aligned} \tag{5}$$

A color, $\vec{c}$, which is a combination of the three is specified thus:

$$\vec{c} = a_r\vec{r} + a_g\vec{g} + a_b\vec{b}. \tag{6}$$

Here a_r is activation of the red primary, a_g the green primary, and a_b the blue. Activation measures the fractional amount of the given primary being added to the combination color. Thus, activation may vary between zero and unity.

To determine how activation is controlled by the input channel the following procedure was followed by Juday et al [9]. First, test exposures were made using only one primary at a time, at each input count level from zero to 255. The transmission of the film was then measured at the peak wavelength of the primary for each count level. A curve was then fit to points of the graph of transmission τ_B, τ_G, τ_R versus counts C_B, C_G, C_R.

The relationship of transmission to counts was found to be exponential to a very good approximation. The best fitting equations are as follows:

$$\tau_B = 10^{.007133 \cdot C_B - 2.513}$$

$$\tau_G = 10^{.007357 \cdot C_G - 2.182} \qquad (7)$$

$$\tau_R = 10^{.006929 \cdot C_R - 2.520}$$

On this basis, one may describe the PFC as actually controlling film density rather than transmission. Density is logarithmically related to transmission. Denoting density D the following relationship holds:

$$D = 10^{-\tau} \qquad (8)$$

Rewriting the equations of best fit (5), in terms of density rather than transmission, and using matrix notation, we obtain the following equation:

$$\begin{pmatrix} D_B \\ D_G \\ D_R \end{pmatrix} = -0.001 \begin{pmatrix} 7.133 & 0 & 0 \\ 0 & 7.357 & 0 \\ 0 & 0 & 6.929 \end{pmatrix} \begin{pmatrix} C_B \\ C_G \\ C_R \end{pmatrix} + \begin{pmatrix} 2.513 \\ 2.182 \\ 2.520 \end{pmatrix} \qquad (9)$$

This equation makes evident that input counts control film density in a linear fashion.

The above implies primary activation control will be exponential rather than linear. Primary activation is transmission at the peak wavelength of the primary normalized to the transmission value resulting from maximum use of the primary. Denoting activation "a", we have the following relations:

$$a_r = \tau_r/\tau_{r_{max}}$$
$$a_g = \tau_g/\tau_{g_{max}} \qquad (10)$$
$$a_b = \tau_b/\tau_{b_{max}}$$

This shows activation is linearly related to transmission. Since transmission is exponentially controlled, primary activation is exponentially controlled as well. The fact that activation is exponentially controlled is found to be responsible for the major features of image sensitivity to the data as will be discussed in Section 6.

4.4 THE MODEL

In this section we present the mathematics of the PFC model. The numerical values of the parameters are those used in all applications of the model reported herein. The model of the PFC, from data values to XYZ Color Space coordinates, involves 4 transformations:

1. From Landsat data values, x_1, x_2, x_4, to input control levels for each primary C_R, C_G, C_B via:

$$C_B = A_1x_1 + B_1$$
$$C_G = A_2x_2 + B_2 \qquad (11)$$
$$C_R = A_4x_4 + B_4$$

Here the A's and B's are the scale and bias factors computed by one of various possible methods.

2. From counts on the input channel to density at the peak wavelengths of the primary via:

$$\begin{pmatrix} D_B \\ D_G \\ D_R \end{pmatrix} = -0.001 \begin{pmatrix} 7.133 & 0 & 0 \\ 0 & 7.357 & 0 \\ 0 & 0 & 6.929 \end{pmatrix} \begin{pmatrix} C_B \\ C_G \\ C_R \end{pmatrix} + \begin{pmatrix} 2.513 \\ 2.182 \\ 2.520 \end{pmatrix} \quad (12)$$

3. From density to primary activation:

$$a_B = 10^{-D_B/0.2021}$$

$$a_G = 10^{-D_G/0.4934} \quad (13)$$

$$a_R = 10^{-D_R/0.1762}$$

4. From activation to X,Y,Z Color Space coordinates:

$$\begin{pmatrix} X \\ Y \\ Z \end{pmatrix} = \begin{pmatrix} 13.53 & 35.90 & 39.74 \\ 10.86 & 57.09 & 32.04 \\ 46.13 & 6.65 & 0.09 \end{pmatrix} \begin{pmatrix} a_B \\ a_G \\ a_R \end{pmatrix} \quad (14)$$

The only nonlinear step in the above is step 3, the relationship of primary activation to film density.

4.5 LIMITATIONS OF THE MODEL

The model presented above has two limitations. One limitation is that "cross-talk" between channels has not been considered. Each filtered calibration exposure of the film was assumed to contribute to the activation of only one film layer. In actuality, a small contribution is given to the activation of the other two as well. This is due to a

slight overlap of each filter's spectral bandpass with the other 2 film layer's spectral sensitivity. Also, since the film dye colorants are held in three layers, spectral absorption in one layer affects exposure of the layers beneath it. In step 2 of the transformation, Equation 10, the matrix relating film densities to input channel counts is diagonal. The presence of cross-talk between channels implies the off-diagonal elements are not truly zero but have small, definite values. The values can be calculated from the spectral curves of the filters and film sensitivities [14]. Alternatively they can be estimated from measurements on film products. An effort is underway to establish the values of the off-diagonal elements and relieve this limitation of the model [15].

A second limitation of the model arises from "inter-image" effects. During film development, the exposed image on each film layer affects the speed of development of the other two layers to some extent. The magnitude of inter-image effects is thought to be comparable to that of cross-talk. However, modeling the effect is very difficult [16].

The model as implemented accounts for the major features of PFC color production. The photographic effects of cross-talk and inter-image effects are assumed to be not so large as to change the characteristic sensitivity of the film.

5

CONCEPTS OF COLORIMETRY-ACCOUNTING FOR HUMAN PERCEPTION OF COLOR DIFFERENCES

A human observer inspects images produced on the PFC and interprets information from the colors perceived along with several other features (e.g., texture). Since our task is the investigation of how spectral information is portrayed in image format we need to consider characteristics of human color perception in the color model.

In this section we will discuss color perception in order to bring out the points relevant to our investigation of imagery. Color perception is not simply the list of hues, red, green, blue and so on. Perception of color differences is not uniform with respect to linear differences in stimuli. Section 5.1 discusses the dimensions of color perception. Section 5.2 describes the concept of a color space designed to be uniform to perception of color differences. The remaining sections elaborate these ideas in application to the PFC.

5.1 DIMENSIONS OF COLOR

Color scientists have empirically determined that specification of color is a three-dimensional problem. Given the spectral energy distribution of a light stimulus, the color of the light may be specified by extracting the three CIE color coordinates X, Y and Z. This is the standard mathematical method of color specification.

Three dimensions of color appear in the descriptive language of color perception as well. Description of a color perception may be broken down into the concepts of lightness, hue, and saturation. "Lightness" is the attribute of a color perception permitting it to be classed as equivalent to some member of the series of achromatic color perceptions (gray levels) ranging from black to white for light-diffusing objects, and ranging from black to perfectly clear and colorless for light-transmitting objects. "Chromaticity" may be described

as a combination of two aspects of color perception, one called "hue" and the other "saturation". Hue is the attribute of a color perception which gives rise to the names blue, green, red, yellow, purple and so on. A chromatic color perception is defined as one possessing a hue. An achromatic color perception is one not possessing a hue. The series of achromatic color perceptions ranging from black to white are commonly referred to as grey levels. Saturation is the attribute of a color perception determining its difference from the achromatic color perception of equivalent lightness. Saturation is thus a description of how deep a hue is or conversely, how grayish and indistinct it is [12].

5.2 THE CONCEPT OF A UNIFORM COLOR SPACE

One would expect the distance between the points in color space which represent two particular colors to be an indication of how different the colors appear to be. However, the "distance to difference" relation is not at all constant in the X Y Z color space. The meaning of a distance in terms of perceptual difference between colors is different for each two points one considers. We say that such a color space is not "perceptually uniform" [12]. The X Y Z space measures distance between colors linearly in terms of energy. However, the human eye judges differences in a way which is more characteristically logarithmic to changes in energy of the stimulus [17].

Color scientists have studied the tabulated results of experiments on perception of magnitudes of color differences. A number of color coordinate spaces have been proposed with the idea of making the "distance to difference" relation more stable [18]. A truly uniform color space with an analytic basis is not in reach of color science in the present state-of-the-art. However, approximations to a uniform color space which are empirically based do exist and are adequate in many applications.

In 1976 the CIE established one coordinate space to become standard. This is the space now referred to as the 1976 CIE L^*, a^*, b^* Uniform Color Space. The coordinates of this space are a non-linear transformation of the X, Y, Z color space coordinates. The equations of definition of L^*, a^*, b^* space are as follows [19]:

$$\begin{aligned} L^* &= 25(100Y/Y_0)^{1/3} - 16 \qquad 1 \leq Y \leq 100 \\ a^* &= 500\ [(X/X_0)^{1/3} - (Y/Y_0)^{1/3}] \\ b^* &= 200\ [(Y/Y_0)^{1/3} - (Z/Z_0)^{1/3}] \end{aligned} \tag{15}$$

Here X_0, Y_0, and Z_0 represent the color produced by adding all three primaries together at full activation. The X Y and Z space is scaled up or down before this transformation such that $Y_0 = 100$.

The authors have adopted L^*, a^*, b^* space as the coordinate system for specification of film colors. In this way we take account of human color discrimination ability in our analysis. The distance between colors, computed as the Euclidean norm of their coordinates in L^*, a^*, b^* space, measures the perceptual difference between the colors in a manner which is reasonably consistent throughout the space.

5.3 LIMITATIONS OF PREVIOUS LACIE ANALYTIC FILM STUDIES

Previous analytic studies of LACIE film products have invoked the 1931 CIE x-y chromaticity diagram as a space for display and analysis of image characteristics [3, 4, 5, 6, 20]. The coordinates of the diagram are formed from X Y Z coordinates by the following relations:

$$\begin{aligned} x &= X/(X + Y + Z) \\ y &= Y/(X + Y + Z) \end{aligned} \tag{16}$$

This space is inadequate in such application for two important reasons. First, the specification of color has empirically been found to be a 3-dimensional problem. The CIE x-y chromaticity diagram is designed to span the two dimensions which together are called the chromaticity of a color. It ignores the third, equally important dimension of colors called lightness. Second, the 1931 CIE chromaticity diagram is not perceptually uniform. This means distance between colors as specified in coordinates of the diagram is not consistently related to the perceived degree of difference between the colors for a human observer. The 1976 CIE Uniform Color Space features a spacing of colors which makes the meaning of distance approximately uniform. In Uniform Color Space, the Euclidean distance between any two colors gives a reliable measure of how distinguishable the colors are to the eye. Given the distance between two colors one can tell whether they will be strikingly different, similar but distinct, or indistinguishable to human perception. One can, furthermore, make statistical computations using the UCS coordinates with the assurance that the meaning of the unit distance is stable. A uniform color space which spans the 3-dimensional gamut of color is the appropriate setting for quantitative and statistical analysis of image products.

5.4 MEANING OF THE UNIT OF DISTANCE IN UNIFORM COLOR SPACE

The unit of distance in color space has a certain meaning in terms of degree of perceived difference between colors. The unit distance was originally adjusted, via parameters in the equations of definition of the space, to correspond to the smallest color difference detectable to the human eye under ideal observing conditions. Under this standard, a 2-1/2 unit difference is generally necessary before observers will agree on the direction of the difference [10].

Ideal observing conditions do not apply to the colors on image products. Boundaries are not sharp and colors to be compared are not

generally adjacent. The authors examined several images for which field average color coordinates had been computed using the PFC model. We attempted to judge the separation in UCS units between colors necessary to make the colors different in a definite direction. The direction of difference is important because the direction conveys the information about the spectral reflectance differences which the Analyst-Interpreter is seeking. A color difference with a discernible direction represents a "usable" color difference for interpretation. We estimate the boundary line of usable color difference to lie between five and ten units of color space distance.

For the reader's reference, Table 1 lists some chosen reference distances with qualitative descriptions of the degree of color difference they represent on an image.

TABLE 1

QUALITATIVE DESCRIPTION OF COLOR DIFFERENCES FOR VARIOUS DISTANCES OF SEPARATION IN UNIFORM COLOR SPACE

Distance	Description
0- 5 units	no difference
5-10 units	boundary of usable difference
15 units	easily discernible difference
30 units	strong contrast
100 units	striking difference, like black on white

5.5 DESCRIPTION OF THE PFC COLOR OBJECT

In this section we detail some aspects of the PFC's color space. We display the boundary of colors attainable to the PFC, which we call the PFC color object, and elucidate its features.

The effective primaries of the PFC enter into the equations of definition of L^*, a^*, b^* space. The color produced by adding the three

primaries together at maximum intensity becomes nominal white and occupies the point $L^* = 100$, $a^* = 0$, $b^* = 0$ in coordinate space. Grey levels producible by the PFC lie on the L^* coordinate axis: $a^* = 0$, $b^* = 0$, $-16 < L^* < 100$. $L^* = -16$ corresponds to absolute black. Since film density cannot become infinite, absolute black is not attainable in the PFC. PFC "black" turns out to be $L^* = 12.5$. The primaries each occupy a point of color space individually as well. Their coordinates follow:

TABLE 2. POSITION OF COLOR PRIMARIES IN L^*, a^*, b^* SPACE

Primary	L^*	a^*	b^*
Red	63.4	39.8	112.7
Green	80.3	-45.6	65.7
Blue	39.4	28.1	-95.7

When considering the set of colors representing all possible combinations of the three primaries we are speaking of the range of colors attainable by the PFC. We can represent this range in color space by a closed surface. All points interior to the surface represent attainable colors and all points exterior to the surface are unattainable to the PFC. Figure 1 shows a sketch of this boundary for the PFC. The shape of the boundary was built up from taking slices of the color space at intervals of 10 in L^*. The color boundary for each slice was detected by computer. Figure 2 shows the color boundary at each slice.

Each diagram of Figure 2 is actually a chromaticity diagram appropriate for PFC colors of the indicated lightness value L^*. The origin of the diagram represents the equivalent grey level against which saturation is judged. Choosing a direction out from the origin is choosing a hue. Choosing a direction into the first quadrant one will find hues dominated by red. In the second quadrant hues are dominated

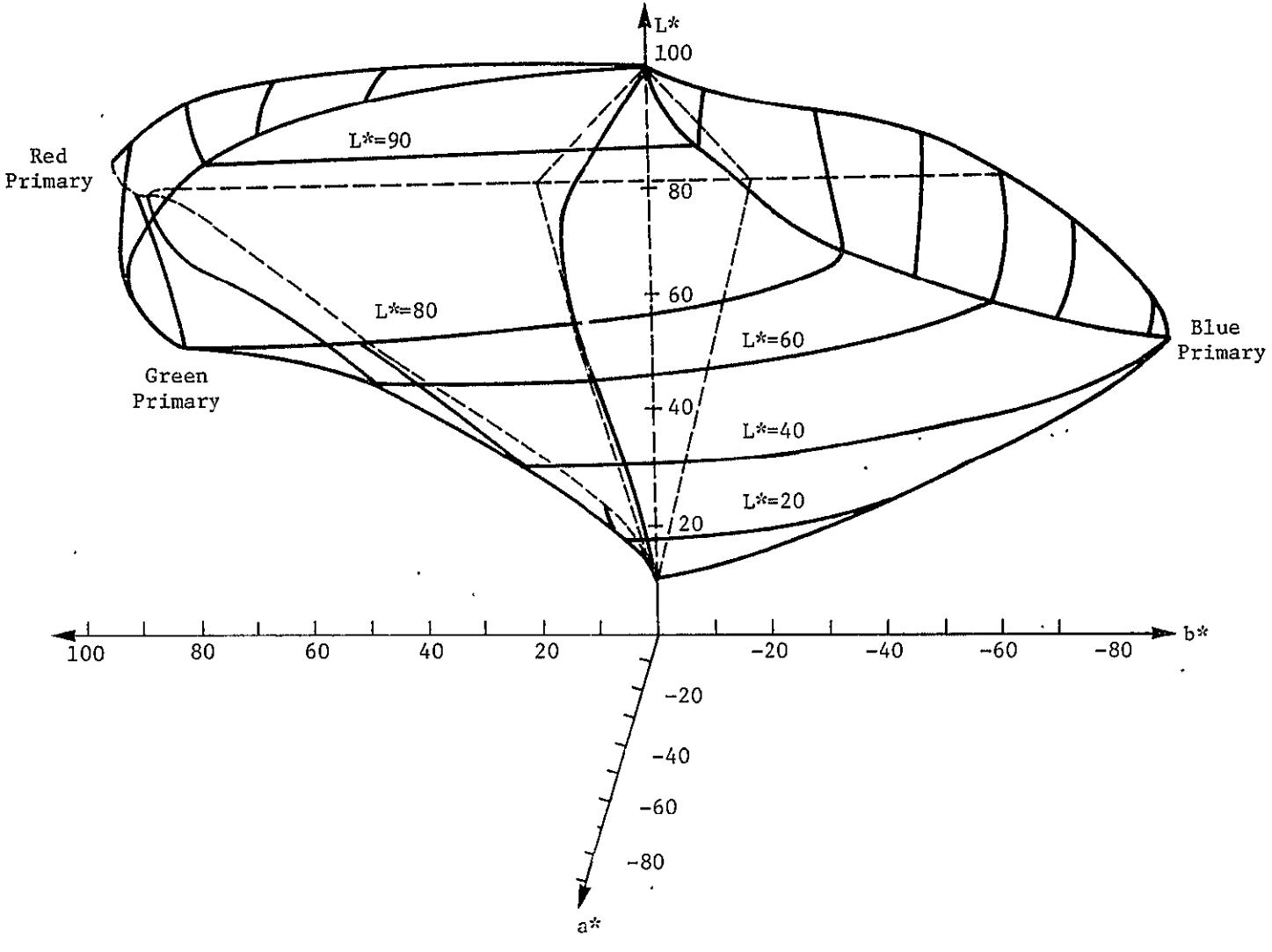

FIGURE 1. BOUNDARY OF COLORS ATTAINABLE BY THE PRODUCTION FILM CONVERTER IN L*,A*,B* UNIFORM COLOR SPACE

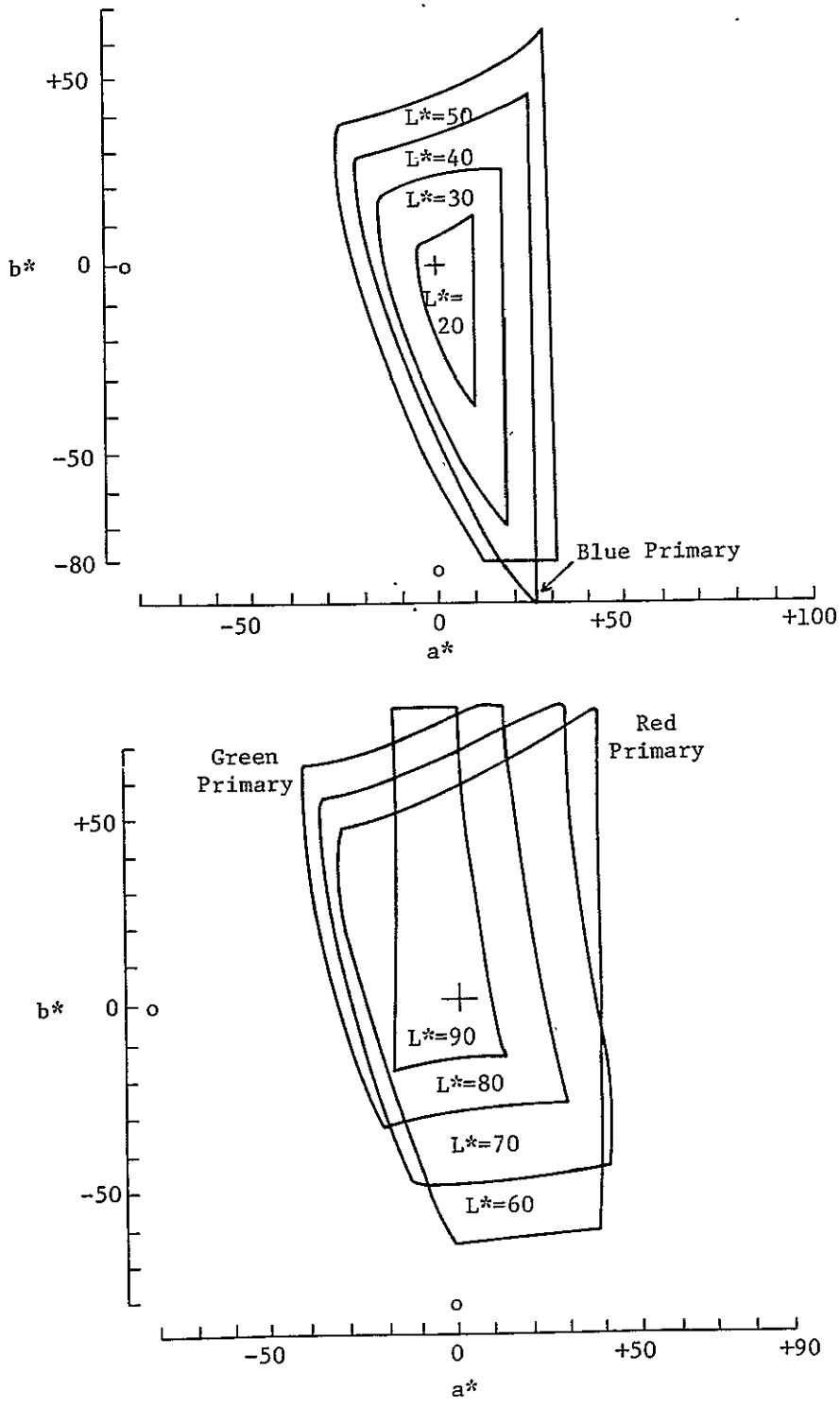

FIGURE 2. COLOR BOUNDARIES OF THE PFC FOR SLICES OF L* FROM 20 TO 90

by green and in the fourth quadrant by blue. As one proceeds along a given direction from the origin to the boundary saturation increases. The boundary of attainable colors is equivalent to the locus of points representing the most saturated color of each hue.

Observe that the boundary of attainable colors narrows to a point at $L^* = 100$ and $L^* = 12.5$. This narrowing is forced by the restriction on lightness at these extremes. To produce colors of lightness near 100 requires all three primaries be used near full intensity and thus little variation in saturation can be achieved. At lightness near PFC black each of the primaries can be little activated so, again, saturation is restricted. Maximum range of color for a fixed lightness is attained at L^* about 60.

Note that the longest dimension of the object in Figure 1 is the line between the red and the blue primaries and spans roughly 200 color space units. This means the PFC is capable of generating a color difference approximately twice as striking as the difference between black and white. The plane with maximum area inside the PFC color object is the plane containing all three primaries.

6
SENSITIVITY ANALYSIS OF IMAGE PRODUCTS

The model of the color production characteristics of the PFC, complete in both physical and psychological/perceptual considerations, has two important potential applications. First, the model may be used as a bridge to more sophisticated methods of using the image generation system. Methods of image generation are under investigation, here at ERIM and at JSC, which promise to provide significant advantages over simple scaling of data channels. Second, the model may be well employed to characterize the performance of image products under current methods of generating them.

In this section we present an analysis of image product sensitivity to data information content for products which use scaled and biased data channels to control primaries of the PFC. The purpose of this analysis is to shed light on the data-to-perception transformation process. We wish to establish whether the data is provided adequate perceptual expansion and whether it is distorted in any way in the process.

6.1 TECHNICAL OBJECTIVE

Our technical objective is the portrayal of image sensitivity, measured in Uniform Color Space units of perceptual distance, to differential motion in data space, measured in Landsat counts. This portrayal should exist over the data range where the concentration of Landsat agricultural data points will be found. The display of sensitivity should be a visual guide to sensitivity at a regular sample of points.

We will first discuss the concept of how a coordinate space is distorted under a non-linear mapping and how that distortion can be presented for assessment (Section 6.2). An examination is made of the

structure of Landsat agricultural data in the subspace of channels 1, 2 and 4 in order to determine an appropriate area for sensitivity assessment (Section 6.3). An experiment is then set up to assess image sensitivity in terms of resolution of data counts (Section 6.4). Interpretation of the result is presented (Section 6.5).

6.2 THE SENSITIVITY ELLIPSE

6.2.1 LOCAL DISTORTION OF SPACE UNDER A NON-LINEAR TRANSFORMATION

To assess image sensitivity involves, according to our definition of the term, a comparison of distances in data space to distances in perception space†. We are concerned with the translation of differences between data points to differences in color by which they will be represented. We have a mapping from one 3-dimensional space to another. We seek to describe how distances are distorted in the transformation.

The transformation from data to perception space distorts distance relationships in a way which is different at each point of data space. This is a consequence of the fact that the transformation is non-linear. A linear transformation applies an expansion of space which is the same at all points of the space it acts on. A non-linear transformation expands space in a way which is a function of the point at which the transformation is applied. We can demonstrate this by writing down the expression which is the linear approximation to a non-linear transformation at the point the transformation is applied. If the transformation was as follows:

$$\begin{aligned} L^* &= f_1\ (x_1, x_2, x_4) \\ a^* &= f_2\ (x_1, x_2, x_4) \\ b^* &= f_3\ (x_1, x_2, x_4) \end{aligned} \qquad (17)$$

† Distance in Uniform Color Space translate to degree of perceived difference between colors. We therefore refer to Uniform Color Space as "perception space".

then the linear approximation formula is [21]:

$$L^* = L_0^* + \frac{\partial f_1}{\partial x_1} dx_1 + \frac{\partial f_1}{\partial x_2} dx_2 + \frac{\partial f_1}{\partial x_4} dx_4$$

$$a^* = a_0^* + \frac{\partial f_2}{\partial x_1} dx_1 + \frac{\partial f_2}{\partial x_2} dx_2 + \frac{\partial f_2}{\partial x_4} dx_4 \qquad (18)$$

$$b^* = b_0^* + \frac{\partial f_3}{\partial x_1} dx_1 + \frac{\partial f_3}{\partial x_2} dx_2 + \frac{\partial f_3}{\partial x_4} dx_4$$

Here, the partial derivatives are to be evaluated at the point the transformation is being approximated, $\left(x_{1_0}, x_{2_0}, x_{4_0}\right)$. The quantity L_0^* is equal to $f_1\left(x_{1_0}, x_{2_0}, x_{4_0}\right)$ and similar equations hold for a_0^* and b_0^*. The quantities dx_1, dx_2, dx_4 are the differential displacements from x_{1_0}, x_{2_0}, x_{4_0} respectively. This set of equations may be conveniently rewritten in matrix notation:

$$\begin{pmatrix} L^* \\ a^* \\ b^* \end{pmatrix} = J(\partial L^*, a^*, b^* / \partial x_1, x_2, x_4) \begin{pmatrix} dx_1 \\ dx_2 \\ dx_4 \end{pmatrix} + \begin{pmatrix} L_0^* \\ a_0^* \\ b_0^* \end{pmatrix} \qquad (19)$$

Here $J(\partial L^*, a^*, b^* / \partial x_1, x_2, x_4)$ is the Jacobian matrix of the transformation and is defined, in accord with the above, as follows:

$$J(\partial L^*, a^*, b^* / \partial x_1, x_2, x_4) = \begin{pmatrix} \frac{\partial f_1}{\partial x_1} & \frac{\partial f_1}{\partial x_2} & \frac{\partial f_1}{\partial x_4} \\ \frac{\partial f_2}{\partial x_1} & \frac{\partial f_2}{\partial x_2} & \frac{\partial f_2}{\partial x_4} \\ \frac{\partial f_3}{\partial x_1} & \frac{\partial f_3}{\partial x_2} & \frac{\partial f_3}{\partial x_4} \end{pmatrix} \qquad (20)$$

This matrix expresses how space is transformed locally, i.e., in the limit of approaching the point of evaluation $\left(x_{1_0}, x_{2_0}, x_{4_0}\right)$. If the transformation (17) is linear, the partial derivatives all are constants, independent of x_1, x_2, and x_4. This implies the local transformation of space is also a global transformation, the same for all points. If the transformation is non-linear, the first partial derivatives will not be constants but functions of x_1, x_2, and x_4. The local transformation matrix is then different at each point of space.

6.2.2 DISPLAY OF SENSITIVITY

The local transformation of space is different depending on the point of data space one is considering. One may expect therefore that some areas of the data will receive more perceptual expansion than others. Mathematically speaking, some volume elements of data space will have larger corresponding volume elements in color space than others. The relevant quantity would be the determinant of the Jacobian matrix for the transformation evaluated at the data point in question. The determinant expresses the ratio of volume elements implied by the transformation about a given point. One approach to the image sensitivity display problem would be to take an array of data space points and tag each point with the value of the determinant evaluated at the point. However this display would be difficult to interpret. Its value would also be limited because it does not indicate visually how nearby areas of the data are related--it does not have directional information.

As a second approach to the problem, imagine taking a set of data points and drawing about each one the boundary which separates it from data points with a color that is different by some small set amount. The boundaries in general will not be spheres. They will be shapes which are expanded in some directions depending on the local stretch introduced by the non-linear color transformation. They will be

larger in volume in some regions of the data space and smaller in others.

The complexity of the data to color transformation prohibits carrying out of the outlined procedure exactly. However, the idea led us to conceive an approach to sensitivity display. We take a point in color space and consider a symmetrical statistical distribution of points around it. A symmetrical distribution has surfaces of equal probability density which are spherical. We then transform this spherical distribution back to data space via the inverse transformation of data to color. Along the way, the distribution will follow the distortion of space introduced by the transformation and become appropriately distorted in shape. Figure 3 indicates schematically what is happening in this process. In data space, the distribution will not be spherical but ellipsoidal. However, its surface still represents a fixed color change equal to the radius of the spherical distribution in color space. Thus the ellipse should be a reasonable characterization of the boundary of color change spoken of above.

For a symmetrical distribution a multivariate normal distribution with diagonal covariance matrix was used. The mathematics of how the distribution could be transformed analytically from one space to another through several non-linear transformations was developed. Details of the derivation are contained in Appendix II. The central result is that the covariance matrix of the distribution about a point transforms according to the following relation:

$$(\mathrm{COV})_{\text{data space}} = J\ (\mathrm{COV})_{\text{color space}} J^{T} \qquad (21)$$

Here J represents the Jacobian matrix of the transformation from color space to data space, evaluated at the point in question, and J^{T} is its

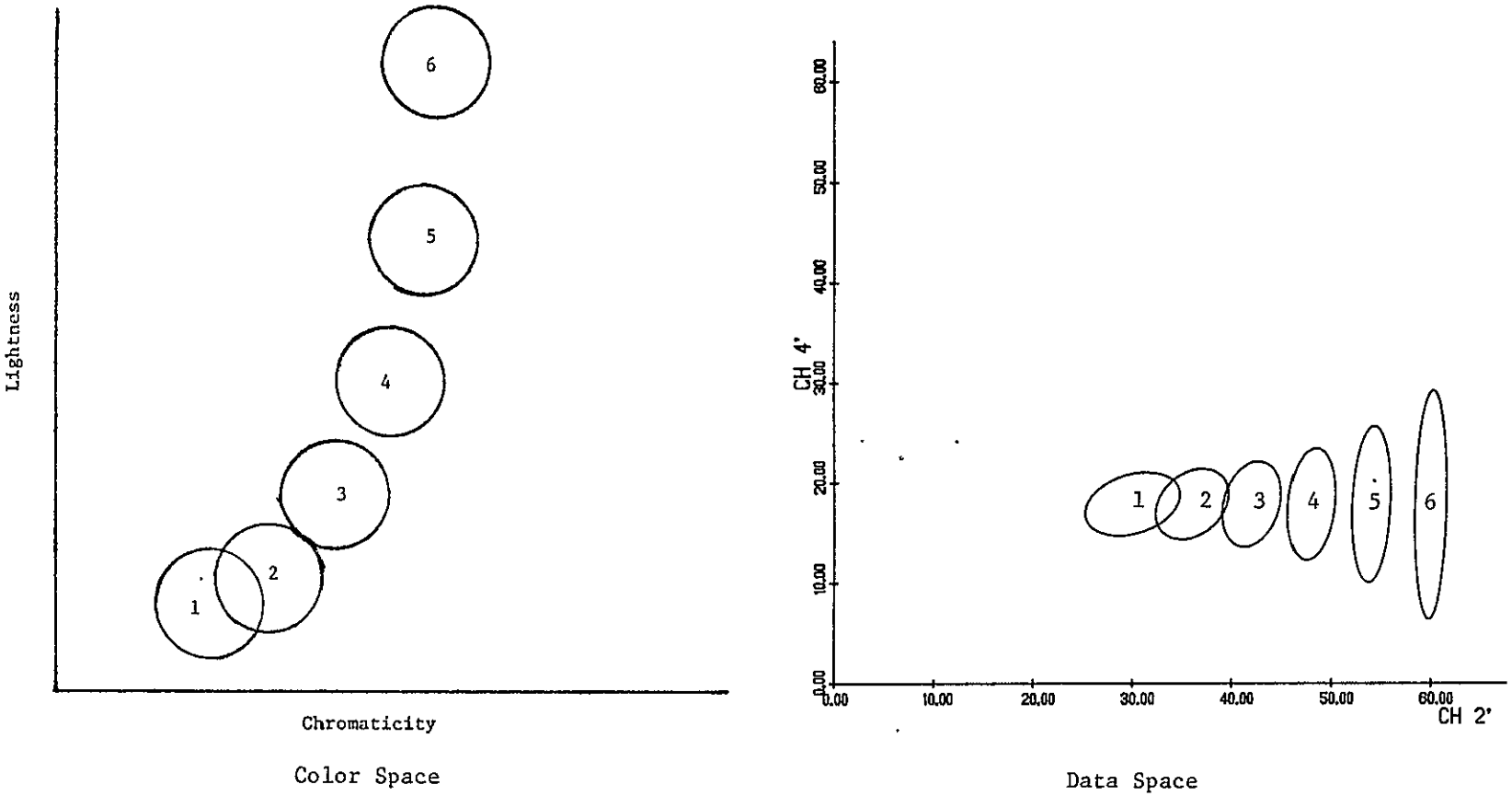

FIGURE 3. DISTRIBUTIONS ARE DISTORTED BY NON-LINEAR TRANSFORMATION (Schematic)

transpose. The equation is an approximation formula which amounts to a linearization of the transformation valid over a small range centered at point of evaluation of the Jacobian.

6.3 STRUCTURE OF LANDSAT DATA IN THE SPACE OF CHANNELS 1, 2 AND 4

We need not be concerned with presenting image sensitivity throughout data space. We are primarily concerned only with the region of space where the concentration of Landsat agricultural data will fall. By choosing an interval along each of the three axes of data space (Channels 1, 2 and 4), one has defined a rectangular box in data space. However, the concentration of data will not fill out this box. The concentration of Landsat agricultural data is known to lie in a 2-dimensional hyperplane of Landsat bands 4, 5, 6 and 7 (Channels 1, 2, 3 and 4) [22]. This data plane represents the region of data space for which it is important to assess image sensitivity. The authors have considered the projection of this hyperplane into the three dimensions of Bands 1, 2 and 4. We find that the plane is spanned by one vector which is very nearly coincident with the Band 4 axis and one vector in the plane of Bands 2 and 3 about 30° from Band 2. We denote these new axes in the data plane by the names channel four prime (CH4') and channel two prime (CH2') respectively. The transformation is as follows (see Appendix III for derivation):

$$\begin{pmatrix} CH1' \\ CH2' \\ CH4' \end{pmatrix} = \begin{pmatrix} .88972 & -.4403 & -.10595 \\ .44655 & .89476 & 0 \\ .09480 & -.04731 & .99270 \end{pmatrix} \begin{pmatrix} CH1 \\ CH2 \\ CH4 \end{pmatrix} \qquad (22)$$

The plane of CH2' and CH4' (CH1' = 0) corresponds to the condition of the Tasselled Cap Yellow coordinate being zero. As the Yellow vector becomes negative, the CH1' value becomes negative. This shifting of the plane is the characteristic effect of the appearance of haze over a scene. A typical scene mean Yellow value is -11.2 [23] which corresponds to CH1' = -11.1.

6.4 DESIGN FOR A SENSITIVITY EXPERIMENT

In this section we will bring the idea of sensitivity characterization together with our knowledge of the data structure to arrive at an appropriate method of display for image sensitivity.

6.4.1 APPROPRIATE SIZE OF THE COLOR SPACE SPHERES

According to the scheme for characterization of sensitivity outlined in Section 6.2, we set up a statistical distribution in color space and then proceed to transform the distribution to data space. What we display will be the surface which corresponds to one standard deviation of the distribution. In color space we defined the distribution to be spherical so the surface is characterized by giving a value for the radius. In data space the surface will be an ellipse which can be plotted.

The assignment of a value to the radius of the distribution in color space is important for the interpretation of the data space ellipse. The radius must represent a distance in color space whose meaning is understood. It would be appropriate for the color space spheres to be the size of one usable color block. We have estimated that a "usable" color difference begins at a separation of five UCS units between colors (Section 5.4). We therefore will give the color space spheres a radius of five UCS units and they will each represent one discriminable color or block of color space.

In accord with the above we may now define the covariance matrix of our color space distribution. For the distribution to be spherically symmetric we require the covariance matrix to be diagonal with equal variances on the diagonal. Thus

$$(COV)_{\text{color space}} = \begin{pmatrix} \sigma^2 & 0 & 0 \\ 0 & \sigma^2 & 0 \\ 0 & 0 & \sigma^2 \end{pmatrix} \tag{23}$$

$$= \sigma^2 \, I$$

where I represents the identity matrix. To have a surface of five units radius to represent one standard deviation we set $\sigma = 5$, $\sigma^2 = 25$.

6.4.2 APPROPRIATE SAMPLE GRID

The sensitivity characterization applies at one point. To display sensitivity of an image over the range of the data requires sampling a grid of points and providing a sensitivity ellipse characterization at each point. The sampling should come from the plane of data concentration discussed in Section 6.3. We can take a regular sample of points from the data space plane and transform them to obtain color space coordinates for the colors they will be mapped to. We then perform the local, linear, inverse transformation on the indicated points in color space and the mathematical distribution, described above, placed about each point. We arrive back at the original regular grid of points in data space but with a sensitivity ellipse now associated with each point.

The fineness of the grid to use remains to be determined. We set the radius of the color space spheres to reflect the size of a usable color change. If we employ a grid spacing which reflects a just significant change in data counts then a comparison will be set up. We will be able to see whether the color resolution of the data meets, exceeds, or fails to meet the inherent resolution of the data.

The inherent resolution of the data is the minimum number of data counts which reliably indicates a real difference in ground reflectance properties. In principle the resolution is one data count. However,

there are a number of sources of noise in Landsat data, some of which are identified and some of which are not. In particular there are day to day differences which have not successfully been accounted for. There has not been a formal look at where the line may be drawn between information and noise in Landsat data. Work has been done at ERIM involving comparison of consecutive day Landsat acquisitions [23] and calibration of Landsat counts with field measured reflectances [24]. These studies informally support a roughly three count spectral distance as on one hand being out of the noise apparent in the data, and on the other hand not being so large as to gloss over significant spectral differences. We postulate that a three count level of resolution is not an inappropriate estimate of the data's reliability.

We would like an image produced from the data to resolve differences of about three counts. We may say the image does resolve three counts at a point in data space if the color ellipse produced there does not extend more than three counts in any direction. To display how well an image product does in this regard, we let the spacing of points we sample in data space reflect the size of the postulated meaningful distance of data space. We take a grid from the plane of data concentration with a spacing of six counts between points. This spacing provides a visual cue to the chosen reference resolution of three counts. Half the distance from a point to one of its four neighbors is three counts. Again, if the instantaneous resolution at a point is three counts or better in all directions, then its associated ellipse will be confined to a three counts radius about the point, i.e., the semi-major axis will be less than three counts.

6.4.3 RANGE OF SAMPLING

A defined range of data space is mapped to the complete range of color accessible to the PFC. This range of data space is defined by the intervals in the data channels which were selected to be mapped to the input, primary control channels. The region of data space defined by the intervals is a rectangular box. The position and dimensions of

the box may be changed by selecting different intervals from the data channels. However, the box is always mapped to the complete space of colors accessible to the PFC as portrayed in Figure 1.

Given a particular set of intervals, data points in an acquisition which fall inside of the box are all differentiated, to within the quantization of the PFC*. Data points which fall outside of the box have exceeded one (or more) of the limits of representation implied in the definition of the intervals in data space. Such a point "saturates" one (or more) of the control channels to 0 or to 255. As a consequence, it does not receive appropriate differentiation. It is represented in the same color as a data point on the boundary of the box.

The plane of data concentration (discussed above) takes a slice out of the box of data which receives differentiation. The slice makes a rectangle in the plane in which we propose to sample sensitivity. Outside of this rectangle in the plane, sensitivity is nonexistent in one or both directions. Therefore we have a limit on the range of points to sample for sensitivity analysis. We place a grid (with a spacing of six counts) into the plane of data concentration and take all the points which fall within the box of data which is fully differentiated.

6.5 SENSITIVITY ANALYSIS OVER THE ACQUISITION HISTORY OF A WINTER WHEAT SEGMENT

Sensitivity analysis according to the approach developed above was performed on acquisitions of Kansas Sample Segment 1154 for the 1975-76 growing season. The four acquisitions span the four biophases of winter wheat development. Analysis was performed for each of two choices of sets of scale and bias factors, i.e., each of two methods of selecting

* The PFC accepts digital input which is quantized to 255 levels. Moreover, the PFC is usually operated in a mode in which these levels are further quantized into groups of 16. In this mode there are 16 levels of exposure per channel.

intervals for expansion out of the data channels. We will present the interval selection procedure which Product One and the Kraus Product represent. We will then present sensitivity plots over the acquisition history of a particular segment, elucidate the pattern which appears in the plots, and analyze the adequacy of resolution presented by the image.

6.5.1 PRODUCT ONE AND KRAUS PRODUCT SELECTION OF INTERVALS

There are two methods of selecting intervals of Channels 1, 2 and 4 for expansion which are used in current operations of film production. The images produced from these selection methods are named Product One and Kraus Product. The history of these methods and their justification will not be dealt with here. We present the formulation of the methods below for reference.

The Product One and Kraus Product algorithms adjust selection of intervals on the basis of statistics of data distribution for a particular acquisition. For each acquisition to be processed the mean value, μ_i, and the standard deviation, σ_i, are computed for each channel of data, i = 1, 2, 3, 4. The algorithms make use of these indications of "where the data lies" in defining intervals of the data channels for expansion.

Product One selects intervals in each channel independent of the rest. The interval chosen is from the mean value minus three times the standard deviation to the mean value plus three times the standard deviation. Mathematically we express this as follows:

$$I_i = \left[\mu_i - 3\sigma_i \, , \, \mu_i + 3\sigma_i\right] \qquad i = 1,2,4 \tag{24}$$

The scale and bias factors necessary to transform the interval I to the interval [0, 225] is found by solving the following simultaneous

equations for A and B:

$$\begin{aligned} 0 &= A(\mu - 3\sigma) + B \\ 255 &= A(\mu + 3\sigma) + B \end{aligned} \tag{25}$$

The Kraus Product maintains a proportion between the intervals to be mapped. The intervals are scaled according to a statistic which involves the mean values of all three channels. This statistic is the "grand mean" and is computed as follows:

$$\mu = (1.1\ \mu_1 + \mu_2 + 2\mu_4)/3 \tag{26}$$

The interval for each channel is then found as follows:

$$\begin{aligned} I_1 &= [0,\ 1/1.1] \cdot 2\mu \\ I_2 &= [0,\ 1] \cdot 2\mu \\ I_4 &= [0,\ 1/2] \cdot 2\mu \end{aligned} \tag{27}$$

Since all the intervals start at zero, a scale factor is all that is required to transform each to [0, 255]. We obtain the scale factors as follows:

$$\begin{aligned} A_1 &= 1.1\ S \\ A_2 &= S \\ A_4 &= 2\ S \end{aligned} \tag{28}$$

where $S = 255/2\mu$.

6.5.2 PRESENTATION OF SENSITIVITY PLOTS

Sensitivity ellipse plots were produced for the four-biophase acquisition history of a Kansas winter wheat segment. The sensitivity

plots for Product One and Kraus Product along with the data signatures for these acquisitions are reproduced in Figures 4 through 15. Figure 4 shows the signature (one standard deviation boundary) of wheat and non-wheat fields for Biophase One*. This is followed, in Figures 5 and 6, by sensitivity ellipse plots for Product One and Kraus Product images corresponding to the data distribution**. Figures 7, 8 and 9 present the results for Biophase Two, and so on for Biophases Three and Four. Overlaying the plot of data concentration on the corresponding sensitivity plot directs attention to the region of the data space which was actually occupied by data points. The sensitivity ellipses which sample this region of data space are the ones which apply to the actual image. For example, the sensitivity ellipses which fall wheat and non-wheat concentrations will depict how well separated the crops appear in the image. Accurate identification of wheat from non-wheat by image interpretation will first depend on appropriate separation in the image.

Notice that each plot has points for which the ellipse shape is contained to 3 counts and other points at which it is violated. Notice also that there is a pattern to the way the ellipse shapes change which is similar in all the plots. The reason for the pattern and its implications will be brought out below.

The boundary of the gird of points in each sensitivity plot represents the boundary of points which do not saturate a control channel. Data points outside of this range in the plane of data concentration "saturate" one or more primaries and appear the same

---

* In this segment the wheat and non-wheat fields are well distinguished and homogeneous within themselves. The normal distribution boundary gives a very good indication of how the data was distributed.

** The scale and bias factors used for Product One were those computed for this acquisition by JSC and listed in the film header information. We derived the segment statistics from the Product One scale and bias values and used the statistics to compute Kraus Product scale values.

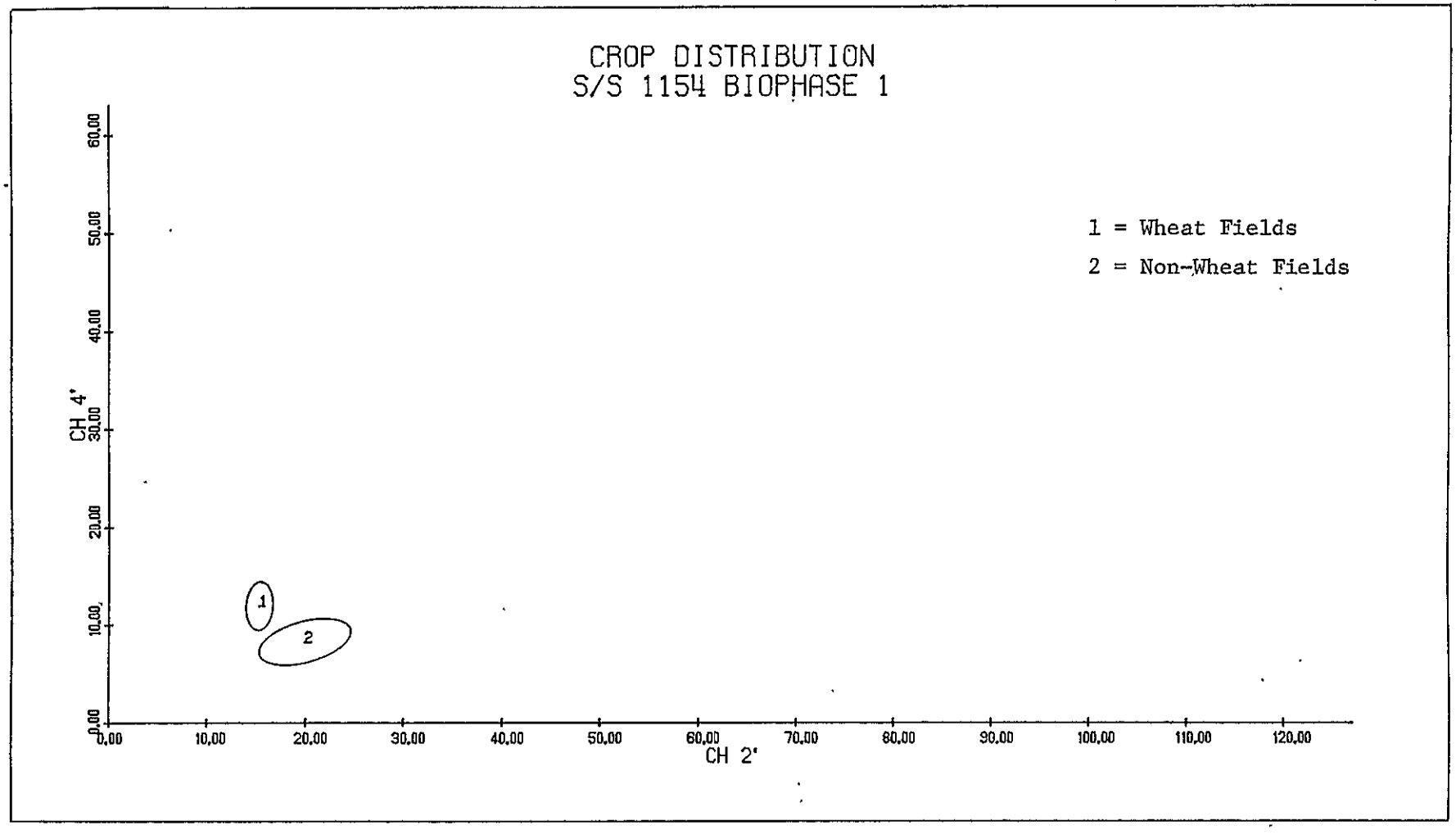

FIGURE 4. CROP DISTRIBUTION FOR A BIOPHASE 1 ACQUISITION

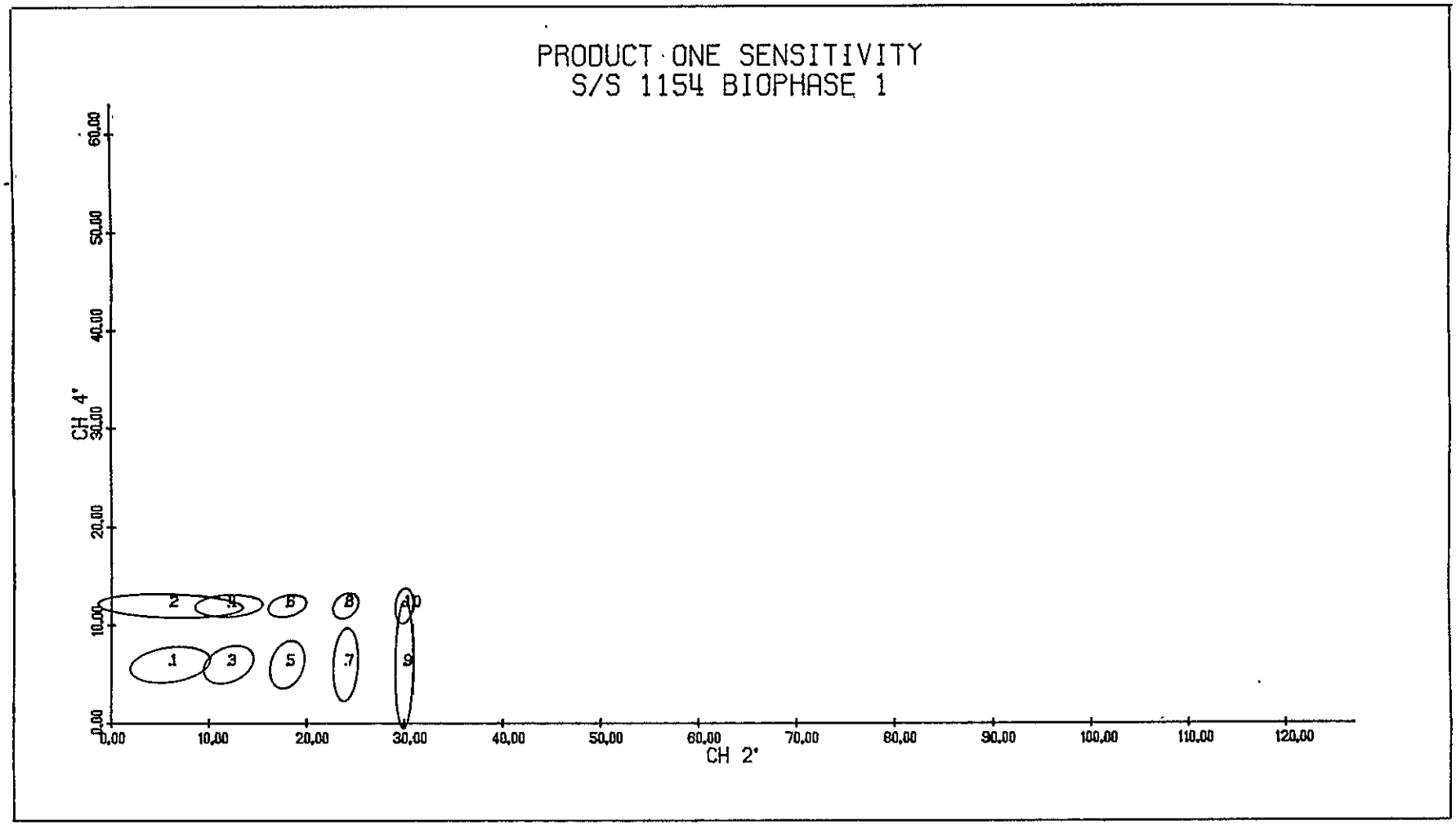

FIGURE 5. PRODUCT ONE SENSITIVITY FOR A BIOPHASE 1 ACQUISITION

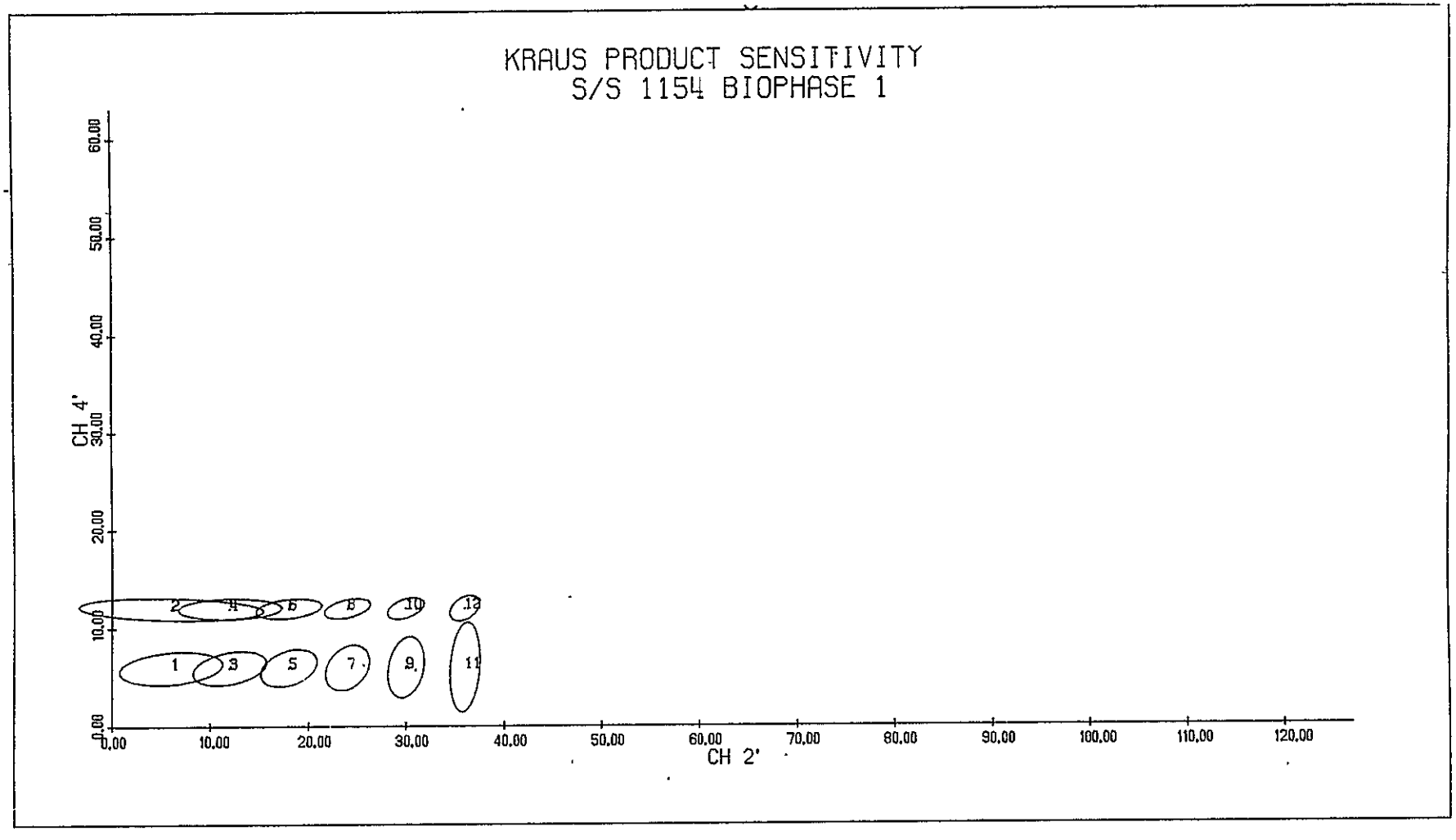

FIGURE 6. KRAUS PRODUCT SENSITIVITY FOR A BIOPHASE 1 ACQUISITION

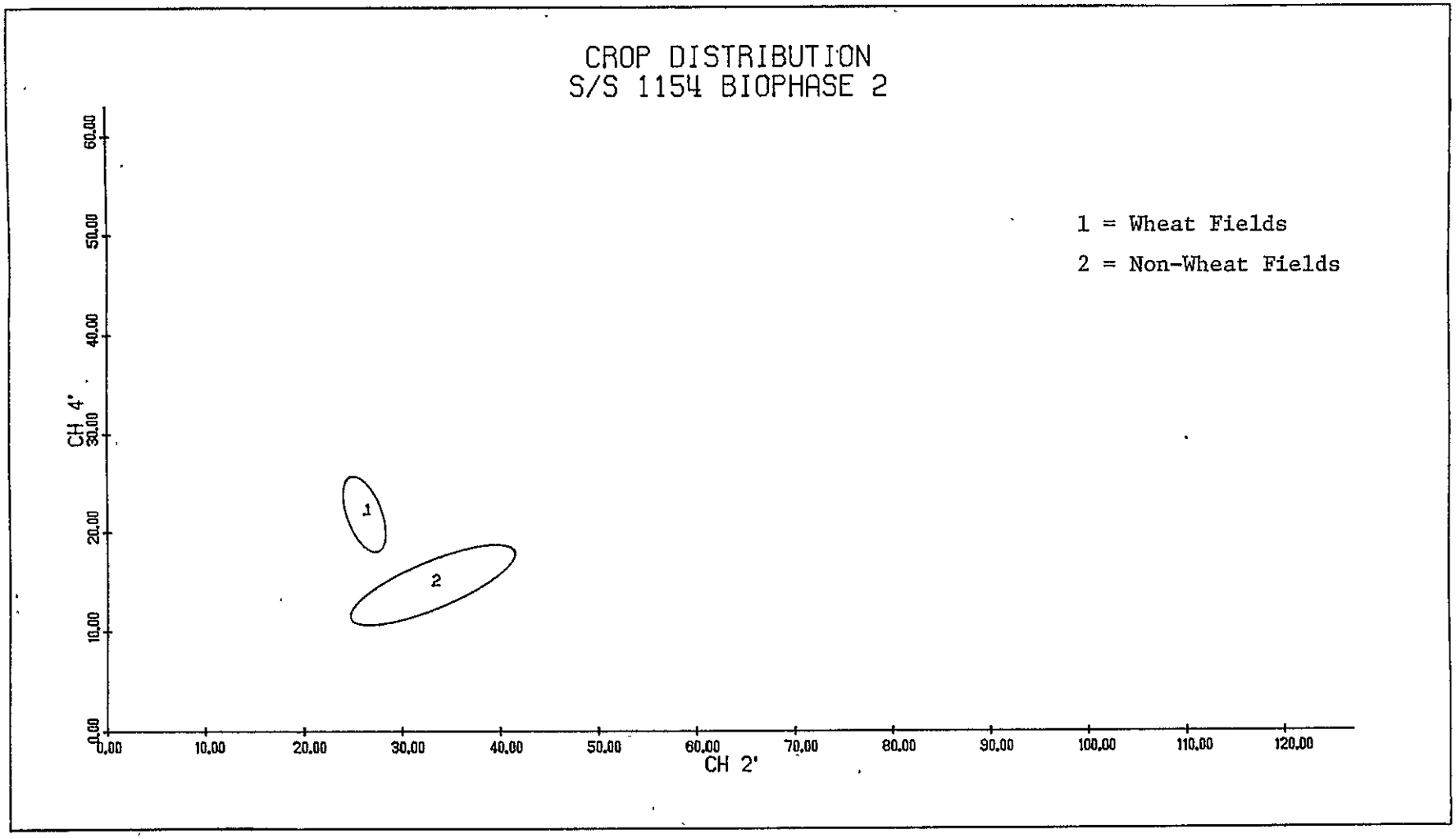

FIGURE 7. CROP DISTRIBUTION FOR A BIOPHASE 2 ACQUISITION

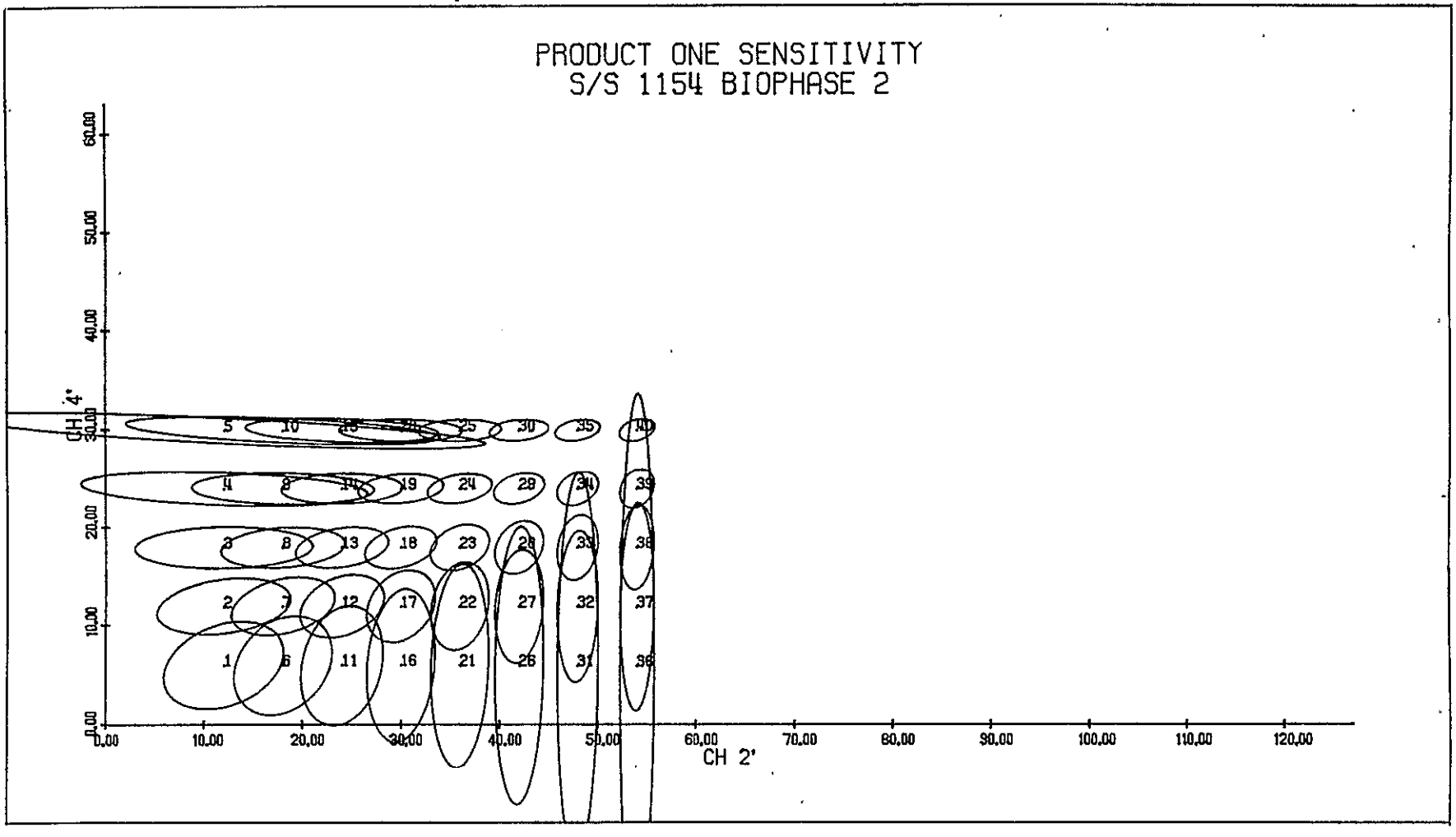

FIGURE 8. PRODUCT ONE SENSITIVITY FOR A BIOPHASE 2 ACQUISITION

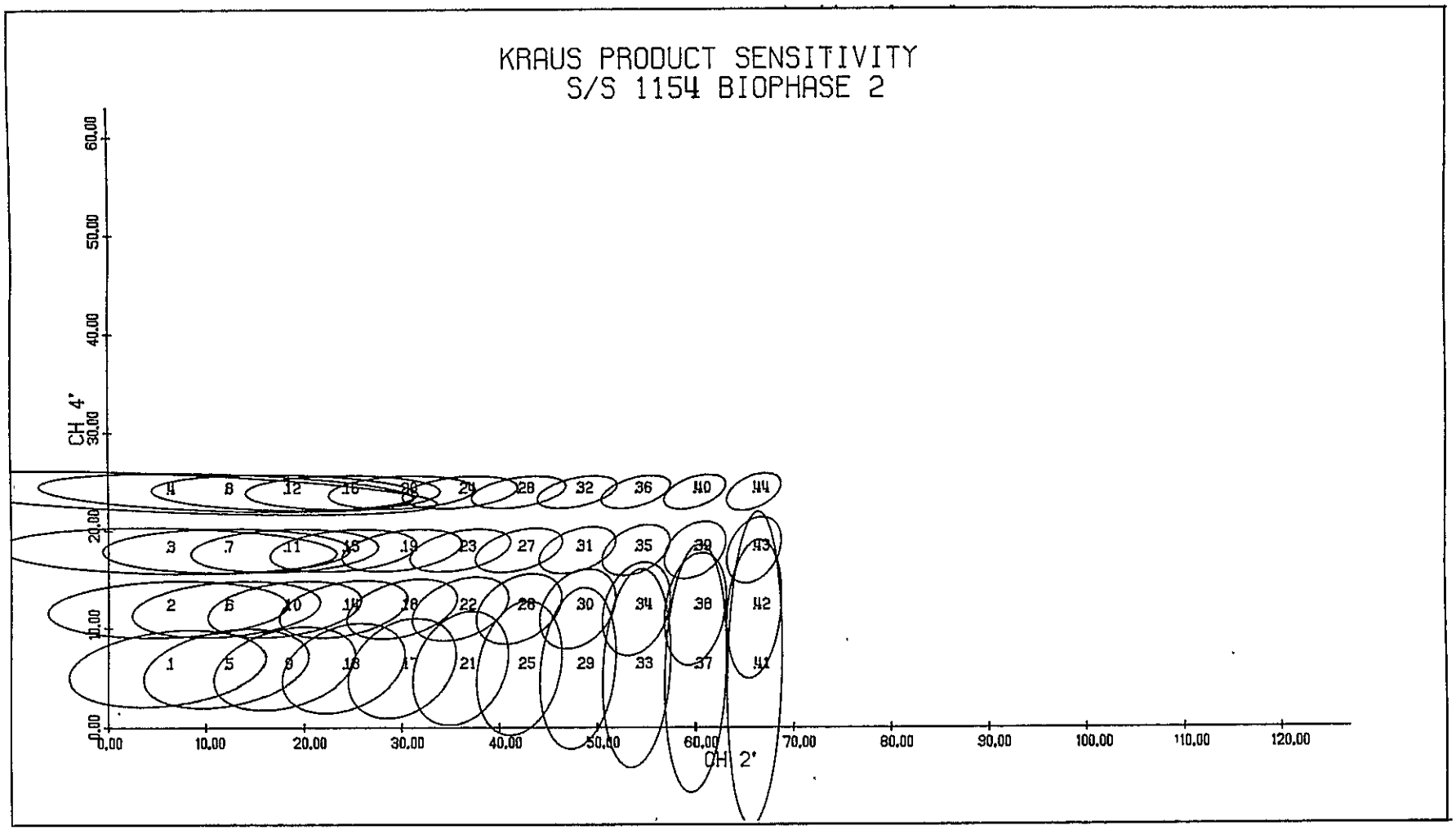

FIGURE 9. KRAUS PRODUCT SENSITIVITY FOR A BIOPHASE 2 ACQUISITION

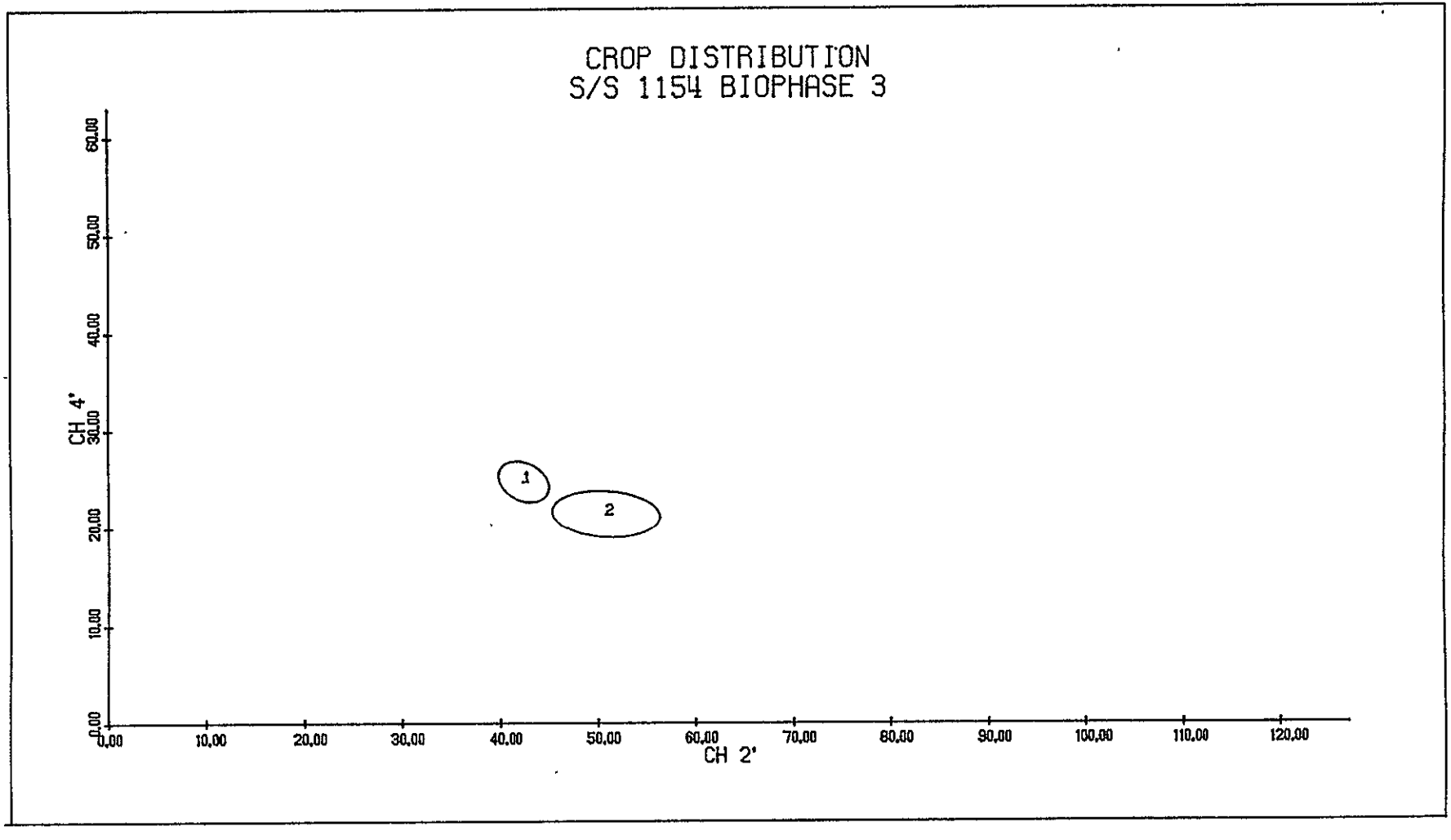

FIGURE 10. CROP DISTRIBUTION FOR A BIOPHASE 3 ACQUISITION

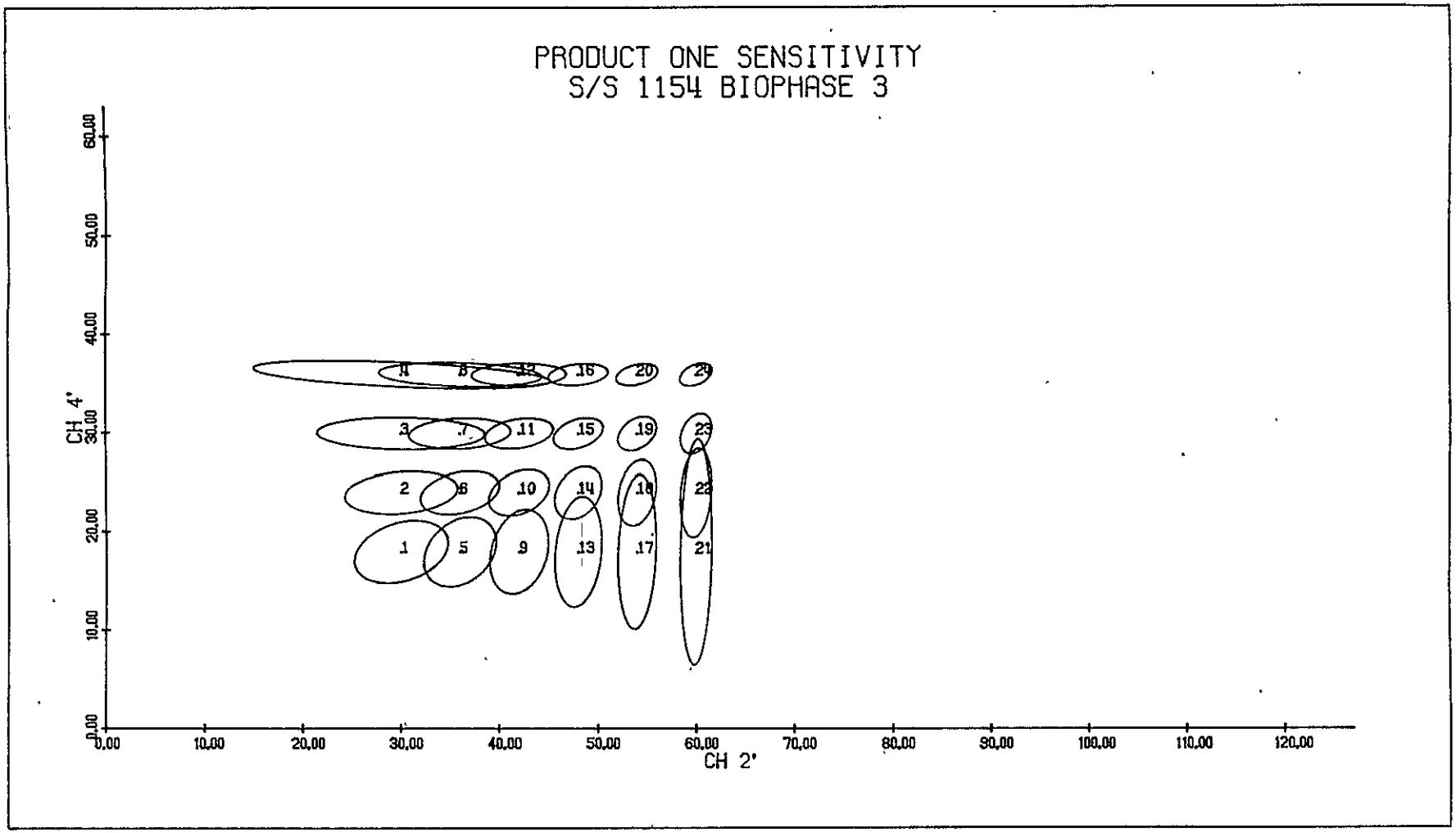

FIGURE 11. PRODUCT ONE SENSITIVITY FOR A BIOPHASE 3 ACQUISITION

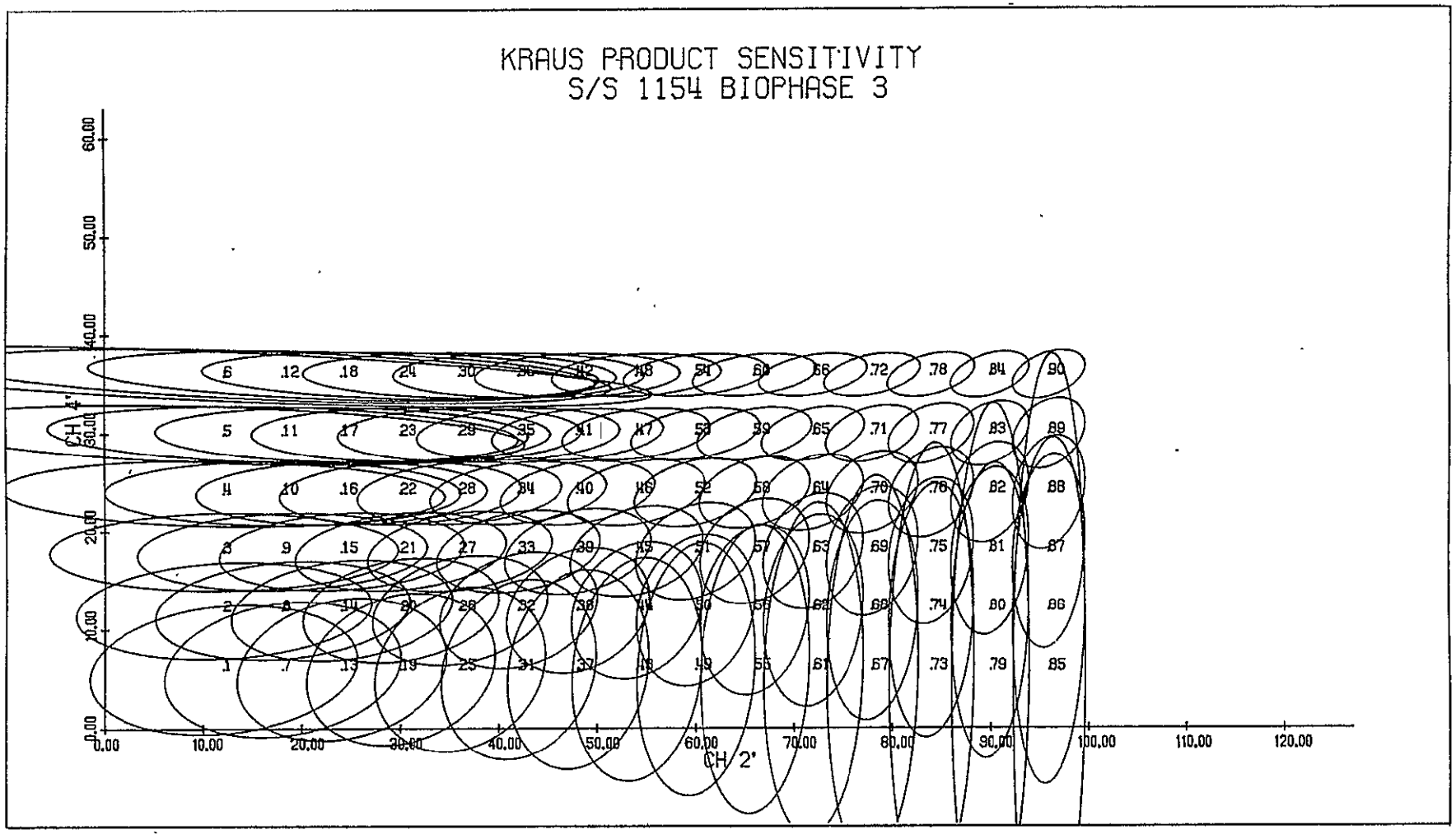

FIGURE 12. KRAUS PRODUCT SENSITIVITY FOR A BIOPHASE 3 ACQUISITION

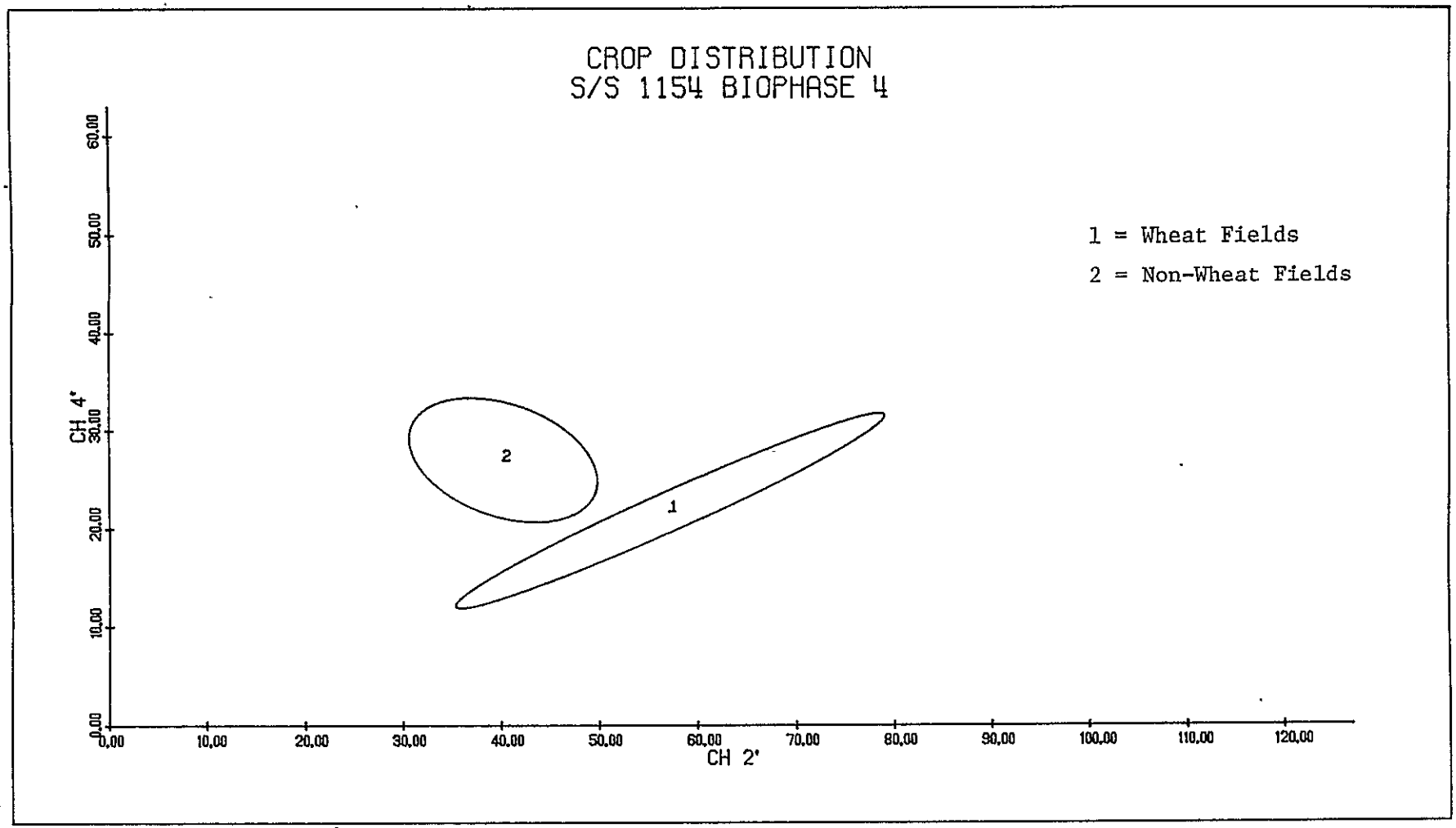

FIGURE 13. CROP DISTRIBUTION FOR A BIOPHASE 4 ACQUISITION

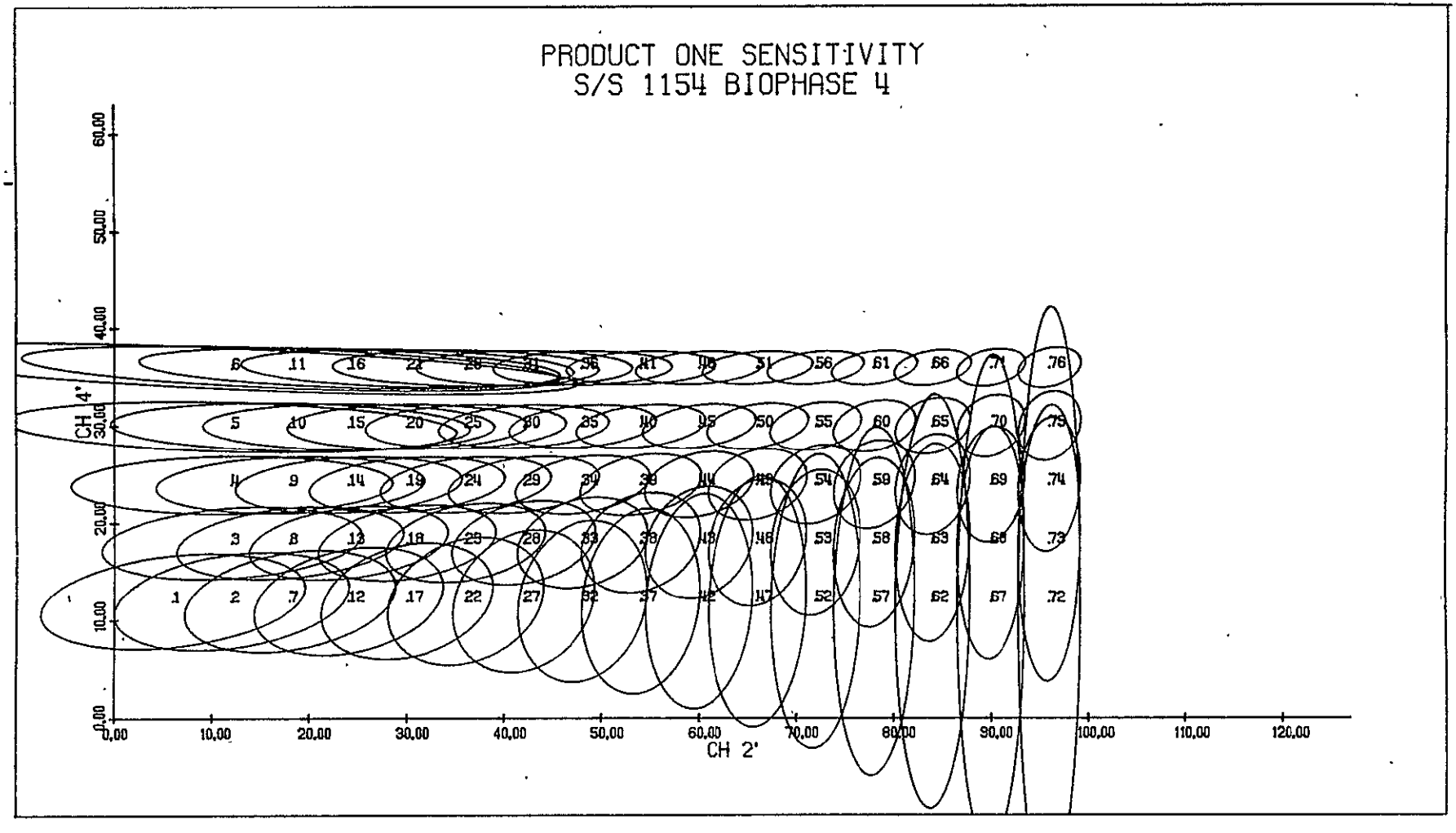

FIGURE 14. PRODUCT ONE SENSITIVITY FOR A BIOPHASE 4 ACQUISITION

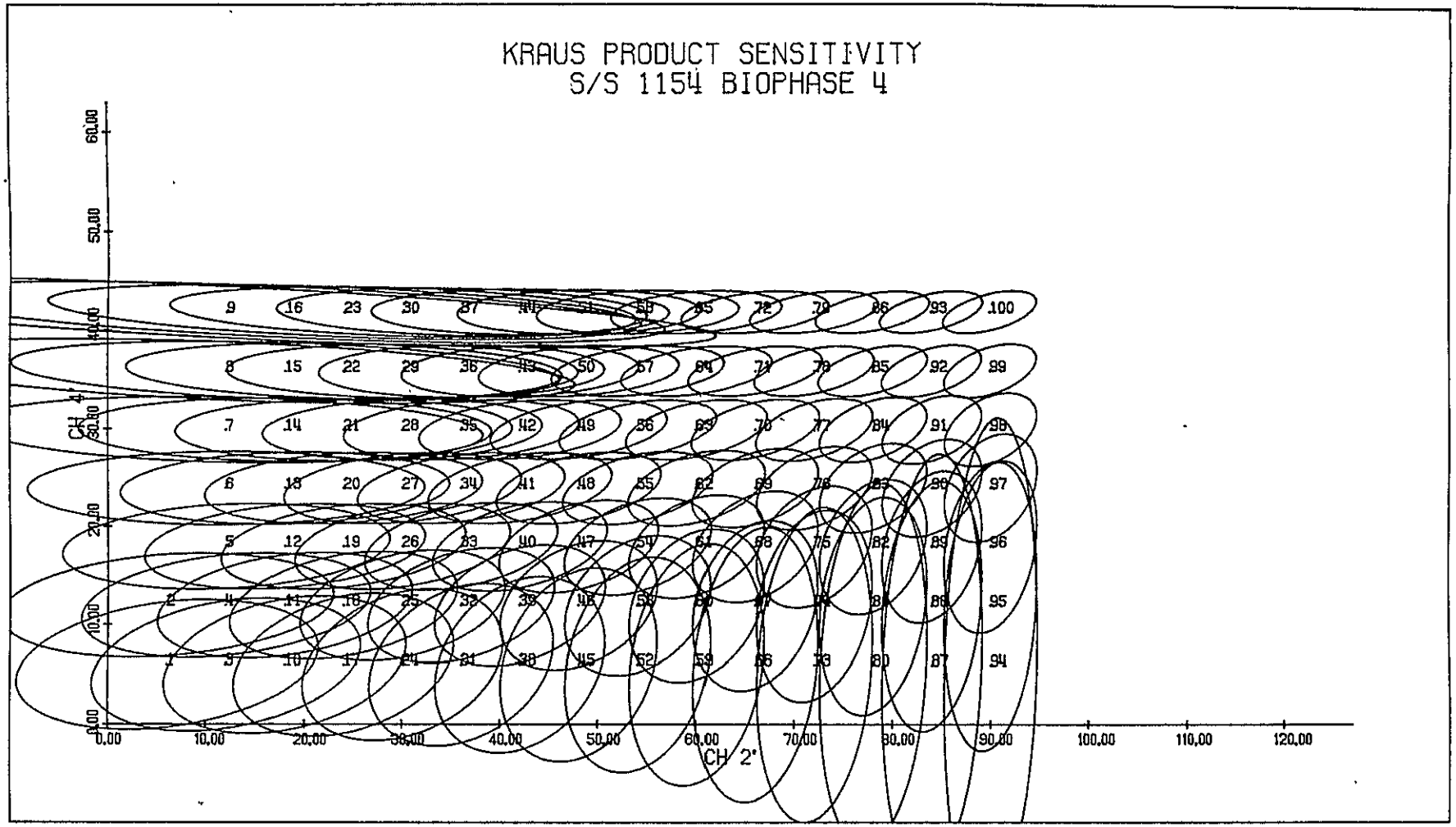

FIGURE 15. KRAUS PRODUCT SENSITIVITY FOR A BIOPHASE 4 ACQUISITION

color as a data point on the boundary. For the reader's reference, Appendix IV lists the points of color space to which each numbered grid point is mapped for each sensitivity plot.

6.5.3 ELUCIDATION OF SENSITIVITY PATTERN

The pattern of shapes of the sensitivity ellipses in the plots presented may be elucidated by consideration of the nature of the transformation from data space to perception space. The transformation involves two non-linear steps. If the steps of the transformation were all linear the ellipses would have the same shape (not necessarily round). This is because a linear transformation distorts space in the same way regardless of the point of application. A non-linear transformation applies a distortion to distances which is different from point to point. The non-linearities in the data to perception mapping cause the shapes of the color space ellipses to migrate in a characteristic manner.

Let us examine one row of ellipses (constant Ch 2' value) along the left of the sample grid. Here we observe sensitivity corresponding to use of the red primary alone. Figure 16 shows the ellipses from the product One Biophase Two sensitivity plot (Figure 8) for CH2' = 12. The migration of shapes observed here is due to the non-linearities of the data-to-perception mapping. One of the non-linearities is in the control of primary activation. The other is in the equations of Uniform Color Space, which represent the non-linear response of the eye in color perception. We will illustrate the characteristic effects of these non-linearities on sensitivity.

To illustrate the influence of the first non-linearity, let us graph activation as a function of input level and then match input level to the data channel axis. Activation is exponentially related

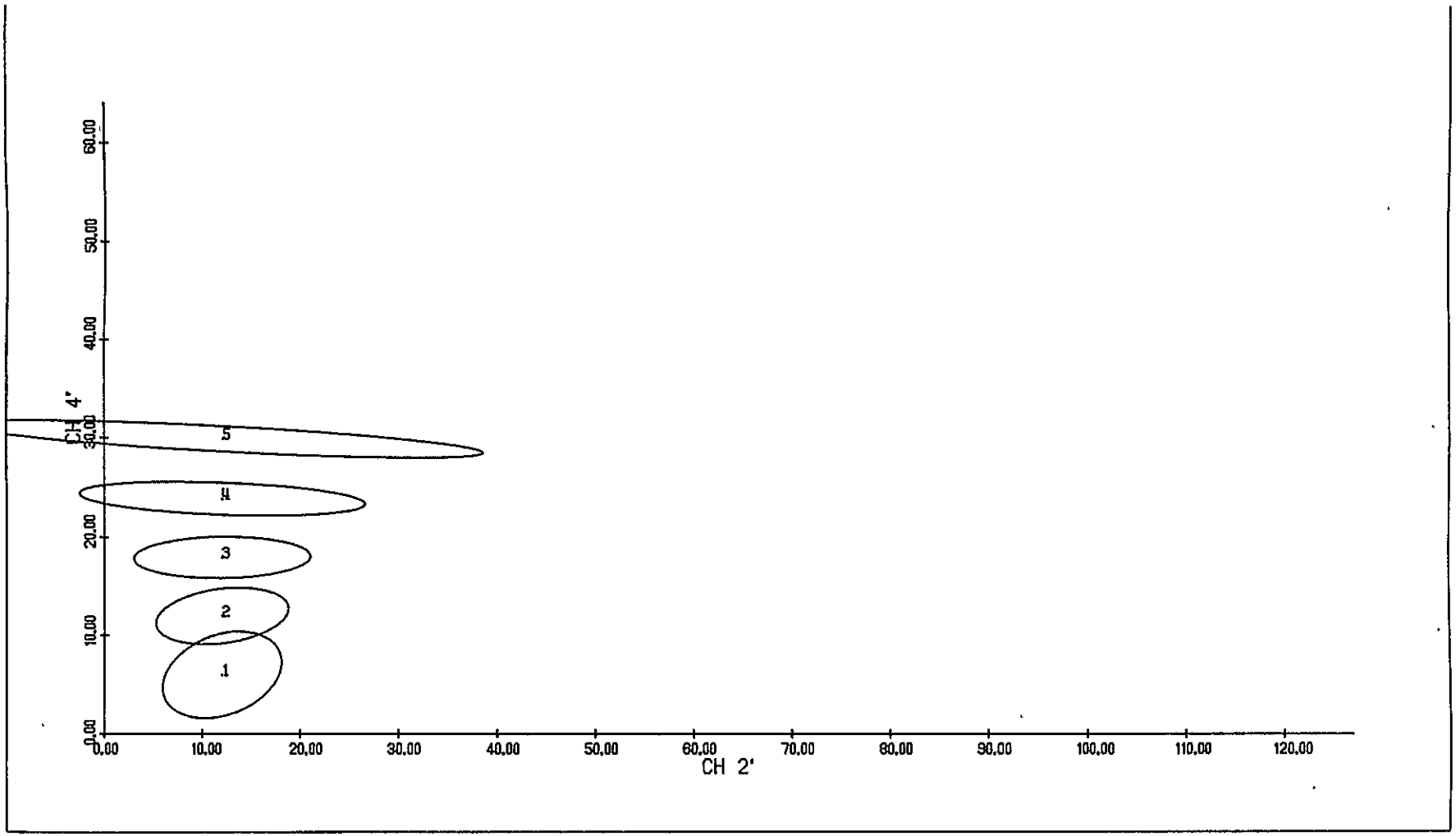

FIGURE 16. ELLIPSES FOR ACTIVATION OF RED PRIMARY ONLY

to input level (see Section 4.3). The general equation relating activation, a, to input level, C, is as follows:

$$a_i = 10^{m \cdot C_i + b}/\tau_{max} \qquad i = B, G, R \qquad (29)$$

where m, b, and τ_{max} are constants for each primary. A graph of this relationship for the red primary (m = 0.006929, b = -2.52, τ_{max} = 0.1762) appears in Figure 17. Note that the curve has a very gentle slope for C_R less than 150. After 200, however, the slope becomes very steep. The change in activation from 0 to 200 counts is about 0.25 while going from 200 to 255 uses the remaining 0.75. The activation variable is far more sensitive to change in input level when the input level is toward the upper end of the scale.

The effect of this on image sensitivity is pronounced. Since input level is a linear expansion of a data channel we may match activation directly with data values. We match the input channel interval, 0 to 255, with the data channel interval selected to cover it. In the following figure (Figure 18) we have matched the graph of red primary activation (Figure 17) with the CH4' axis of the sensitivity ellipses for use of the red primary in isolation. The increased sensitivity of activation to input toward the upper end of the data interval is reflected in the narrowing of the ellipses. Moving toward the top of the CH4' interval the dimension of the ellipses parallel to the CH4' axis becomes small. This implies color is varying rapidly in this direction and sensitivity to differences in CH4' is large.

The second non-linearity in the transformation occurs in the equations of Uniform Color Space. The UCS transformation involves cube roots. The effect on sensitivity is counter to the exponential transformation discussed above. Under a cube root transformation, sensitivity becomes greater near the low end of the scale of activation.

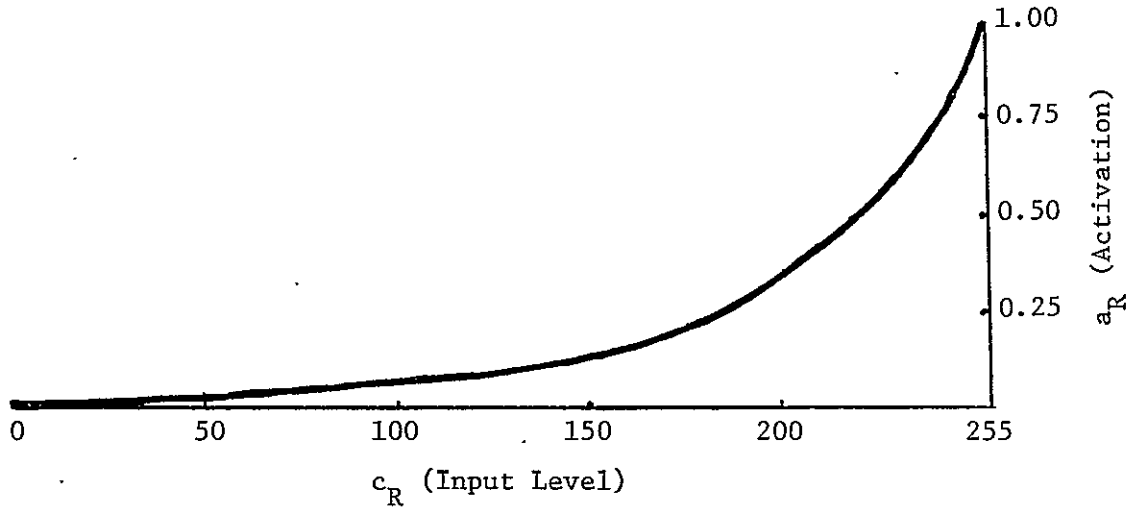

FIGURE 17. ACTIVATION OF THE RED PRIMARY VS. COUNTS ON INPUT CHANNEL

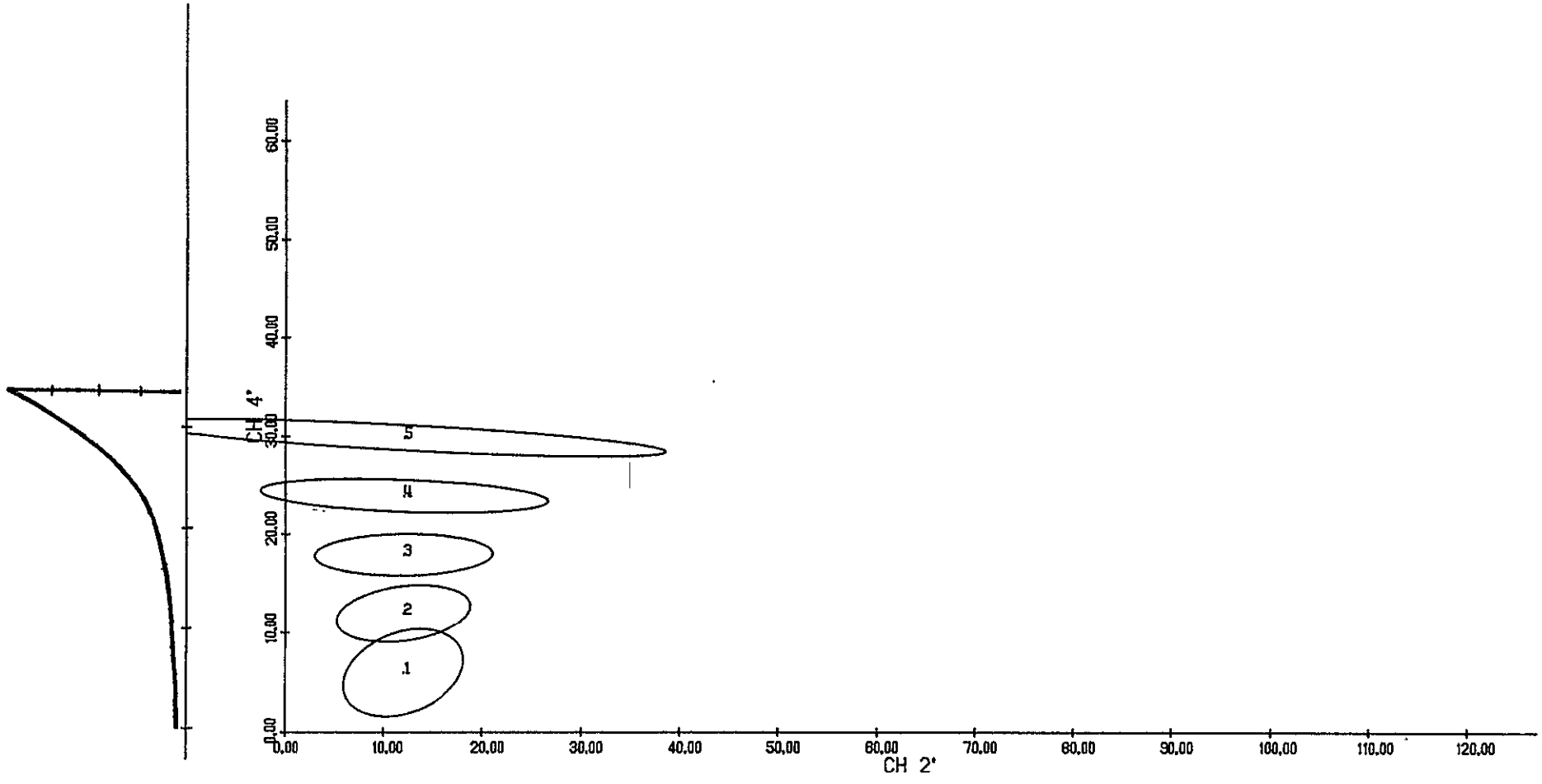

FIGURE 18. MATCHING ACTIVATION WITH DATA CHANNEL

We can illustrate the influence of the color space non-linearity by removing the non-linearity in activation. We modify the mathematics of the model so that activation scales linearly with input:

$$a_i = C_i/255 \qquad i = B, G, R \tag{30}$$

A sensitivity ellipse plot (of the Biophase Two acquisition with Product One intervals) produced under this modification is presented in Figure 19. This figure shows the eye's responsiveness to linear changes in energy of a stimulus. Note that the sensitivity to change increases as the size of the stimulus decreases, i.e., as you move downward in CH2' and/or CH4'.

The effect of the perception transformation runs counter to the effect of exponential activation control. However, it loses in the tug-of-war by a wide margin. There is a mismatch between density control of activation as implemented in the PFC and the physiology of human color perception. As a result, the sensitivity ellipse plots all show a pattern characteristic of exponential translation of data to perception space, rather than uniform translation.

Let us now assemble the complete pattern of sensitivity. The sensitivity of the blue and green primaries in isolation follows the same pattern as the red primary; sensitivity is greatest toward the upper end of the data interval. This is represented by the bottom row of ellipses in each plot. Consider the ellipses of the Biophase Three sensitivity plot (Figure 11) for CH4' = 18. In isolation they appear as follows in Figure 20.

For combinations of the three primaries, sensitivity depends on where each falls on the curve of activation. Near highest activation of all three the overall sensitivity is finest. Near lowest activation sensitivity is poorest. This is indicated schematically in Figure 21.

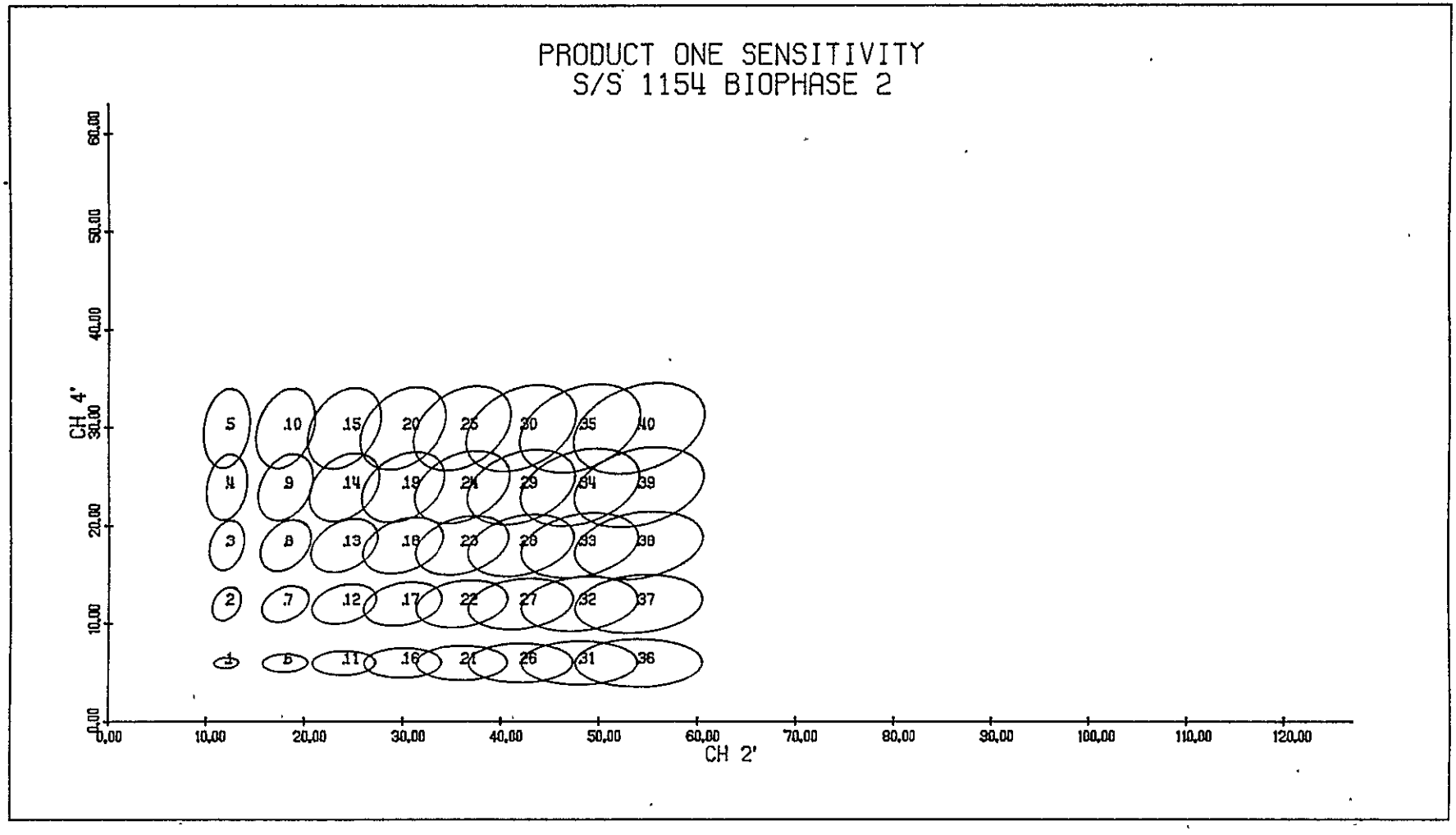

FIGURE 19. PRODUCT ONE SENSITIVITY WITH HYPOTHETICAL LINEAR CONTROL OF PRIMARY ACTIVATION

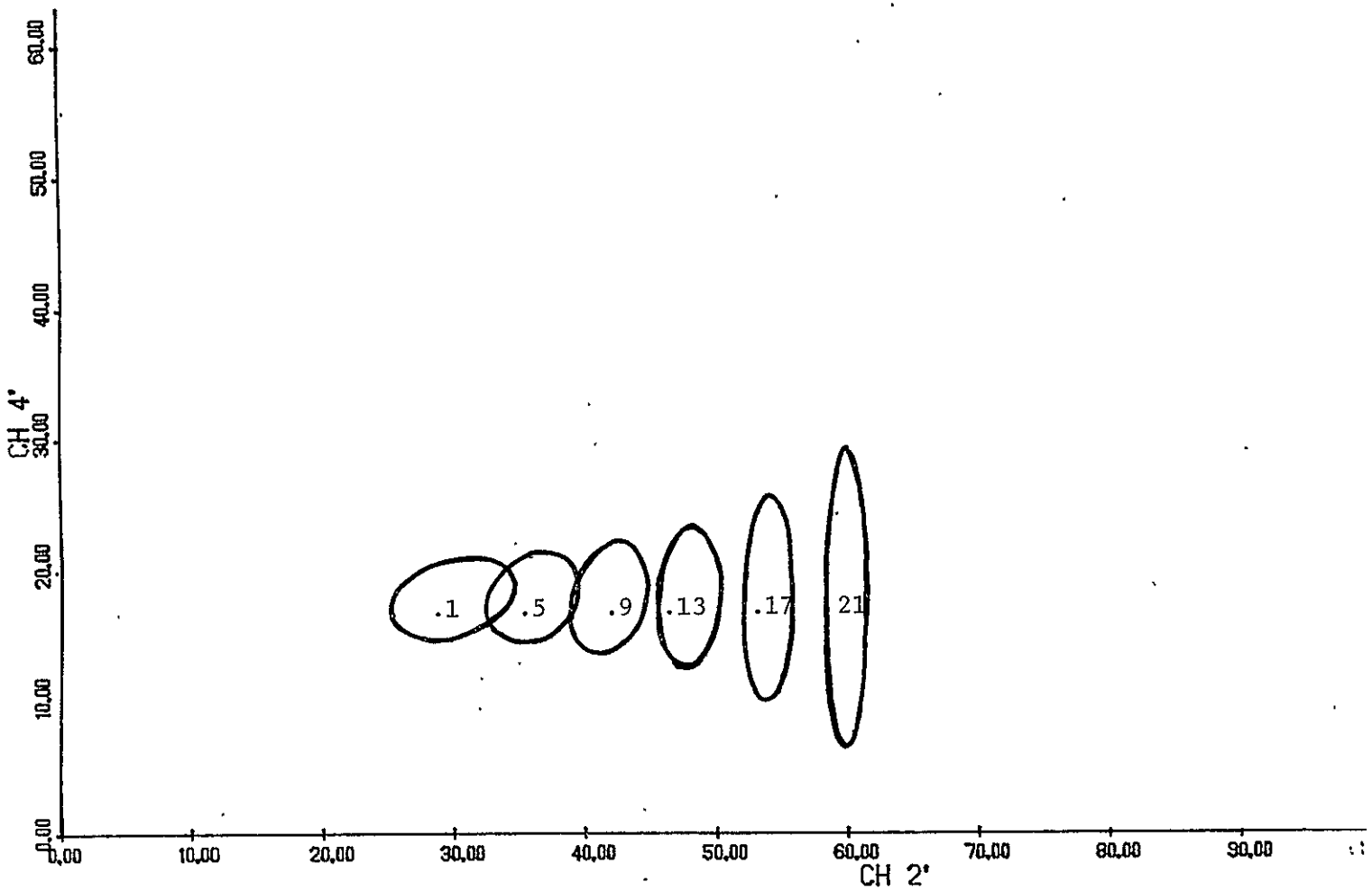

FIGURE 20. ELLIPSES FOR ACTIVATION OF BLUE AND GREEN PRIMARIES

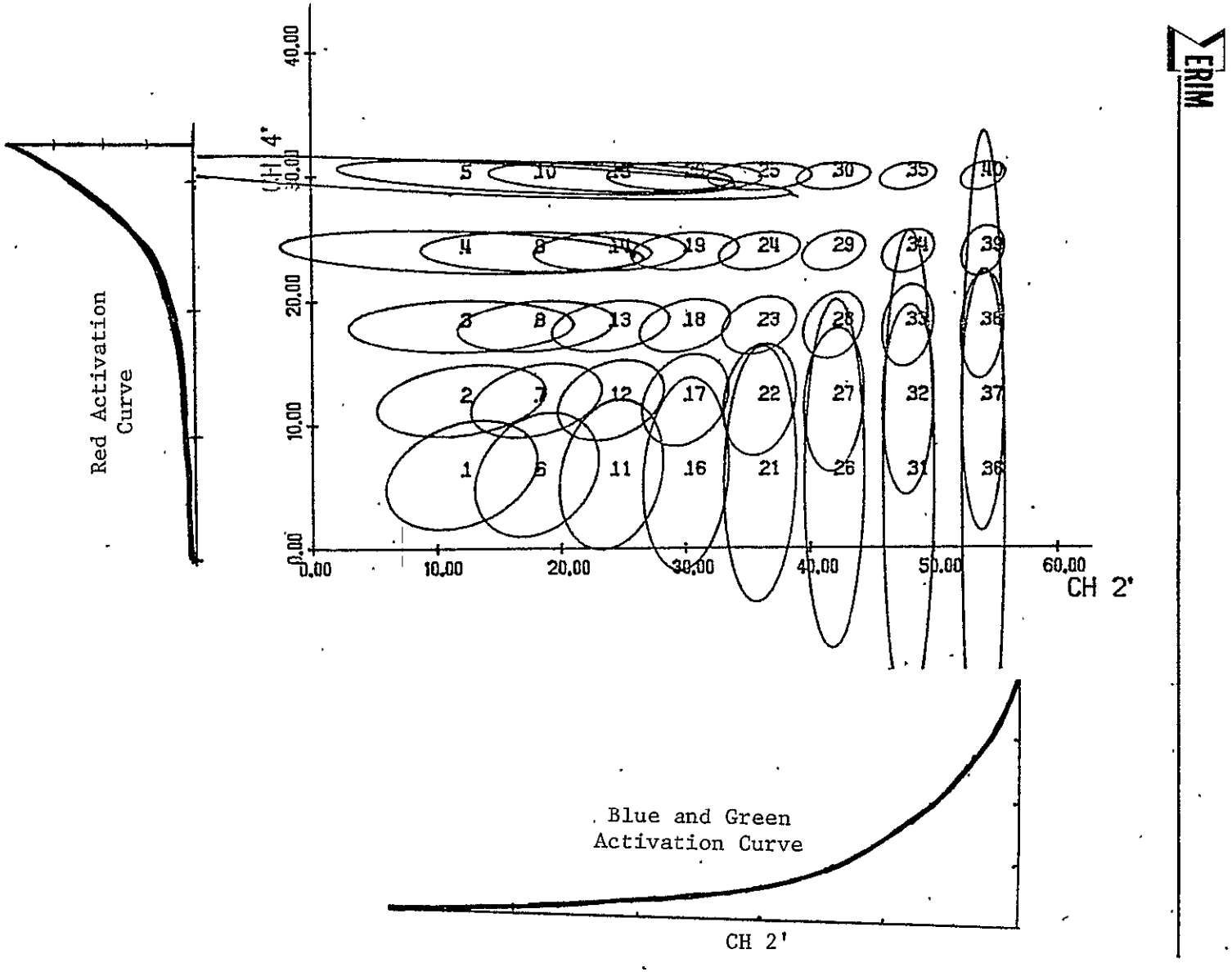

FIGURE 21. ACTIVATION CURVES MATCHED WITH SENSITIVITY PLOT
(for Product One, Biophase 2 Image)

Ellipses are small and distinct from one another in the upper right of the grid which corresponds to high activations. The ellipses are large and overlapping in the lower left which corresponds to low activation.

6.5.4 ANALYSIS OF RESOLUTION

In this section we evaluate the Product One and Kraus Product images on the basis of how well they resolve the data for the human eye. As a hypothesis of evaluation we will say there is a resolution size to Landsat information which may be expressed as a number of data channel counts. We will also say there is a resolution size of color perception which may be expressed as a number of UCS units. Our task is then to establish whether the resolvable unit of data space is transformed to a resolvable color difference in image format. In this way we measure the adequacy of resolution of the image product.

Our design of sensitivity display facilitates evaluation of image resolution. The design (discussed in Section 6.4) provides that the ellipse boundary represent one resolvable unit in color space. In addition, the spacing of evaluation points (ellipse centers) samples the data space at a fineness which corresponds to the hypothesized resolution level of the data. This arrangement makes it possible to check the adequacy of image resolution straightforwardly by examining a sensitivity ellipse plot. In areas of the data plane where color resolution exceeds the baseline resolution (3 counts) in all directions sensitivity ellipses will be smaller than 3 counts (in length of semi-major axis).

The spacing of grid points provides a visual cue to the reference resolution since half the distance from a point to one of its four neighbors is a 3 count threshold. Although the ellipses display information for all directions, it will prove convenient in portions of the subsequent analysis to concentrate on the directions of CH2' and CH4'.

Let us first characterize Product One sensitivity under various circumstances. Comparing the Product One plots for each Biophase (Figure 5, 8, 11, 14) we observe that the overall sensitivity of a

Product One image is very much a function of the range of data it is asked to cover. In Biophase One the range is very small. The scene consists primarily of bare soil and soil with sprouting crops which is still nearly bare. From the sensitivity ellipse plot of Biophase One, Figure 5(a), we see that data is resolved down to 1 1/2 or 2 counts over most of the range*. In Biophase Four, on the other hand, one usually finds a sharp contrast of fields which are very green, with fields which are harvested and bare or covered with crop stubble. Inspecting the sensitivity plot of Biophase Four one finds resolution in the center of the range to be about 7 counts. One concludes that PFC Product One has good resolution for acquisitions in which the data range is small but has less than desirable resolution in acquisitions with typical data variability.

Let us look more closely at the Biophase Two acquisition. This acquisition has a data distribution with average variability for an agricultural scene. Figure 22 gives a breakdown of the data range into regions according to sensitivity. It also shows where the concentration of data points fell for this acquisition. The demarcation line of good vs. poor sensitivity for CH4 was drawn through the line of sensitivity ellipses above which the 3 count reference on resolution is consistently met or exceeded. Similarly, for CH2' the line was drawn through the column of ellipses to the right of which the 3 count criterion is met or exceeded. We observe that the data concentration lies outside the region of all around good sensitivity. Developed wheat falls in a region of good CH4' sensitivity but poor CH2' sensitivity. Non-wheat for the acquisition falls in a region of poor CH4' resolution and CH2' resolution which ranges from good to poor. Under current methods of using the PFC it will always be true that the best image sensitivity

*This statement is not to be taken to mean that Biophase One acquisition imagery is free of problems. The so-called "spectral distortion" of Product One Imagery may exist independent of the quality of image resolution.

occurs in the upper corner of the data range selected, away from the middle of the range where the data is concentrated.

Let us turn to examination of the Kraus Product. We observe that for each of the plots reproduced here the Kraus Product sensitivity is distinctly poorer than that of Product One. This is to be expected since the Kraus algorithm characteristically does not follow data variability as closely as Product One. Figure 23 presents a breakdown of sensitivity for the Biophase Two acquisition using the Kraus Product. This may be compared with Figure 22 for Product One. The data concentration falls much lower in CH2' sensitivity than it did for Product One but remains about the same in CH4' sensitivity. Comparing the sensitivity plot for this image (Figure 9) we find that the concentration of data falls around grid points 19. From the shape of the ellipses associated with these points, we surmise that the image gives four to five times as much perceptual expansion to CH4' variation as CH2' variation.

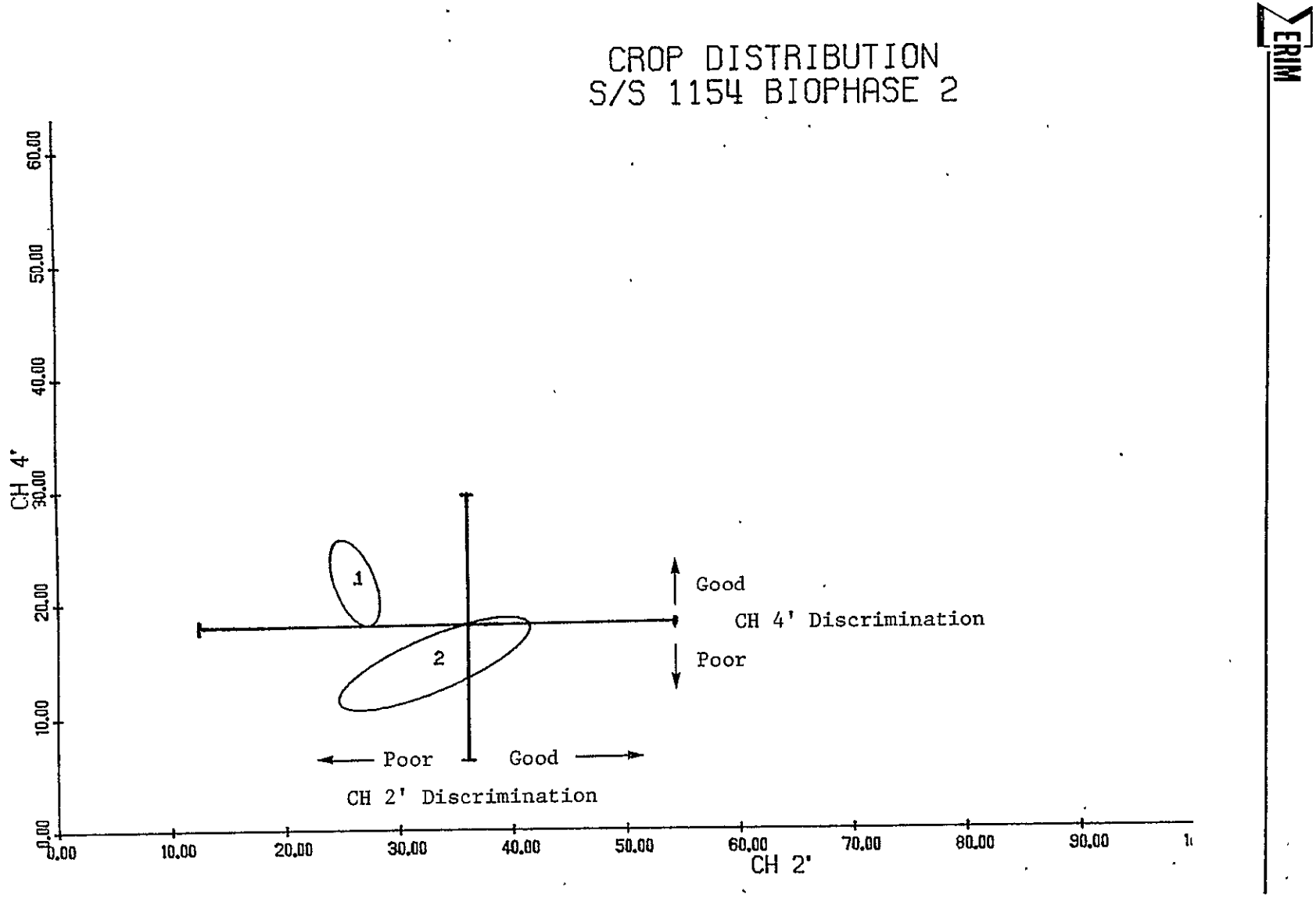

FIGURE 22. BREAKDOWN OF DATA PLANE ACCORDING TO SENSITIVITY FOR PRODUCT ONE IMAGE OF A BIOPHASE 2 ACQUISITION

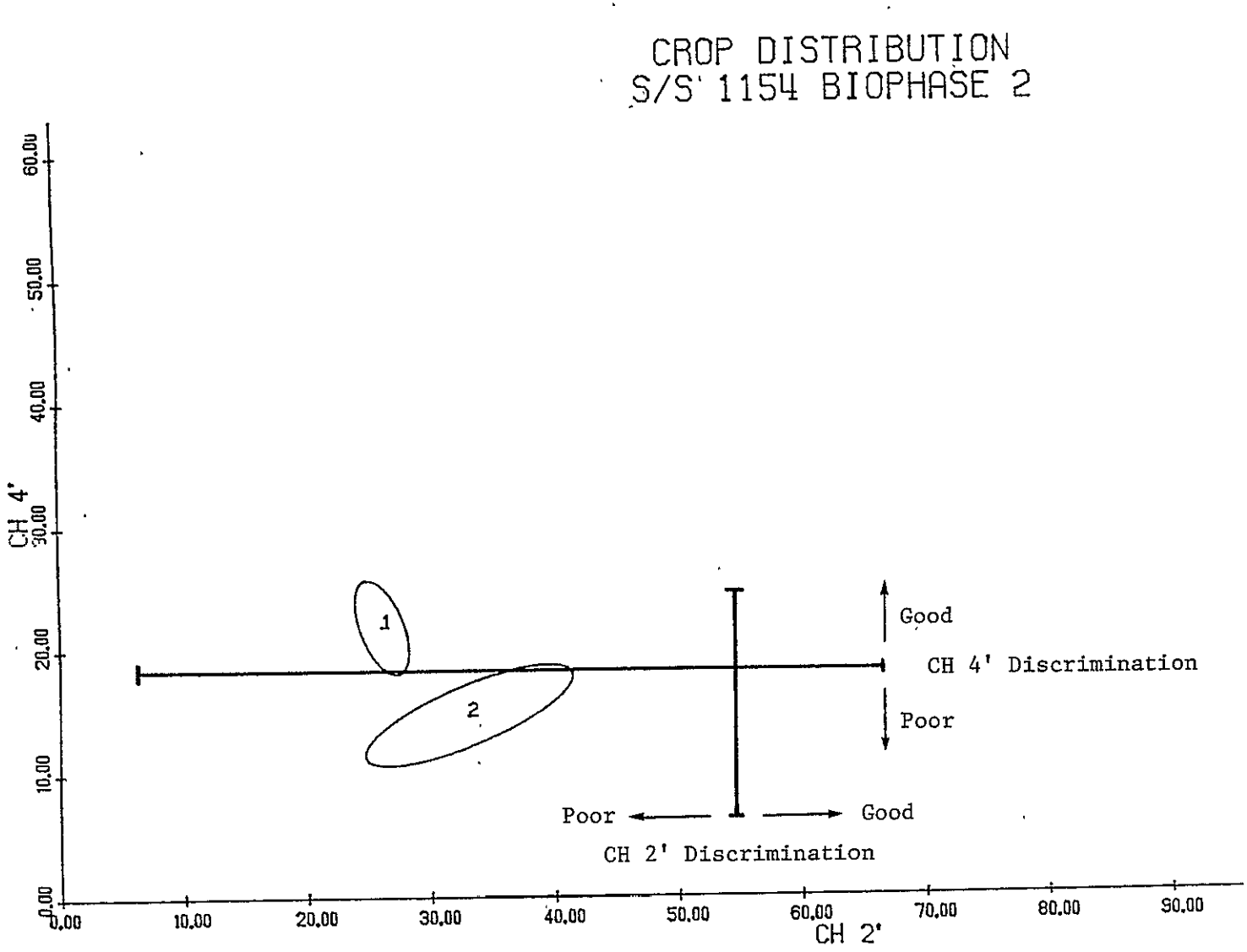

FIGURE 23. BREAKDOWN OF DATA PLANE ACCORDING TO SENSITIVITY FOR KRAUS PRODUCT IMAGE OF A BIOPHASE 2 ACQUISITION

CROP DISCRIMINATION ANALYSIS

Sensitivity analysis presented above shows Product One has problems in data resolution when the data spans its full natural range. We initiated an analysis of Product One in terms of probability of misclassification to resolve the question of how important this lack of resolution might be to crop discriminability. In particular we also wanted to compare the loss of information due to dropping Channel 3 with the loss due to poor resolution.

7.1 EXPERIMENT DESIGN

We sought an acquisition for study to provide a two-class discrimination problem. The acquisition of Kansas Sample Segment 1154 for Julian Day 124 was selected for its good separation of winter wheat and non-wheat crops. This is the same Biophase Two acquisition used in the sensitivity analysis above.

Signatures of the two crop distributions in data space were computed and transformed into their color space counterparts. In the transformation, Product One procedure was used employing bias and scale values as originally computed by JSC. To simulate the finite color resolution of the human eye, statistical noise of 5 color space units was added to the color space signatures.* This assures that points separated by less than 5 UCS units cannot be classified as different, just as on an image the eye cannot distinguish the colors to be different.

*Adding noise to the distributions involves adding the covariance matrix of the noise source to the covariance matrix of the distribution. The noise is uniform with standard deviation of 5 units. Its covariance matrix is therefore

$$(COV)_{noise} = 5^2 I$$

where I is the identity matrix.

Our experimental purpose was to determine, step by step, where information relevant to crop discrimination was being lost in the data-to-perception transformation. We proceeded to compute probabilities of misclassification between wheat and non-wheat distributions when represented in each of the following coordinate spaces:

1. Landsat 4-space: Channels 1, 2, 3 and 4.
2. Landsat 3-space: Channels 1, 2 and 4.
3. Color space assuming infinite color resolution by the eye: L*, a*, b*.
4. Color space assuming resolution of 5 units by the eye: L*, a*, b*.

7.2 RESULTS AND INTERPRETATION

Table 3 presents the probability of misclassification between the two distributions in each coordinate space.

TABLE 3. PROBABILITY OF MISCLASSIFICATION ANALYSIS RESULTS FOR PRODUCT ONE

Coordinate Space	Percentage Correct Classification	
	Wheat	Non-Wheat
1. Landsat 4 channels	97.2	94.6
2. Landsat 3 channels	87.8	95.2
3. Color space assuming infinite color resolution	84.8	95.0
4. Color space assuming 5 unit color resolution	81.8	91.6

We do not claim these results represent how an Analyst Interpreter would perform in working this acquisition. We expect the rankings observed to indicate where information losses occur and their relative importance.

Step 1, from Landsat 4-space to Landsat 3-space, involves simply dropping one channel of the data from use in classification. We ignore Channel 3 input and consider only the channels which go into making Product One, namely Channels 1, 2 and 4. The result is a substantial decline in the accuracy of wheat recognition. Recognition of wheat drops from 97.2% to 87.8%.

Step 2 takes us from Landsat data distributions to color space distributions with the assumption of infinite color resolution. Classification accuracy can change at this step due to distortion of the shapes of distributions with respect to one another. A further 3 percentage point drop in wheat recognition occurs at this point.

Step 3 takes account of the finite color resolution of the eye. This results in a decline of 3 percentage points in wheat recognition and a decline of 4.4 percentage points in non-wheat recognition.

The factors in information loss, are then, in order of importance, as follows:

1. Dropping Channel 3 input.
2. Insufficient resolution of data into color.
3. Distortion of shape of distribution in transformation to color.

The importance of Channel 3 input for classification has been recognized empirically and the AI is routinely provided a product which includes Channel 3 (Product Two). However, the price is that this image does not contain Channel 1 information. We expect that much of the information of Landsat data lies in the interrelationship of the four channels considered simultaneously. For this reason, interpreting two images with subsets of bands is not the same as interpreting one image with all the information. Data feature extraction transformations exist which reduce the dimensionality of Landsat data without significant loss

of information. The linear Tasselled Cap transformation, developed by Kauth and Thomas of ERIM, is a prime example. There is impetus for investigating ways of converting Landsat features to a single color image with full retention of information.

8

CONCLUSIONS AND RECOMMENDATIONS

Based on our analysis on sensitivity of image products we present two conclusions concerning products which depend on scaling and biasing of data channels for control of PFC primaries: 1) the images do not provide a uniform representation of data variation but distort distance relationships in characteristic ways, and 2) overall sensitivity in the region of data concentration does not meet the criterion of making a significant difference in data counts (3 counts) appear as a significant difference in color (5 UCS units) when the data fill their normal range.

The observation on sensitivity applies even to Product One which is the "maximum contrast" method of selecting data intervals (scale and bias factors). The Kraus Product, which generally covers larger data intervals than Product One, appears to be significantly less sensitive than Product One.

From our analysis of crop discrimination properties, we conclude that the present method of film generation leads to loss of information (in a probability-of-misclassification sense) by two major processes. In order of importance they are: 1) neglecting the input of one channel of data in any one image, and 2) failing to provide sufficient color resolution of the data.

It has been recognized for some time that the technique of scaling and biasing data channels for image production has inherent problems relating to consistency of interpretation of colors [4, 5, 6]. The problem is inherent because the simple technique of scaling and biasing requires a large alteration of the data-to-color map for each acquisition. Alternative techniques to Product One's selection of data intervals have been proposed which compromise between contrast and stability of interpretation [3, 7, 8]. However, the conclusion

of this study is that the scaling and biasing approach cannot provide an image which portrays the data as fully as it could be or as fully as we would like it portrayed for interpretation in most instances. The scaling and biasing approach tends to distort distance relationships in data space and provides less than desirable resolution when the data variation is typical of a developed, non-hazy agricultural scene.

Our recommendation is that impetus be given to advanced techniques of producing images which take advantage of the known structure of Landsat data and the understanding that has been developed of the color production properties of the image production system.

APPENDIX I

DETAILS OF MODELING THE COLOR PRODUCTION CHARACTERISTICS OF THE PRODUCTION FILM CONVERTER

1.0 OBJECTIVE

Establish a means for the analysis and comparison of image products generated by different algorithms -- initially the Product 1 algorithm and the algorithms proposed by Kaneko, Kraus, and Hocutt.

2.0 APPROACH

Given an algorithm which produces, pixel by pixel, PFC gun numbers R, G and B, specify the colors corresponding to the mixtures of PFC primaries in the coordinates of a perceptually uniform color space (CIE 1976 (L^*,a^*,b^*) Unifrom Color Space). Establish analytic measures of performance on the algorithms which express the success of an algorithm in separating wheat from non-wheat for the human eye.

3.0 THE TRANSFORMATION

Our understanding of the technical details of the transformation from R,G,B gun numbers to L^*,a^*,b^* coordinates is based on private communication with Richard Juday of JSC. To make the transformation it is necessary to know the chromaticities of the effective primaries being used and to know the relationship of gun settings to the amount of primary activated.

3.1 PRIMARY UNITS

It is our understanding that gun numbers 0-255 are not linear measures of primary activation for the PFC image. The gun settings are related to density produced in the film. Primary activation must measure transmission which is related exponentially to density. The correspondence of gun numbers to primary activation is contained in Table 1. Each gun number is associated with one of 65 levels of primary activation. One defines activation coordinates (a_R, a_G, a_B) as follows:

TABLE 1. CORRESPONDENCE OF PFC GUN NUMBERS TO PRIMARY ACTIVATION
Source: Richard Juday

N	R	B	G
0	2	0	3
1	9	5	40
2	30	45	42
3	45	64	67
4	57	74	77
5	68	82	86
6	74	92	94
7	84	103	102
8	91	109	110
9	96	110	114
10	103	120	123
11	108	125	130
12	113	129	136
13	118	133	139
14	121	137	141
15	125	142	143
16	129	151	146
17	132	153	151
18	139	155	153
19	144	157	157
20	147	163	157
21	153	166	161
22	158	166	165
23	166	172	171
24	168	179	176
25	171	182	179
26	172	182	187
27	175	183	187
28	179	186	189
29	180	186	190
30	183	187	193
31	186	189	195
32	189	190	195
33	191	191	195
34	191	192	195
35	192	194	195
36	193	195	195
37	194	196	195
38	195	197	195
39	196	198	196
40	197	200	197
41	199	201	202
42	202	204	202
43	205	205	204
44	206	205	206
45	207	208	212
46	209	210	213
47	213	211	214
48	215	213	218
49	216	215	223
50	218	217	225
51	220	219	227
52	222	221	229
53	223	223	231
54	226	224	232
55	227	226	234
56	228	227	235
57	229	228	236
58	229	229	237
59	231	230	238
60	234	231	240
61	237	232	241
62	239	233	242
63	242	233	243
64	244	234	244

$$a_R = N_R/64$$

$$a_G = N_G/64$$

$$a_B = N_B/64$$

It follows that $0 \leq a_i \leq 1$ $\quad i = R,G,B.$

3.2 XYZ TRANSFORMATION

The activation coordinates (a_R, a_G, a_B) form a color space. The axes are linear measures of the three additive primaries of the PFC. As such, there is a linear relationship between the basis vectors of (a_R, a_G, a_B) space and CIE XYZ space. The relation may be expressed in matrix notation:

$$\begin{pmatrix} X \\ Y \\ Z \end{pmatrix} = \begin{pmatrix} X_R & X_G & X_B \\ Y_R & Y_G & Y_B \\ Z_R & Z_G & Z_B \end{pmatrix} \begin{pmatrix} a_R \\ a_G \\ a_B \end{pmatrix}$$

To determine the values of the matrix elements one must first compute the x,y chromaticity coordinates of the primaries and of the light used in viewing the film product.

The x chromaticity of the light table is found by evaluation of the following integral:

$$x_T = \int_\lambda \bar{x}(\lambda)\, L(\lambda)\, d\lambda/T$$

where

$\bar{x}(\lambda)$ is the color matching function of the X tristimulus value

$L(\lambda)$ is the relative energy distribution of the light source

T is the normalizing denominator,
$T = \int \bar{x}Ld\lambda + \int \bar{y}Ld\lambda + \int \bar{z}Ld\lambda$

The x chromaticity of the red primary is found by evaluation of this integral:

$$X_R = \int_\lambda \bar{x}(\lambda)\ L(\lambda)\ \tau_R(\lambda)\ d\lambda/T$$

where

$\tau_R(\lambda)$ is the film transmission for the red primary

T is the normalizing denominator

$$T = \int \bar{x}\ L\ \tau_R d\lambda + \int \bar{y}\ L\ \tau_R d\lambda + \int \bar{z}\ L\tau_R d\lambda$$

To find y, one replaces $\bar{x}$ with $\bar{y}$ in the above equations. For chromaticities of the green and blue primaries one uses τ_G and τ_B in place of τ_R. Each integral is approximated by a sum over 10 nm intervals from λ = 400 nm to λ = 750 nm using the data of Table 2. The computed chromaticities are listed beneath the table.

The three primary lights added together must give the color of the light table, (x_T y_T Y_T), being used to view the film. Y_T is set equal to 100 as nominal white. One may determine Y_R, Y_G, Y_B in terms of their chromaticity and the combination light by solving a set of three simultaneous equations (See Addendum). Carrying out this computation one obtains the following:

$$Y_R = 32.04$$

$$Y_G = 57.09$$

$$Y_B = 10.86$$

One now computes X_i and Z_i from these relations:

$$X_i = \frac{x_i}{y_i} Y_i$$

$$Z_i = \frac{1 - x_i - y_i}{y_i} Y_i$$

$$i = R,G,B.$$

TABLE 2. SPECTRAL ENERGY DISTRIBUTION OF LIGHT TABLE, COLOR MATCHING FUNCTIONS AND TRANSMISSIONS AS A FUNCTION OF WAVELENGTH. Source: Richard Juday

λ	$\bar{x}$	$\bar{y}$	$\bar{z}$	L_λ	τ_G	τ_B	τ_R
400	.0143	.0004	.0679	1.105	.020	.080	.000
410	.0435	.0012	.2074	.951	.020	.092	.000
420	.1344	.0040	.6456	2.192	.016	.107	.000
430	.2839	.0116	1.3856	6.063	.014	.116	.000
440	.3483	.0230	1.7471	2.891	.015	.139	.000
450	.3362	.0880	1.7721	2.530	.016	.165	.000
460	.2908	.0600	1.6692	2.829	.020	.175	.000
470	.1954	.0910	1.2876	2.865	.023	.170	.000
480	.0956	.1390	.8130	2.782	.047	.145	.000
490	.0320	.2080	.4652	3.072	.079	.110	.000
500	.0048	.3230	.2720	2.889	.115	.074	.000
510	.0093	.5030	.1582	3.093	.151	.045	.000
520	.0633	.7100	.0782	3.392	.190	.028	.005
530	.1655	.8620	.0422	4.141	.207	.018	.005
540	.2904	.9540	.0203	7.628	.198	.013	.015
550	.4334	.9950	.0087	8.140	.176	.010	.035
560	.5945	.9950	.0039	8.570	.155	.010	.074
570	.7621	.9520	.0021	8.694	.124	.010	.115
580	.9163	.8700	.0017	7.699	.116	.010	.150
590	1.0263	.7757	.0011	7.424	.093	.015	.172
600	1.0622	.6310	.0008	6.058	.071	.012	.182
610	1.0026	.5030	.0003	5.019	.051	.011	.187
620	.8544	.3810	.0002	3.790	.037	.010	.188
630	.6424	.2650	.0000	2.783	.036	.000	.190
640	.4479	.1750	.0000	2.173	.021	.000	.193
650	.2835	.1070	.0000	1.617	.019	.000	.205
660	.1649	.0610	.0000	1.192	.016	.000	.218
670	.0874	.0320	.0000	1.362	.014	.000	.218
680	.0468	.0170	.0000	.667	.013	.000	.218
690	.0227	.0082	.0000	.513	.013	.000	.218
700	.0114	.0041	.0000	.495	.015	.000	.218
710	.0058	.0021	.0000	.363	.018	.000	.218
720	.0029	.0010	.0000	.374	.018	.000	.218
730	.0014	.0005	.0000	.359	.018	.000	.218
740	.0007	.0003	.0000	.294	.018	.000	.218
750	.0003	.0001	.0000	.301	.018	.000	.218

(5.4780	8.710660	1.012205)	(1.356728	1.088513	4.623864)	7
(.3603	.573036	.066588)	(.191923	.153981	.654094)	
x_G	y_G	z_G	x_B	y_B	z_B	

Chromaticity Coordinates for Light Table and the Three Film Colors

	x	y
Red	.5529	.4458
Green	.3603	.5730
Blue	.1919	.1540
Light Table	.3684	.4131

The resulting transformation matrix is specified:

$$\begin{pmatrix} X_R & X_G & X_B \\ Y_R & Y_G & Y_B \\ Z_R & Z_G & Z_B \end{pmatrix} = \begin{pmatrix} 39.73 & 35.90 & 13.53 \\ 32.04 & 57.09 & 10.86 \\ .0934 & 6.646 & 46.13 \end{pmatrix}$$

3.3 L^*,a^*,b^* TRANSFORMATION

L^*,a^*,b^* space is defined as a transformation of XYZ space. Once the conversion to XYZ has been made the coordinates of L^*,a^* and b^* follow from the equations of definition:

$$L^* = 25\ (Y)^{1/3} - 16 \qquad 1 \leq Y \leq 100$$

$$a^* = 500\ [(X/X_o)^{1/3} - (Y/Y_o)^{1/3}]$$

$$b^* = 200\ [(Y/Y_o)^{1/3} - (Z/Z_o)^{1/3}]$$

This space was adopted in 1976 as the CIE standard uniform color space. Figure 1 shows a sketch, in L^*,a^*,b^* space, of the boundary of possible object-colors (inner boundary) and the spectrum locus boundary (outer boundary).

The total difference $\Delta E_{CIE}(L^*,a^*,b^*)$ between two colors represented in this space is simply the Euclidean distance between them calculated as

$$\Delta E_{CIE}(L^*,a^*,b^*) = [(\Delta L^*)^2 + (\Delta a^*)^2 + (\Delta b^*)^2]^{1/2}\ \dagger$$

Euclidean distance in this space has approximately the same significance, in terms of measuring distinguishability between two colors, everywhere in the space, regardless of orientation. For example, suppose the a^* and b^* components of two pixels are equivalent, but the L^* component differs by 10 counts. These two pixels are as perceptually separable as two other pixels whose L^*,a^* components are equal, and differ by 10 in the b^* components.

$\dagger$CIE Proceedings, 18th Session, Appendix 2, 1975.

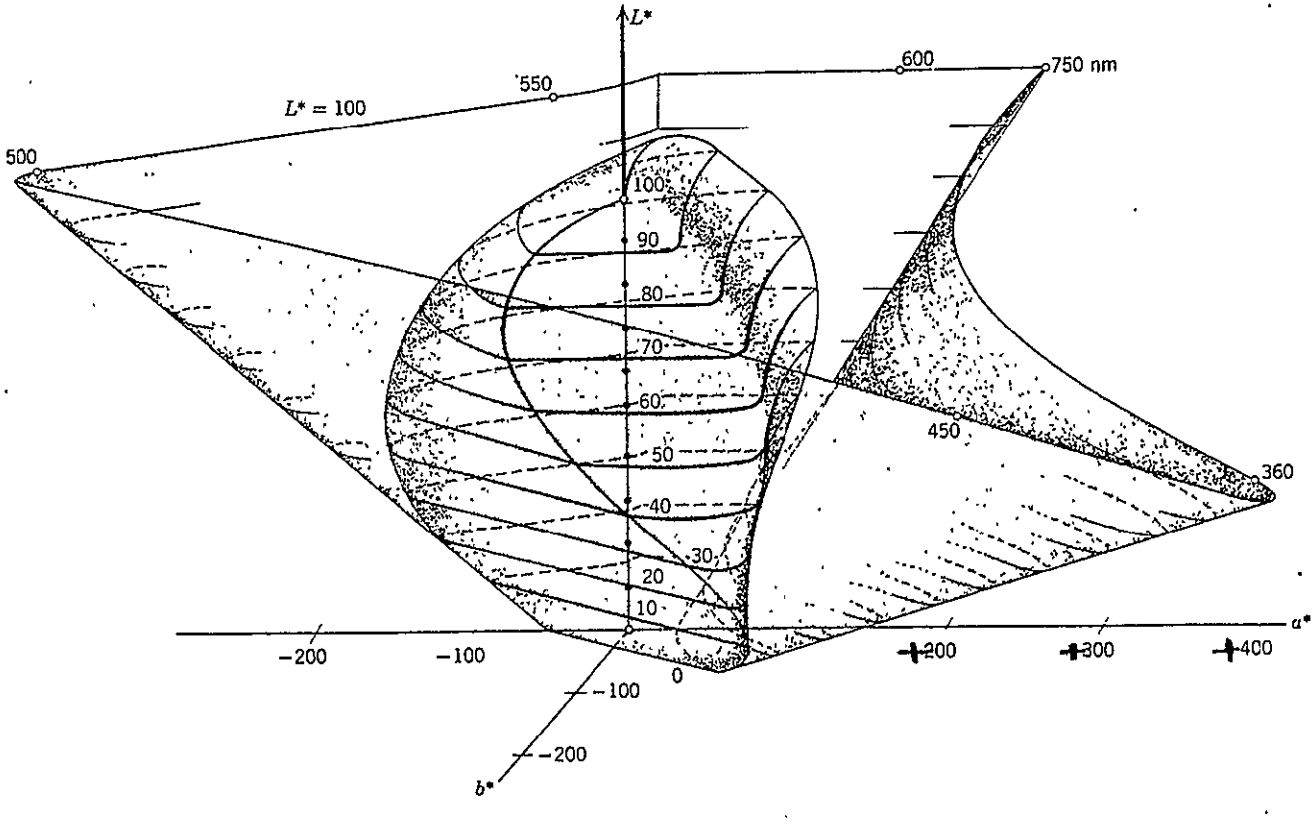

Sketch of (L^*,a^*,b^*) object-color space with inner boundary generated by optimal color stimuli with respect to CIE standard illuminant D_{65} and the CIE 1964 supplementary standard observer. The colors of all object-color stimuli fall within this boundary. This is also the gamut within which the color-difference formula $\Delta E(L^*a^*b^*)$ is intended to be valid. Note that the spectrum locus of the monochromatic stimuli is generally well outside the boundary of object-color stimuli.

FIGURE 1. (L^*,a^*,b^*) OBJECT-COLOR SPACE. (From Judd and Wyszecki, Color in Business, Science and Industry)

4.0 APPLICATION

A computer program has been implemented which does the following:

1. Applies given bias and scale factors to three channels of Landsat data to determine 3 "gun numbers" R,G,B. (The data may, optionally, be haze and sun angle corrected data.)

2. Determines activations of the 3 primaries by looking up the gun number in Table 1.

3. Performs the transformation to XYZ space and then L^*,a^*,b^* space according to the relations reviewed above.

5.0 ANALYSIS

We intend to establish analytic measures of performance on image products using L^*,a^*,b^* color coordinates. Potential points for comparison of products include these four:

1. Distinguishability of wheat from not-wheat, e.g., what is the distance in L^*,a^*,b^* units which separate mean wheat color from not-wheat at selected times during the growing season?

2. Portion of accessible color space used by the technique employed.

3. Consistency of color versus reflectance of an object, from time to time and scene to scene.

4. Early season separability of wheat as detectable to an analyst interpreter.

In addition to comparing gun mapping algorithms, we will investigate the effect of scene haze on the image product and the utility of preprocessing for haze and sun angle correction as well as examining the effect of employing a data transformation, like the Tasselled Cap, before color mapping.

ADDENDUM

EXPRESSION OF $Y_R Y_G Y_B$ IN TERMS OF THEIR CHROMATICITIES AND (x_T, y_T, Y_T)

(Source: Richard Juday)

By definition:

1. $x_T = X_T/(X_T + Y_T + Z_T)$

2. $y_T = Y_T/(X_T + Y_T + Z_T)$

3. $Y_T = Y_R + Y_B + Y_G$

and

$$X_T = X_R + X_G + X_B$$

$$Z_T = Z_R + Z_G + Z_B$$

and

$$X_i = \frac{x_i}{y_i} Y_i \qquad i = R,G,B$$

$$Y_i = \frac{y_i}{y_i} Y_i$$

$$Z_i = \frac{z_i}{y_i} Y_i$$

Substituting back into Equations (1), (2), and (3), one can rewrite

$$x_T = \frac{\sum \frac{x_i}{y_i} Y_i}{\sum \left(\frac{x_i}{y_i} + \frac{y_i}{y_i} + \frac{1 - x_i - y_i}{y_i} \right) Y_i}$$

$$= \frac{\sum \frac{x_i}{y_i} Y_i}{\sum \frac{1}{y_i} Y_i}$$

$$y_T = \frac{\sum Y_i}{\sum \frac{1}{y_i} Y_i}$$

$$Y_T = \sum Y_i$$

where all summations are over i = R,G,B.

Simplifying we have:

$$x_T \sum \frac{1}{y_i} Y_i - \sum \frac{x_i}{y_i} Y_i = 0$$

$$\text{implies} \quad \sum \frac{x_T - x_i}{y_i} Y_i = 0$$

$$y_T \sum \frac{1}{y_i} Y_i - \sum \frac{y_i}{y_i} Y_i = 0$$

$$\text{implies} \quad \sum \frac{y_T - y_i}{y_i} Y_i = 0$$

$$\sum Y_i = Y_T$$

Evaluating the summation, we have 3 equations in the 3 unknowns Y_R, Y_G, and Y_B.

$$\left(\frac{x_T - x_R}{y_R}\right) Y_R + \left(\frac{x_T - x_G}{y_G}\right) Y_G + \left(\frac{x_T - x_B}{y_B}\right) Y_B = 0$$

$$\left(\frac{y_T - y_B}{y_R}\right) Y_R + \left(\frac{y_T - y_G}{y_G}\right) Y_G + \left(\frac{y_T - y_B}{y_B}\right) Y_B = 0$$

$$1 \cdot Y_R + 1 \cdot Y_G + 1 \cdot Y_B = Y_T$$

Upon solving for Y_R, Y_G and Y_B and substituting the known values of the chromaticities one finds

$$Y_R = 32.04$$

$$Y_G = 57.09$$

$$Y_B = 10.86$$

APPENDIX II

ANALYTIC TRANSFORMATION OF A COVARIANCE MATRIX THROUGH A NON-LINEAR TRANSFORMATION BY LOCAL LINEAR APPROXIMATION

1. INTRODUCTION

Task 2 has a subtask on analysis of Landsat false color imagery. One of our needs in this area is a way to characterize the sensitivity of the image as a function of where one is in data space. As our representation of data space we have brightness, greenness and yellowstuff dimensions of the Tasselled-Cap transformed data space. As our representation of color space we have the 1976 CIE L*a*b* Uniform Color Space in which Euclidean distance is correlated to distinguishability between colors for the human eye. We wish to see what variation in data space corresponds to small variation about a given point in color space. We propose taking a regular sample of points in color space and considering a uniform, Gaussian probability distribution about each of them. In other words we associated with each sample point a mean vector, which is the coordinates of the point itself, and a diagonal covariance matrix.

$$\vec{r}_o = \begin{pmatrix} L_o^* \\ a_o^* \\ b_o^* \end{pmatrix} \qquad \mathrm{COV}(\vec{r}) = \begin{pmatrix} \sigma^2 & 0 & 0 \\ 0 & \sigma^2 & 0 \\ 0 & 0 & \sigma^2 \end{pmatrix}$$

The surfaces of equal probability density for this distribution are spheres about the point. If one transforms the distribution back to data space, and approximates the resulting distribution with Gaussian statistics, the new surfaces will not be spheres but ellipsoids. The shape and size of the ellipsoids will reflect how sensitive the image is to variation in that area of the data.

The transformation of points from color space to data space involves non-linear mappings. To transform the covariance matrix one must, in general, resort to approximation methods based on Taylor series expansions of the functions involved. Such an approximation scheme is accurate for small variation about a fixed point which is the kind of problem to be dealt with here. I have been working on this problem and have derived general formulas for the transformed mean vector and covariance matrix. I present them in this memo.

2. STATEMENT OF PROBLEM

Given --

1. Vector function $\vec{\psi}$

$$\vec{\psi}(\vec{x}) = \begin{pmatrix} \psi_1(x_1 x_2 \cdots x_N) \\ \vdots \\ \psi_N(x_1 x_2 \cdots x_N) \end{pmatrix}$$

2. on the random vector $\vec{x}$

$$\vec{x} = \begin{pmatrix} x_1 \\ \vdots \\ x_N \end{pmatrix}$$

3. distributed with

$$\text{mean } \vec{x}_o = \begin{pmatrix} x_{1_o} \\ \vdots \\ x_{N_o} \end{pmatrix} \quad \text{and COV } \vec{x} = \left(\text{COV}(x_i x_j)\right)_{NxN}$$

Find --

1. $E(\vec{\psi}(\vec{x}))$ the expected value of each component of $\vec{\psi}$ and
2. $\text{COV}(\vec{\psi}(\vec{x})) = \left(\text{COV}(\psi_i \psi_j)\right)_{NxN}$

the covariance matrix of the variables $\psi_1 \cdots \psi_N$

3. ANALYSIS

The approach to estimating $E(\vec{\psi})$ and $COV(\vec{\psi})$ will involve breaking the functions ψ_i down into their Taylor series about the point $\vec{x}_o$. In other words each function will be expressed in terms of its derivatives at the point $\vec{x}_o$ and powers of the variables $(x_1 - x_{1_o})$, ... $(x_N - x_{N_o})$. The statistical expectation operator $E(\ )$ can be applied to such a polynomial or product of polynomials in a straightforward way.

3.1 DEFINITIONS AND NOTATION

The expectation operator $E(\psi(x_1,x_2 \ldots x_N))$ is defined by the following equation:

$$E(\psi) = \int_{-\infty}^{\infty} \ldots \int \psi(x_1,x_2,\ldots x_N)\ p(x_1,x_2,\ldots x_N) dx_1 \ldots d_{x_N}$$

where p is the probability density of $\vec{x}$. Intuitively, if you take a large sample of vectors drawn at random from the distribution p and compute $\psi(\vec{x})$ for each the average will approach $E(\psi)$. $E(\psi)$ is the mean of the transformed distribution.

The covariance of two variables, x_i, x_j, is defined to be

$$COV(x_i x_j) = E[(x_i - x_{i_o})(x_j - x_{j_o})]$$

The Taylor series for a function, ψ, of 2 variables, μ, v, is as follows:

$$\psi(\mu,v) = \psi(\mu_o v_o) + \left[\frac{\partial\psi}{\partial\mu}(\mu - u_o) + \frac{\partial\psi}{\partial v}(v - v_o)\right]$$

$$+ \frac{1}{2!}\left[\frac{\partial^2\psi}{\partial\mu^2}(\mu - \mu_o)^2 + 2\frac{\partial^2\psi}{\partial v^2}(\mu - \mu_o)(v - v_o) + \frac{\partial^2\psi}{\partial v^2}(v - v_o)^2\right.$$

$$\left. + \ldots + \frac{1}{n!}\left[\frac{\partial^n\psi}{\partial\mu^n}(\mu - \mu_o)^n + \ldots\right] + \ldots,\right.$$

all derivatives being evaluated at (μ_o,v_o).

The general term of the series can be interpreted in terms of an n-th differential $d^n\psi$ of the function $\psi(\mu,v)$:

$$d^nF = \sum_{r=o}^{n} \binom{n}{r} \frac{\partial^n\psi}{\partial\mu^r\partial v^{n-r}} \Bigg|_{(\mu_o v_o)} (\mu - \mu_o)^r (v - v_o)^{n-r}$$

where $\binom{n}{r} = \frac{n!}{r!(n-r)!}$ are the coefficients of the binomial formula, appropriate to the expansion of $(a+b)^n$.

The series can now be more concisely written:

$$\psi(\mu,v) = \psi(\mu_o v_o) + d\psi + \frac{1}{2!} d^2\psi + \frac{1}{3!} d^3\psi + \ldots + \frac{1}{n!} d^n\psi + \ldots$$

If ψ is a function of 3 variables the coefficients of $d^n\psi$ are those appropriate to a trinomial expansion $(a+b+c)^n$ and so on for higher dimensions.

3.2 CALCULATION OF $E(\vec{\psi}(\vec{x}))$

Apply the expectation operator to the Taylor series for ψ_i:

$$E(\psi_i) = E(\psi_i(\vec{x}_o)) + E(d\psi) + \frac{1}{2!} E(d^2\psi) + \ldots$$

Evaluating the terms on the right:

$$E(\psi_i(\vec{x}_o)) = \psi_i(\vec{x}_o)$$

$$Ed\psi = E\left(\frac{\partial\psi_i}{\partial x_1}(x_1 - x_{1_o}) + \ldots + \frac{\partial\psi_i}{\partial x_N}(x_N - x_{N_o})\right)$$

$$= \frac{\partial\psi_i}{\partial x_1} E(x_1 - x_{1_o}) + \ldots \frac{\partial\psi_i}{\partial x_N} E(x_N - x_{N_o})$$

$$= 0$$

since the expected value of $x_i - x_{i_o}$ is zero.

Thus

$$E(\psi_i(\vec{x})) = \psi_i(\vec{x}_o) + \frac{1}{2!} E(d^2\psi_i) + \frac{1}{3!} E(d^3\psi) + \ldots$$

For 2 dimensions the second term is

$$E(d^2\psi_i) = E\left(\frac{\partial^2\psi_i}{\partial\mu^2}(\mu - \mu_o)^2 + 2\frac{\partial^2\psi_i}{\partial\mu\partial v}(\mu - \mu_o)(v - v_o) + \frac{\partial^2\psi_i}{\partial v^2}(v - v_o)^2\right)$$

$$= \frac{\partial^2\psi_i}{\partial\mu^2} COV(\mu^2) + 2\frac{\partial^2\psi_i}{\partial\mu\partial v} COV(\mu v) + \frac{\partial^2\psi_i}{\partial v^2} COV(v^2)$$

The covariances here are part of the given information. Calculating higher terms in the series necessitates calculating higher "moments of the distribution":

$$E(\mu - \mu_o)^p (v - v_o)^q.$$

If the distribution is normal, and has a diagonal covariance matrix, these moments may be evaluated from the moment generating function

$$m(t_1, t_2) = e^{\frac{1}{2}(\sigma_\mu^2 t_1 + \sigma_v^2 t_2)}$$

where $\sigma_\mu^2 = COV(\mu^2)$.

The moments are found by differentiation:

$$E(\mu - \mu_o)^p (v - v_o)^q = \left.\frac{\partial^{p+q} m}{\partial^p t_1 \partial^q t_2}\right|_{t_1=0, t_2=0}$$

(See Addendum I).

For a linear transformation

$$\begin{pmatrix} \psi_1 \\ \psi_2 \end{pmatrix} = A \begin{pmatrix} \mu \\ \nu \end{pmatrix}$$

where A is a constant coefficient matrix. In this case $d^n\psi = 0$ for $n \geq 2$. The exact expression for $E(\vec{\psi})$, in 2 dimensions, is then the following:

$$E(\psi_i) = \psi_i(\mu_o, \nu_o)$$

3.3. CALCULATION OF THE TRANSFORMED COVARIANCE MATRIX

By definition

$$COV(\psi_i\psi_j) \equiv E(\psi_i - E\psi_i)(\psi_j - E\psi_j)$$

It follows that

$$\begin{aligned} COV(\psi_i\psi_j) &= E(\psi_i\psi_j - \psi_i E\psi_j - \psi_j E\psi_i + E\psi_i E\psi_j) \\ &= E\psi_i\psi_j - E\psi_i E\psi_j - E\psi_i E\psi_j + E\psi_i E\psi j \\ &= E\psi_i\psi_j - E\psi_i E\psi_j. \end{aligned}$$

We will evaluate these last two terms, $E\psi_i\psi_j$ and $E\psi_i E\psi_j$, by multiplying power series, then subtract to arrive at $COV(\psi_i\psi_j)$.

$$\begin{aligned} \psi_i\psi_j = \psi_{i_o}\psi_{j_o} &+ (\psi_i\, d\psi_j + \psi_{j_o}\, d\psi_i) \\ &+ \frac{1}{2!}(\psi_i\, d^2\psi_j + \psi_{j_o}\, d^2\psi_i) \\ &+ d\psi_i d\psi_j + \ldots \end{aligned} \tag{1}$$

where ψ_{i_o} means $\psi_i(x_{1_o} \ldots x_{N_o})$.

$$E\psi_i\psi_j = \psi_{i_o}\psi_{j_o} + 0 + \frac{1}{2!}\left[E(\psi_{i_o} d^2\psi_j) + E(\psi_{j_o} d^2\psi_i)\right] + E(d\psi_i d\psi_j) + \ldots \tag{2}$$

$$E\psi_i E\psi_j = \psi_{i_o}\psi_{j_o} + \frac{1}{2!}\left[E(\psi_{i_o} d^2\psi_j) + E(\psi_{j_o} d^2\psi_i)\right] + \ldots$$

Subtracting

$$COV(\psi_i\psi_j) = E\psi_i\psi_j - E\psi_j E\psi_j = E(d\psi_i d\psi_j) + \ldots$$

This equation gives a first "linear" approximation to the covariance terms of the transformed variables. One can, it happens, write a matrix equation for the transformed covariance matrix in terms of the original covariance matrix, provided only this first term desired. To see this, rewrite the above equation along the following lines:

$$COV(\psi_i\psi_j) = E\left(\frac{\partial\psi_i}{\partial x_1}(x_1 - x_{1_o}) + \ldots + \frac{\partial\psi_i}{\partial x_N}(x_N - x_{N_o})\right) \times \left(\frac{\partial\psi_j}{\partial x_1}(x_1 - x_{1_o}) + \ldots + \frac{\partial\psi_j}{\partial x_N}(x_N - x_{N_o})\right)$$

$$COV(\psi_i\psi_j) = \left(\frac{\partial\psi_i}{\partial x_1}, \ldots, \frac{\partial\psi_i}{\partial x_N}\right) E \begin{pmatrix} x_1'^2 & x_1'x_2' \ldots x_1'x_N' \\ x_2'x_1' & x_2'^2 \ldots \\ \vdots & \vdots \\ x_N'x_1' & \cdot \end{pmatrix}_{NxN} \begin{pmatrix} \frac{\partial\psi_i}{\partial x_1} \\ \vdots \\ \frac{\partial\psi_i}{\partial x_N} \end{pmatrix}$$

where $x_1' = (x_1 - x_{1_o})$, etc.

The expression E $\left[(x_i' x_j')_{NxN}\right]$ appearing in this equation, is, by definition, the covariance matrix: $(\text{COV } x_i x_j)_{NxN}$. Each term of the transformed covariance matrix is formed from the original covariance matrix by the above equation. The entire covariance matrix, COV($\vec{\psi}$), can be written down thus:

$$\left(\text{COV } \psi_i \psi_j\right)_{NxN} = \begin{pmatrix} \frac{\partial \psi_1}{\partial x_1} & \cdots & \frac{\partial \psi_1}{\partial x_N} \\ \frac{\partial \psi_2}{\partial x_1} & \cdots & \vdots \\ \vdots & & \\ \frac{\partial \psi_N}{\partial x_1} & \cdots & \frac{\partial \psi_N}{\partial x_N} \end{pmatrix} \left(\text{COV}(x_i x_j)\right)_{NxN} \begin{pmatrix} \frac{\partial \psi_1}{\partial x_1} & \cdots & \frac{\partial \psi_N}{\partial x_1} \\ \frac{\partial \psi_1}{\partial x_2} & \cdots & \vdots \\ \vdots & & \\ \frac{\partial \psi_1}{\partial x_N} & \cdots & \frac{\partial \psi_N}{\partial \psi_N} \end{pmatrix}$$

The first matrix on the right is the Jacobian matrix of the transformation $\vec{\psi}(\vec{x})$. Denoting it J, the equation becomes:

$$\left(\text{COV } \psi_i \psi_j\right)_{NxN} = J \left(\text{COV } x_i x_j\right)_{NxN} J^T$$

If $\vec{\psi}$ is a linear transformation on $\vec{x}$ of the form $\vec{\psi} = A\vec{x}$, then J = A and

$$\left(\text{COV } \psi_i \psi_j\right)_{NxN} = A \left(\text{COV } x_i x_j\right)_{NxN} A^T$$

This expression is exact because the higher differentials of a linear transform are zero.

For a general, nonlinear transformation this degree of approximation may not be adequate. In particular, if $d\psi = 0$ at the point of evaluation the approximation obviously fails. In Addendum II the series approximation to COV $\psi_i \psi_j$ is reworked, retaining terms to fourth order in differentials of ψ.

ADDENDUM I

MOMENT GENERATING FUNCTION OF THE MULTIVARIATE NORMAL DISTRIBUTION

We will consider a bivariate distribution with zero mean for simplicity of notation but the results will have obvious generalization to N dimensions and arbitrary origin. The moment generating function of a distribution is defined by the following:

$$m(t_1,t_2) = E\, e^{(xt_1+yt_2)}$$

$$= \int_{-\infty}^{\infty}\int e^{(xt_1+yt_2)}\, p(x,y)\, dxdy$$

where $p(x,y)$ is the probability density function of distribution (and variables x and y have mean values of zero). Now, consider taking the partial of $m(t_1,t_2)$ with respect to t_1 and evaluating at $t_1 = t_2 = 0$:

$$\frac{\partial m(0,0)}{\partial t_1} = \int_{-\infty}^{\infty}\int x\, e^{o}\, p(x,y)\, dxdy$$

Since $e^{o} = 1$ this is just $E(x)$ - the first moment of x about zero. Any moment can be evaluated from this relation:

$$E(x^p y^q) = \frac{\partial^{p+q} m(0,0)}{\partial x^p \partial y^q}$$

Density of the bivariate normal distribution for independent random variables x and y is expressed as follows:

$$p(x,y) = \frac{1}{\sqrt{2\pi}\,\sigma_x}\ \frac{1}{\sqrt{2\pi}\,\sigma_y}\ e^{-\frac{1}{2}\left(\frac{x^2}{\sigma_x^2}+\frac{y^2}{\sigma_y^2}\right)}$$

where σ_x is the standard deviation of x.

Thus the moment generating function is evaluated from the following expression:

$$m(t_1,t_2) = \frac{1}{2\pi\sigma_x\sigma_y} \iint_{-\infty}^{\infty} e^{-\frac{1}{2}\left(\frac{x^2}{\sigma_x^2} - 2xt_1\right)} e^{-\frac{1}{2}\left(\frac{y^2}{\sigma_y^2} - 2yt_2\right)} dxdy$$

Complete the squares in the exponents:

$$m(t_1,t_2) = \frac{1}{2\pi\sigma_x\sigma_y} e^{\frac{1}{2}\left(\sigma_x^2 t_1^2 + \sigma_y^2 t_2^2\right)} \iint_{-\infty}^{\infty} e^{-\frac{1}{2}\left(\frac{x}{\sigma_x} - \sigma_x t_1\right)^2 - \frac{1}{2}\left(\frac{y}{\sigma_y} - \sigma_y t_2\right)^2} dxdy$$

Substitute

$$u = \frac{x}{\sigma_x} - \sigma_x t_1 \qquad v = \frac{y}{\sigma_y} - \sigma_y t$$

$$dx = \sigma_x\, du \qquad dy = \sigma_y\, dv$$

to arrive at this simplification:

$$m(t_1t_2) = \frac{1}{2\pi} e^{\frac{1}{2}\left(\sigma_x^2 t_1^2 + \sigma_y^2 t_2^2\right)} \iint_{-\infty}^{\infty} e^{-\frac{1}{2}\left(u^2 + v^2\right)} dudv$$

The integral here is known to have the value 2π. The moment generating function of bivariate normal distribution for independent random variables x,y is as stated:

$$m(t_1,t_2) = e^{\frac{1}{2}\left(\sigma_x^2 t_1^2 + \sigma_y^2 t_2^2\right)}$$

C-2

This may be generalized to N dimensions for correlated variables with arbitrary mean values:

$$m(\vec{t}) = e^{\vec{t}_o \cdot \vec{x}_o} e^{\frac{1}{2}\left(t_1^2\sigma_1^2 + 2t_1t_2\,\mathrm{COV}(x_1x_2) + \ldots + 2t_{N-1}t_N\mathrm{COV}(x_{N-1}x_N) + t_N^2\sigma_N^2\right)}$$

where $\vec{t} = (t_1, t_2 \ldots t_N)$, and $\vec{x}_o$ is the mean vector.

ADDENDUM II

FURTHER TERMS IN THE POWER SERIES FOR $COV(\psi_i\psi_j)$

To increase the accuracy of the approximation for $COV(\psi_i\psi_j)$ presented above, it is necessary to retain further terms of the power series. Note that if $d\psi = 0$ the first order approximation fails entirely. The following computations parallel those of the text in approximating

$$COV(\psi_i\psi_j) = E(\psi_i\psi_j) - E\psi_i E\psi_j$$

but retains terms through 4th partials of ψ.

$$\psi_i(x_1 \cdots x_n) \simeq \psi_{i_o} + d\psi_i + \frac{1}{2!} d^2\psi_i + \frac{1}{3!} d^3\psi_i + \frac{1}{4!} d^4\psi_i$$

$$\begin{aligned}
\psi_i\psi_j \simeq\ & \psi_{i_o}\psi_{j_o} + \left(\psi_{i_o} d\psi_j + \psi_{j_o} d\psi_i\right) \\
& + \frac{1}{2!}\left(\psi_{i_o} d^2\psi_j + \psi_{j_o} d^2\psi_i\right) \\
& + d\psi_i d\psi_j \\
& + \frac{1}{3!}\left(\psi_{i_o} d^3\psi_j + \psi_{j_o} d^3\psi_i\right) \\
& + \frac{1}{2!}\left(d\psi_i d^2\psi_j + d\psi_j d^2\psi_i\right) + \frac{1}{3!}\left(d\psi_i d^3\psi_i + d\psi_j d^3\psi_i\right) \\
& + \frac{1}{4!}\left(\psi_{i_o} d^4\psi_j + \psi_{j_o} d^4\psi_i\right) \\
& + \frac{1}{2!}\frac{1}{2!}\left(d^2\psi_i d^2\psi_j\right) \\
& + \frac{1}{4!}\left(d\psi_i d^4\psi_j + d\psi_j d^4\psi_i\right) \\
& + \frac{1}{2!3!}\left(d^2\psi_i d^3\psi_j + d^2\psi_j d^3\psi_i\right) \\
& + \frac{1}{2!4!}\left(d^2\psi_i d^4\psi_j + d^2\psi_j d^4\psi_i\right) \\
& + \frac{1}{3!3!}\left(d^3\psi_i d^3\psi_j\right) \\
& + \frac{1}{3!4!}\left(d^3\psi_i d^4\psi_j + d^3\psi_j d^4\psi_i\right) \\
& + \frac{1}{4!4!}\left(d^4\psi_i d^4\psi_j\right)
\end{aligned} \tag{1}$$

$$E\psi_i \simeq \psi_{i_o} + \frac{1}{2!} Ed^2\psi_i + \frac{1}{3!} Ed^3\psi_i + \frac{1}{4!} Ed^4\psi_i$$

$$\begin{aligned} E\psi_i E\psi_j \simeq \psi_{i_o}\psi_{j_o} &+ \frac{1}{2!}\left(\psi_{i_o} Ed^2\psi_j + \psi_{j_o} Ed^2\psi_i\right) \\ &+ \frac{1}{3!}\left(\psi_{i_o} Ed^3\psi_j + \psi_{j_o} Ed^3\psi_i\right) \\ &+ \frac{1}{4!}\left(\psi_{i_o} Ed^4\psi_j + \psi_{j_o} Ed^3\psi_i\right) \\ &+ \frac{1}{2!2!}\left(Ed^2\psi_i Ed^2\psi_j\right) \\ &+ \frac{1}{2!}\frac{1}{3!}\left(Ed^2\psi_i Ed^3\psi_j + Ed^2\psi_j Ed^3\psi_i\right) \\ &+ \frac{1}{3!3!}\left(Ed^3\psi_i Ed^3\psi_j\right) \\ &+ \frac{1}{2!4!}\left(Ed^2\psi_i Ed^4\psi_j + Ed^2\psi_j Ed^4\psi_i\right) \\ &+ \frac{1}{3!4!}\left(Ed^3\psi_i Ed^4\psi_j + Ed^3\psi_j Ed^4\psi_i\right) \\ &+ \frac{1}{4!4!}\left(Ed^4\psi_i Ed^4\psi_j\right) \end{aligned} \qquad (2)$$

Subtracting

$$E(\psi_i\psi_j) - E\psi_i E\psi_j \simeq E(d\psi_i d\psi_j)$$
$$+ \frac{1}{2!}\left[E\left(d\psi_i d^2\psi_j\right) + E\left(d\psi_j d^2\psi_i\right)\right]$$
$$+ \frac{1}{3!}\left[E\left(d\psi_i d^3\psi_j\right) + E\left(d\psi_j d^3\psi_i\right)\right]$$
$$+ \frac{1}{4!}\left[E\left(d\psi_i d^4\psi_j\right) + E\left(d\psi_j d^4\psi_i\right)\right]$$
$$+ \frac{1}{2!2!}\,\mathrm{COV}\left(d^2\psi_i d^2\psi_j\right)$$
$$+ \frac{1}{3!3!}\,\mathrm{COV}\left(d^3\psi_i d^3\psi_j\right)$$
$$+ \frac{1}{4!4!}\,\mathrm{COV}\left(d^4\psi_i d^4\psi_j\right)$$
$$+ \frac{1}{2!3!}\left[\mathrm{COV}\left(d^2\psi_i d^3\psi_j\right) + \mathrm{COV}\left(d^2\psi_j d^3\psi_i\right)\right]$$
$$+ \frac{1}{3!4!}\left[\mathrm{COV}\left(d^3\psi_i d^4\psi_j\right) + \mathrm{COV}\left(d^3\psi_j d^4\psi_i\right)\right]$$

where

$$\mathrm{COV}\left(d^2\psi_i d^2\psi_j\right) = E\left(d^2\psi_i d^2\psi_j\right) - Ed^2\psi_i Ed^2\psi_j$$

and so on. Evaluating the expression for $\mathrm{COV}(\psi_i\psi_j)$ requires knowledge of two things:

1. The partials of $\vec{\psi}$ through 4th order.
2. The moments of the distribution of $\vec{x}$ up to $E\left(x_1^4 \ldots x_N^4\right)$.

APPENDIX III

PROJECTION OF THE TASSELLED CAP HYPERPLANE INTO THE SUBSPACE OF CHANNELS 1, 2, AND 4

III.1 THE TASSELLED CAP PLANE [22]

Tasselled Cap 4-space is a simple rotation and translation of axes for the 4-space of Landsat data Channels 1, 2, 3 and 4. The new axes align with the principal components of variation found in Landsat agricultural data. The first two principal components together account for about 96% of the data variation within a typical scene which implies that the data lies primarily in a two-dimensional hyperplane of the data 4-space. This plane, referred to as the "Tasselled Cap Plane", has axes which bear the descriptive names of Brightness and Green. The third principal component accounts for most of the remaining variance. The average value of this component over a scene varies with the amount of haze through which the scene is viewed and it has the descriptive name of Yellowness. The remaining component accounts for only a fraction of a percent of the variance and bears the name Nonesuch.

The matrix representing the transformation to Tasselled Cap coordinates is as follows:

$$\begin{pmatrix} \text{Brightness} \\ \text{Greenness} \\ \text{Yellowness} \\ \text{Nonesuch} \end{pmatrix} = \begin{pmatrix} 0.33231 & 0.60316 & 0.67581 & 0.26278 \\ -0.28317 & -0.66006 & 0.57755 & 0.38833 \\ -0.89952 & 0.42830 & 0.07592 & -0.04080 \\ -0.01594 & 0.13068 & -0.45187 & 0.88232 \end{pmatrix} \begin{pmatrix} \text{CH1} \\ \text{CH2} \\ \text{CH3} \\ \text{CH4} \end{pmatrix} \quad (1)$$

III.2 THE BRIGHTNESS-GREENNESS PLANE IN THE SPACE OF CHANNELS 1, 2 AND 4

To reduce dimensionality from 4 to 3 we assign nonesuch the value of zero:*

$$-0.01594 \cdot CH1 + 0.13068 \cdot CH2 - 0.45187 \cdot CH3 + 0.88232 \cdot CH4 = 0 \quad (2)$$

This allows us to solve for Channel 3 in terms of the other channels so that it can be eliminated:

$$CH3 = (-0.01594 \cdot CH1 + 0.13068 \cdot CH2 + 0.88232 \cdot CH4)/0.45187 \quad (3)$$

We eliminate CH3 from the equation of Yellowness:

$$a_1 CH1 + a_2 CH2 + a_4 CH4 = \text{Yellowness} \quad (4)$$

where a_1, a_2 and a_4 represent the following values:

$$\begin{aligned} a_1 &= -0.89952 + 0.07592 \cdot (-0.01594/0.45187) \\ a_2 &= \ \ 0.42830 + 0.07592 \cdot (0.13068/0.45187) \\ a_4 &= -0.04080 + 0.07592 \cdot (0.88232/0.45187) \end{aligned} \quad (5)$$

For a given value of Yellowness the equation (4) provides the definition of a plane, in the space of Channels 1, 2 and 4, which corresponds to the Tasselled Cap hyperplane of Landsat 4-space. We will now establish the rotation of axes in Channels 1, 2 and 4 space which places two axes in this plane and one orthogonal to it.

The vector (a_1, a_2, a_4) is perpendicular to the plane. Thus it will represent one of our new axes and we will call it Channel 1 prime

*This condition is true, approximately, for all typical scenes.

(CH1'). We evaluate the vector and normalize its magnitude to unity thus:

$$\overrightarrow{CH1'} = \vec{a}/|\vec{a}| \tag{6}$$

$$\overrightarrow{CH1'} = (-0.90220,\ 0.45026,\ 0.10744)/\sqrt{0.9022^2 + 0.45026^2 + 0.10744^2} \tag{7}$$

$$\overrightarrow{CH1'} = (-0.88972,\ 0.44403,\ -0.10595) \tag{8}$$

We choose a second axis to be in the plane of Channels 1 and 2 (Channel 4 = 0) and perpendicular to CH1' (in the Tasselled Cap plane) and normalize to unity:

$$\overrightarrow{CH2'} = (0.44403,\ 0.88972,\ 0)/\sqrt{0.44403^2 + 0.88972^2} \tag{9}$$

$$\overrightarrow{CH2'} = (0.44655,\ 0.89476,\ 0) \tag{10}$$

Finally the third axis is chosen perpendicular to the first two:

$$\begin{aligned} \overrightarrow{CH4'} &= \overrightarrow{CH1'} \times \overrightarrow{CH2'} \\ \overrightarrow{CH4'} &= (0.09480,\ -0.04731,\ 0.99270) \end{aligned} \tag{11}$$

The complete transformation is written as follows:

$$\begin{pmatrix} CH1' \\ CH2' \\ CH4' \end{pmatrix} = \begin{pmatrix} -0.90220, & 0.45026, & 0.10744 \\ 0.44655, & 0.89476, & 0 \\ 0.09480, & -0.04731, & 0.99270 \end{pmatrix} \begin{pmatrix} CH1 \\ CH2 \\ CH4 \end{pmatrix} \tag{12}$$

With regard to this transformation we make the following observations:

1. CH1' is essentially the Yellowness component of the data (differing only by the factor of 1.014 introduced in normalization to unity).

2. CH2' lies in the plane of Channels 1 and 2 and forms an angle of about 26° within Channel 2.

3. CH4' is very nearly coincident with Channel 4.

4. This is all under the condition of Nonesuch = 0.

APPENDIX IV

POINTS OF L*, a*, b* UNIFORM COLOR SPACE WHICH CORRESPOND TO THE POINTS OF DATA SPACE SAMPLED FOR SENSITIVITY ANALYSIS

PRODUCT ONE

Biophase One (Figure 5)

Grid Point No.	L*	a*	b*
1	19.3	8.5	8.6
2	35.6	21.9	33.4
3	25.6	2.2	1.2
4	38.8	17.8	20.0
5	36.7	-6.3	-4.1
6	46.0	9.9	6.5
7	54.2	-16.3	-7.2
8	59.7	-2.2	-4.6
9	79.9	-28.0	-8.0
10	82.6	-17.1	-12.4

KRAUS PRODUCT

Biophase One (Figure 6)

Grid Point No.	L*	a*	b*
1	23.6	10.1	-0.9
2	42.5	25.1	29.5
3	28.2	5.0	-3.4
4	44.7	22.1	22.6
5	35.5	-2.0	-3.5
6	48.8	16.6	17.1
7	46.0	-10.9	-0.2
8	55.9	7.7	14.2
9	60.7	-21.4	6.9
10	67.3	-4.7	15.7
11	80.4	-33.6	18.7
12	84.2	-20.3	22.7

PRODUCT ONE

Biophase Two (Figure 8)

Grid Point No.	L*	a*	b*
1	14.8	0.1	-1.6
2	19.5	7.0	4.8
3	28.2	15.6	18.0
4	42.3	25.6	40.4
5	63.4	37.8	74.1
6	19.1	-3.1	-3.5
7	22.9	3.6	1.0
8	30.5	12.9	12.1
9	43.7	23.9	32.7
10	64.1	36.9	65.3
11	24.7	-6.7	-4.8
12	27.5	-0.4	-2.0
13	33.9	9.1	6.5
14	45.8	21.2	24.6
15	65.3	35.3	55.5
16	31.7	-10.6	-5.6
17	33.8	-5.1	-4.5
18	38.8	4.2	1.5
19	49.1	17.2	16.5
20	67.3	32.8	44.8
21	40.3	-14.8	-5.8
22	41.7	-10.2	-6.1
23	45.5	-1.6	-2.6
24	54.1	11.7	8.9
25	70.4	28.8	33.6
26	50.9	-19.7	-5.3
27	51.8	-15.7	-7.0
28	54.5	-8.2	-5.7
29	61.2	4.7	2.2
30	75.2	23.0	22.6

PRODUCT ONE

Biophase Two (Figure 8)
(Continued)

Grid Point No.	L*	a*	b*
31	63.6	-25.2	-4.1
32	64.1	-21.8	-7.0
33	65.9	-15.4	-7.7
34	70.9	-3.6	-3.2
35	82.5	15.0	12.2
36	79.0	-31.7	-2.0
37	79.1	-28.6	-6.0
38	80.2	-23.2	-8.5
39	83.8	-12.9	-7.1
40	92.8	4.9	3.3

KRAUS PRODUCT

Biophase Two (Figure 9)

Grid Point No.	L*	a*	b*
1	17.4	6.6	-5.8
2	23.6	12.9	3.8
3	33.5	20.5	19.8
4	47.9	29.5	43.4
5	19.7	4.2	-6.9
6	25.3	11.0	1.5
7	34.6	19.1	16.4
8	48.6	28.6	39.3
9	22.7	1.5	-7.5
10	27.5	8.4	-0.2
11	36.1	17.2	13.3
12	49.5	27.4	35.2
13	26.3	-1.6	-7.4
14	30.4	5.2	-1.4
15	38.1	14.5	10.7
16	50.8	25.6	31.2
17	30.7	-5.3	-6.5
18	34.1	1.4	-1.7
19	40.9	11.1	8.6
20	52.7	23.0	27.6
21	36.0	-9.3	-4.7
22	38.7	-3.0	-1.2
23	44.5	6.8	7.4
24	55.2	19.5	24.4
25	42.3	-13.7	-2.1
26	44.4	-8.0	0.2
27	49.2	1.5	7.2
28	58.6	15.0	22.0
29	49.7	-18.6	1.5
30	51.2	-13.4	3.0
31	55.1	-4.4	8.3
32	63.2	9.2	20.7

KRAUS PRODUCT

Biophase Two (Figure 9)
(Continued)

Grid Point No.	L*	a*	b*
33	58.3	-23.8	6.3
34	59.4	-19.4	6.9
35	62.4	-11.2	10.7
36	69.1	2.1	20.8
37	68.3	-29.6	12.3
38	69.0	-25.8	12.2
39	71.3	-18.6	14.7
40	76.7	-5.9	22.5
41	79.9	-36.0	19.7
42	80.3	-32.8	19.0
43	81.9	-26.6	20.3
44	86.1	-15.0	26.1

PRODUCT ONE

Biophase Three (Figure 11)

Grid Point No.	L*	a*	b*
1	20.3	4.1	-4.3
2	27.4	12.6	6.0
3	40.1	22.9	25.7
4	60.1	35.4	57.5
5	25.7	-0.7	-6.1
6	31.4	8.2	1.3
7	42.6	19.8	18.2
8	61.4	33.6	48.0
9	33.4	-6.6	-6.3
10	37.5	1.9	-1.6
11	46.8	14.7	11.6
12	63.9	30.3	38.1
13	43.7	-13.5	-4.3
14	46.4	-5.8	-2.3
15	53.5	7.0	6.8
16	68.1	24.6	28.9
17	57.1	-21.4	0.0
18	58.7	-15.1	-0.2
19	63.6	-3.1	4.9
20	75.3	15.5	21.6
21	74.3	-30.8	7.1
22	75.0	-25.7	5.0
23	78.1	-15.5	6.8
24	86.7	2.6	17.7

KRAUS PRODUCT

Biophase Three (Figure 12)

Grid Point No.	L*	a*	b*
1	17.0	6.0	-16.9
2	20.1	9.6	-12.3
3	24.8	14.0	-5.1
4	31.4	19.1	5.2
5	40.2	24.9	19.5
6	51.6	31.6	38.2
7	18.8	4.7	-18.0
8	21.7	8.3	-13.9
9	26.0	12.8	-7.3
10	32.3	18.1	2.5
11	40.8	24.2	16.3
12	52.1	31.2	34.7
13	20.9	3.1	-18.8
14	23.5	6.8	-15.3
15	27.5	11.4	-9.2
16	33.4	17.0	-0.0
17	41.7	23.3	13.2
18	52.7	30.5	31.1
19	23.3	1.3	-19.3
20	25.6	5.0	-16.3
21	29.2	9.7	-11.0
22	34.8	15.5	-2.4
23	42.7	22.2	10.1
24	53.4	29.7	27.5
25	26.0	-0.5	-19.6
26	28.0	2.9	-17.1
27	31.3	7.7	-12.4
28	36.4	13.7	-4.6
29	43.9	20.7	7.2
30	54.3	28.6	23.9

KRAUS PRODUCT

Biophase Three (Figure 12)
(Continued)

Grid Point No.	L*	a*	b*
31	29.1	-2.7	-19.5
32	30.9	0.6	-17.5
33	33.8	5.4	-13.5
34	38.5	11.6	-6.5
35	45.5	18.9	4.4
36	55.4	27.2	20.4
37	32.7	-5.1	-19.0
38	34.1	-1.8	-17.5
39	36.7	2.8	-14.2
40	40.9	9.0	-8.0
41	47.4	16.6	2.0
42	56.9	25.4	17.1
43	36.6	-7.6	-18.2
44	37.9	-4.6	-17.1
45	40.1	-0.0	-14.4
46	43.8	6.1	-9.1
47	49.8	13.9	-0.0
48	58.7	23.1	14.0
49	41.1	-10.4	-16.9
50	42.1	-7.6	-16.3
51	44.0	-3.3	-14.2
52	47.3	2.7	-9.7
53	52.6	10.7	-1.6
54	60.9	20.4	11.2
55	46.0	-13.4	-15.2
56	46.9	-10.8	-15.0
57	48.4	-6.8	-13.4
58	51.3	-0.9	-9.7
59	56.1	7.0	-2.7
60	63.6	17.0	8.9

KRAUS PRODUCT

Biophase Three (Figure 12)
(Concluded)

Grid Point No.	L*	a*	b*
61	51.6	-16.7	-13.0
62	52.2	-14.3	-13.1
63	53.5	-10.5	-12.1
64	55.9	-4.9	-9.2
65	60.1	2.8	-3.2
66	67.0	13.0	7.1
67	57.7	-20.3	-10.3
68	58.2	-18.0	-10.7
69	59.3	-14.6	-10.1
70	61.3	-9.3	-7.9
71	64.9	-1.7	-3.0
72	71.0	8.4	6.0
73	64.6	-24.1	-6.9
74	64.9	-22.1	-7.6
75	65.7	-18.9	-7.5
76	67.4	-14.1	-6.0
77	70.5	-6.8	-2.0
78	75.8	3.2	5.7
79	72.1	-28.2	-2.9
80	72.3	-26.4	-3.9
81	72.9	-23.5	-4.2
82	74.3	-19.1	-3.3
83	76.9	-12.3	-0.2
84	81.5	-2.5	6.2
85	80.5	-32.8	1.6
86	80.6	-31.1	0.4
87	81.0	-28.5	-0.1
88	82.1	-24.5	0.2
89	84.2	-18.2	2.4
90	88.1	-8.9	7.7

PRODUCT ONE

Biophase Four (Figure 14)

Grid Point No.	L*	a*	b*
1	13.7	3.2	1.3
2	15.3	1.7	-0.2
3	19.4	7.3	5.9
4	26.0	13.9	16.3
5	35.8	21.4	32.2
6	49.5	30.0	54.4
7	17.3	0.1	-1.6
8	21.0	5.0	3.7
9	27.1	12.5	13.3
10	36.5	20.4	28.5
11	49.9	29.3	50.3
12	19.6	-1.6	-2.9
13	22.8	3.8	1.6
14	28.5	10.9	10.4
15	37.5	19.2	24.7
16	50.5	28.5	45.9
17	22.2	-3.4	-4.1
18	25.0	1.8	-0.2
19	30.2	9.0	7.5
20	38.7	17.7	20.9
21	51.3	27.5	41.2
22	25.2	-5.3	-5.1
23	27.6	-0.3	-2.0
24	32.3	6.9	4.7
25	40.2	15.9	17.0
26	52.3	26.2	36.5
27	28.5	-7.3	-6.1
28	30.7	-2.6	-3.6
29	34.8	4.5	2.1
30	42.1	13.7	13.2
31	53.6	24.6	31.6
32	32.3	-9.4	-6.9
33	34.1	-5.0	-5.1
34	37.8	1.8	-0.3
35	44.4	11.2	9.5
36	55.2	22.6	26.7
37	36.6	-11.5	-7.6
38	38.1	-7.5	-6.4

PRODUCT ONE

Biophase Four (Figure 14)
(Continued)

Grid Point No.	L*	a*	b*
39	41.2	-1.0	-2.5
40	47.2	8.3	6.0
41	57.3	20.1	21.7
42	41.3	-13.8	-8.2
43	42.6	-10.1	-7.6
44	45.3	-4.0	-4.5
45	50.5	5.1	2.7
46	59.8	17.2	16.9
47	46.5	-16.1	-8.6
48	47.6	-12.8	-8.5
49	49.9	-7.2	-6.4
50	54.5	1.6	-0.3
51	62.9	13.9	12.2
52	52.3	-18.6	-9.0
53	53.2	-15.6	-9.4
54	55.1	-10.5	-8.0
55	59.1	-2.1	-3.1
56	66.6	10.0	7.7
57	58.7	-21.3	-9.2
58	59.4	-18.6	-10.0
59	61.0	-13.9	-9.4
60	64.4	-6.1	-5.7
61	71.1	5.8	3.5
62	65.8	-24.2	-9.3
63	66.3	-21.7	-10.6
64	67.6	-17.4	-10.6
65	70.5	-10.2	-7.9
66	76.3	1.1	-0.3
67	73.6	-27.3	-9.2
68	74.0	-25.0	-10.9
69	75.0	-21.1	-11.5
70	77.5	-14.6	-9.9
71	82.5	-3.8	-3.8
72	82.2	-30.6	-9.0
73	82.4	-28.5	-11.1
74	83.3	-25.0	-12.3
75	85.3	-19.1	-11.6
76	89.6	-9.0	-7.0

KRAUS PRODUCT

Biophase Four (Figure 15)

Grid Point No.	L*	a*	b*
1	15.3	5.3	-6.8
2	18.5	9.0	-1.9
3	16.8	3.8	-7.4
4	19.8	7.6	-3.0
5	24.0	12.1	3.6
6	29.9	17.1	13.1
7	37.7	22.7	25.7
8	47.5	28.9	41.9
9	59.9	35.9	62.2
10	18.5	2.2	-7.8
11	21.2	6.1	-3.9
12	25.2	10.7	2.2
13	30.8	16.0	11.2
14	38.3	21.8	23.4
15	48.0	28.2	39.3
16	60.2	35.5	59.3
17	20.5	0.4	-8.0
18	23.0	4.3	-4.5
19	26.6	9.0	1.1
20	31.9	14.6	9.4
21	39.1	20.7	21.1
22	48.6	27.4	36.6
23	60.6	34.9	56.4
24	22.9	-1.5	-7.8
25	25.0	2.2	-4.8
26	28.3	7.1	0.1
27	33.3	12.9	7.9
28	40.2	19.3	19.0
29	49.3	26.4	34.0
30	61.2	34.2	53.4
31	25.5	-3.7	-7.3
32	27.3	-0.0	-4.8
33	30.4	4.9	-0.4
34	34.9	10.8	6.6
35	41.4	17.6	17.1

KRAUS PRODUCT

Biophase Four (Figure 15)
(Continued)

Grid Point No.	L*	a*	b*
36	50.3	25.0	31.5
37	61.8	33.2	50.4
38	28.5	-6.0	-6.5
39	30.1	-2.4	-4.5
40	32.7	2.3	-0.6
41	36.9	8.4	5.7
42	43.0	15.5	15.4
43	51.5	23.4	29.1
44	62.7	31.9	47.5
45	31.8	-8.5	-5.4
46	33.2	-5.1	-3.7
47	35.5	-0.4	-0.5
48	39.3	5.7	5.1
49	44.9	13.1	14.0
50	52.9	21.3	26.9
51	63.8	30.4	44.6
52	35.6	-11.2	-3.8
53	36.7	-8.0	-2.6
54	38.7	-3.4	0.0
55	42.1	2.6	4.9
56	47.2	10.1	13.0
57	54.7	18.8	25.0
58	65.1	28.4	41.9
59	39.7	-14.0	-1.9
60	40.7	-11.1	-1.0
61	42.4	-6.8	1.1
62	45.3	-0.8	5.3
63	50.0	6.8	12.4
64	56.9	15.8	23.5
65	66.8	25.9	39.5
66	44.4	-17.0	0.4
67	45.2	-14.3	1.0
68	46.6	-10.3	2.6
69	49.1	-4.5	6.1
70	53.3	3.0	12.4

KRAUS PRODUCT

Biophase Four (Figure 15)
(Concluded)

Grid Point No.	L*	a*	b*
71	59.6	12.3	22.4
72	68.9	22.9	37.4
73	49.6	-20.2	3.3
74	50.2	-17.7	3.5
75	51.3	-14.0	4.7
76	53.5	-8.6	7.6
77	57.1	-1.1	12.9
78	62.9	8.3	21.9
79	71.5	19.3	35.7
80	55.3	-23.5	6.6
81	55.7	-21.3	6.5
82	56.7	-18.0	7.3
83	58.5	-12.9	9.6
84	61.6	-5.7	14.1
85	66.7	3.6	22.0
86	74.6	15.1	34.5
87	61.6	-27.1	10.4
88	61.9	-25.2	10.1
89	62.6	-22.1	10.6
90	64.1	-17.5	12.3
91	66.8	-10.7	16.0
92	71.3	-1.4	22.8
93	78.4	10.2	34.0
94	68.5	-31.0	14.8
95	68.7	-29.2	14.3
96	69.2	-26.5	14.4
97	80.4	-22.3	15.6
98	72.7	-15.9	18.5
99	76.6	-7.0	24.3
100	82.9	4.6	34.3

MEMO TO: Richard Juday, JSC

FROM: Ron Balon

SUBJECT: Comparison of our Respective Analysis on Sensitivity of Image Products.

APPENDIX V

COMPARISON OF THE AUTHORS' SENSITIVITY DISPALY METHOD WITH A METHOD DEVELOPED BY RICHARD JUDAY OF JSC

1.0 INTRODUCTION

Last quarter, under ERIM's task on analysis of False Color Image Products, Ric Cicone and myself developed a technique for graphic display of image product sensitivity. This work was similar in many respects to work on assessment of image sensitivity which you have been carrying out. The purpose of this memo is to compare the two techniques. The aims of the comparison will be, 1) to establish whether they are producing consistent results, (if they were not, we would have to re-assess the accuracy of the implementation of the techniques) and 2) to assist your understanding of our technique and the insights it provides.

2.0 COMPARISON OF A SPECIFIC EXAMPLE

We received an explanation of your approach to image sensitivity assessment in your letter of January 17, 1978. The technique described involves computing the change in color units, Δc, corresponding to a small motion in data space, $|\delta|$, and using the ratio $\Delta c/|\delta|$ as a measure of sensitivity. Motions were sampled in two directions to correspond to changes in Brightness and Greeness (in the Kauth coordinate system) within the plane of data concentration for a particular acquisition.

During the last quarterly SR&T review Ric Cicone received samples of your work. They are the graphs presented in Fig. 1 and 2. We understand the graphs were created by computing the sensitivity measure $\Delta\, \dot{c}/|\delta|$ for a fine grid of points in the Tasselled Cap plane and then connecting the points into "iso-sensitivity" lines.

To compare techniques, I generated a sensitivity ellipse plot according to our technique, using the same bias and scale values given for your example and the same values of YELLOWNESS and NONESUCH. Our usual method is to display sensitivity in a "CH2' to CH4'" plane. This is the hyperplane of the Tasselled Cap projected into the three dimensional space of CH1, CH2, CH4. For this comparison, however, we transformed results to the Tasselled Cap, Brightness and Greeness

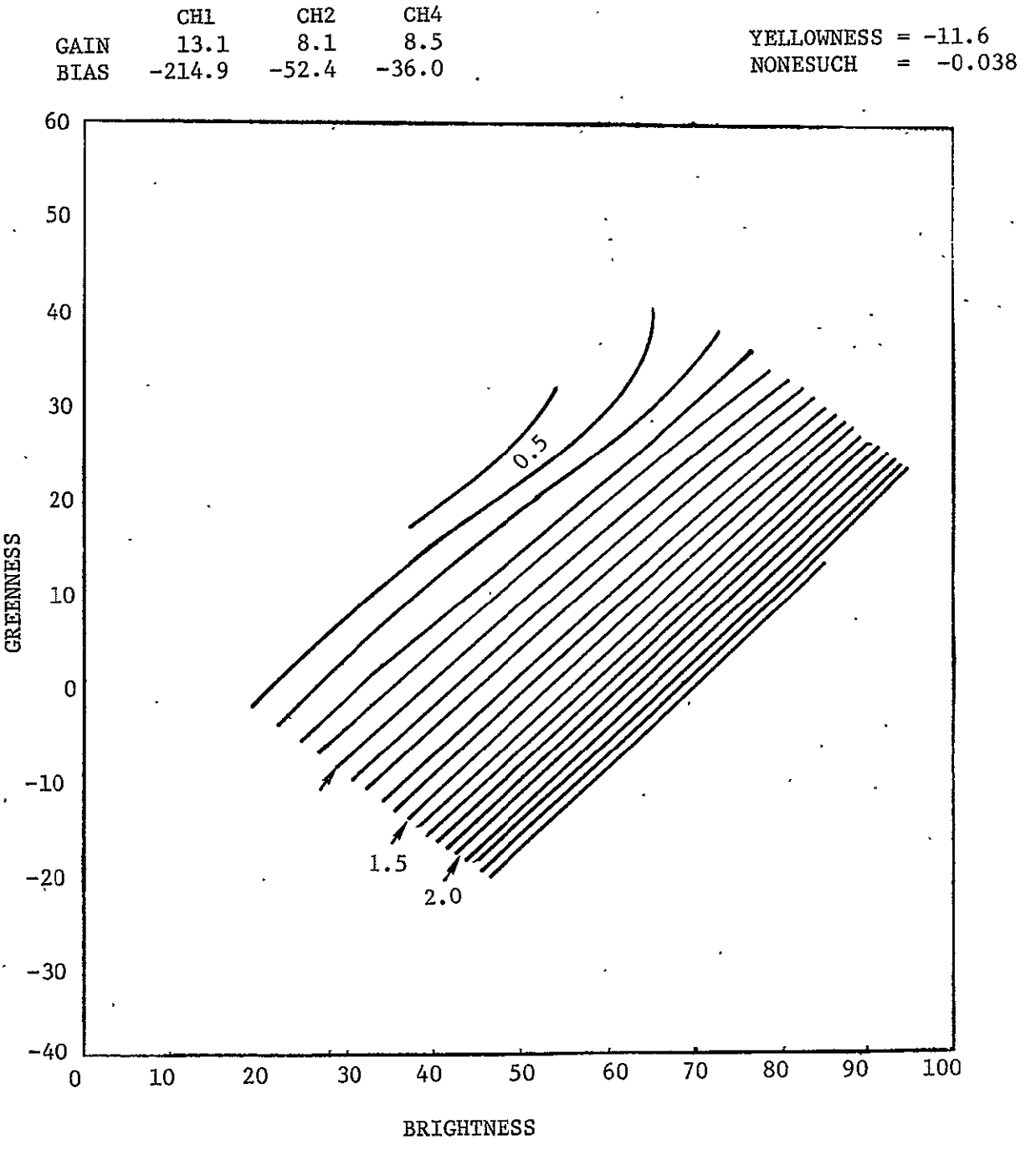

FIGURE 1. PRODUCT ONE BRIGHTNESS SENSITIVITY AFTER RICHARD JUDAY

	CH1	CH2	CH4
GAIN	13.1	8.1	8.5
BIAS	-214.9	-52.4	-36.0

YELLOWNESS = -11.6
NONESUCH = -0.038

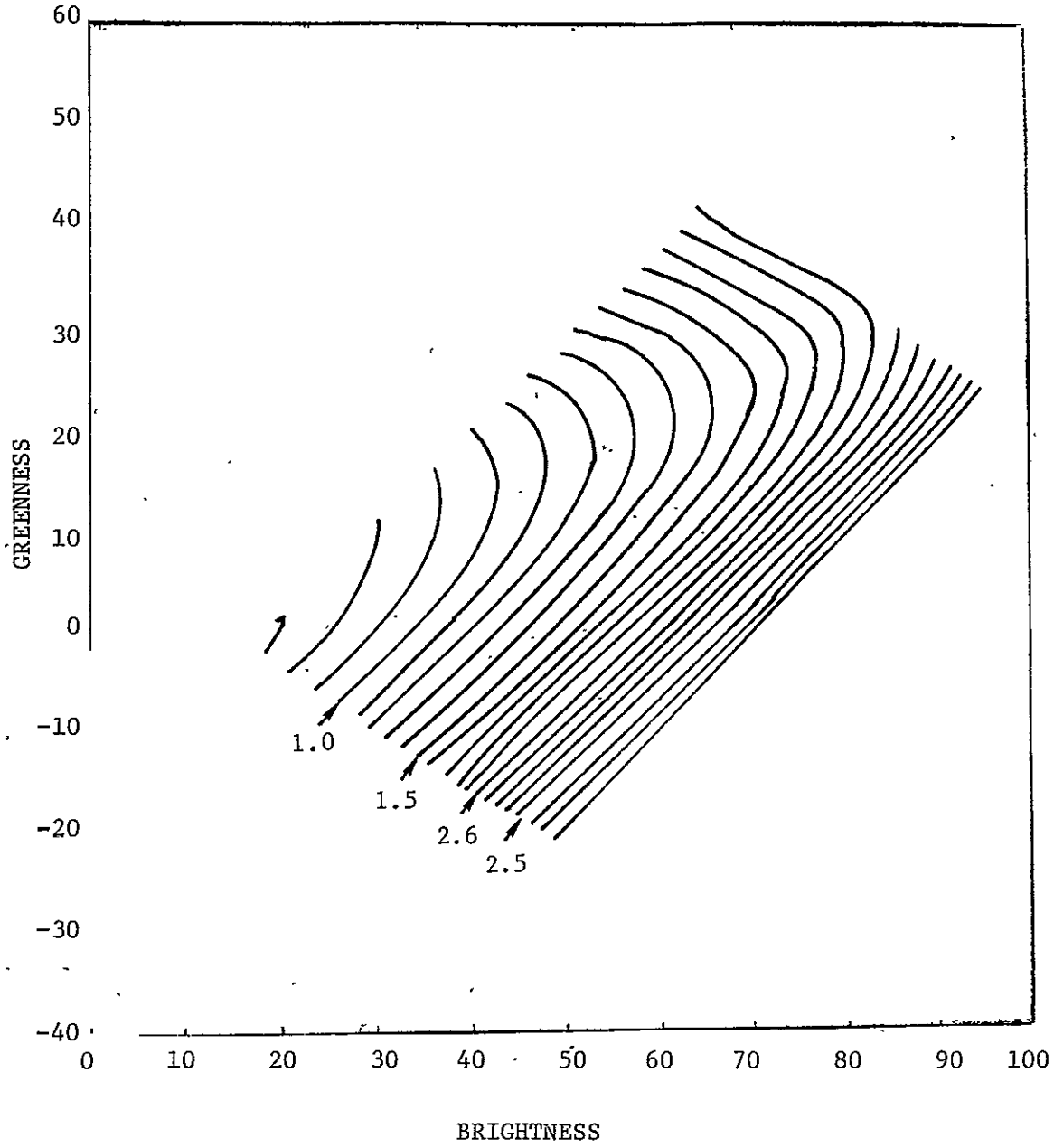

FIGURE 2. PRODUCT ONE GREENNESS SENSITIVITY AFTER RICHARD JUDAY

coordinates as you have been using them.

Our sensitivity display technique involves setting up a symmetrical (spherical) statistical distribution about a point in color space and then mapping the point and its distribution into data space. We arrange that the one standard deviation surface of the distribution represents a distance of one perceptible step in color space. Based on some examination of images for which field average color coordinates have been computed, we estimate the perceptible step to be about 5 units and use $\sigma = 5$.* The initially spherical distribution will become distorted in following the shear introduced by the transformation.

Interpretation of the displayed ellipses is straightforward. The boundary of the ellipse represents how far one must move, in a given direction, away from the given data point before a perceptible color difference will occur. For our display we take a uniform sample of points from the plane of data concentration, transform them to color space and then perform the inverse transformation of each point with the ball of radius five placed, around it. The shapes and sizes of the resulting ellipses in data space show directly how the space is broken up into colors.

The sensitivity ellipse plot produced for comparison is shown in Figure 3. Explanation of the characteristic pattern of shapes of these ellipses is easier in CH2' to CH4' space. I will therefore not deal with the question in this context, but will proceed with the comparison of results.

The information shown in the Brightness and Greeness iso-sensitivity graphs is contained within the sensitivity ellipse plot and can be extracted from it. The ellipse boundaries give sensitivity information in all directions. For comparison we are interested in looking more closely at the directions of Brightness and Greenness. Figure 4 shows the sensitivity ellipse plot with two vectors drawn from the center of each ellipse. One vector is parallel to the Greenness dimension and one is parallel to Brightness. The length of the vector corresponds to the $|\delta|$, motion in data space, in the sensitivity formula $\Delta c/|\delta|$. The quantity Δc, in this case, is the constant 5.

---

* The field average color coordinates were computed assuming 16-level quanitization by the PFC. Thus, this factor was empirically taken into account in estimating a perceptible step to be 5 UCS units.

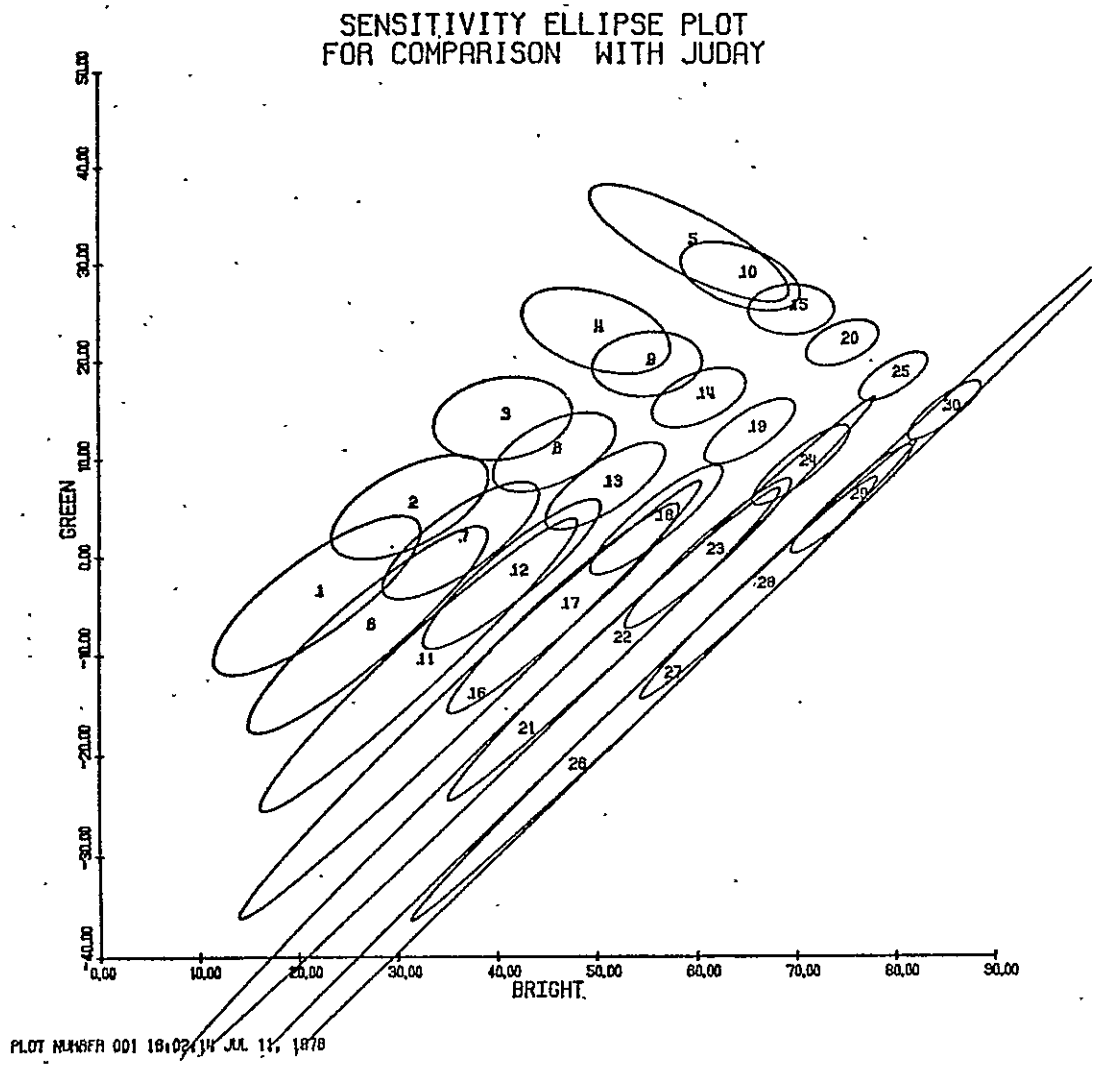

FIGURE 3. SENSITIVITY ELLIPSE PLOT FOR COMPARISON WITH JUDAY

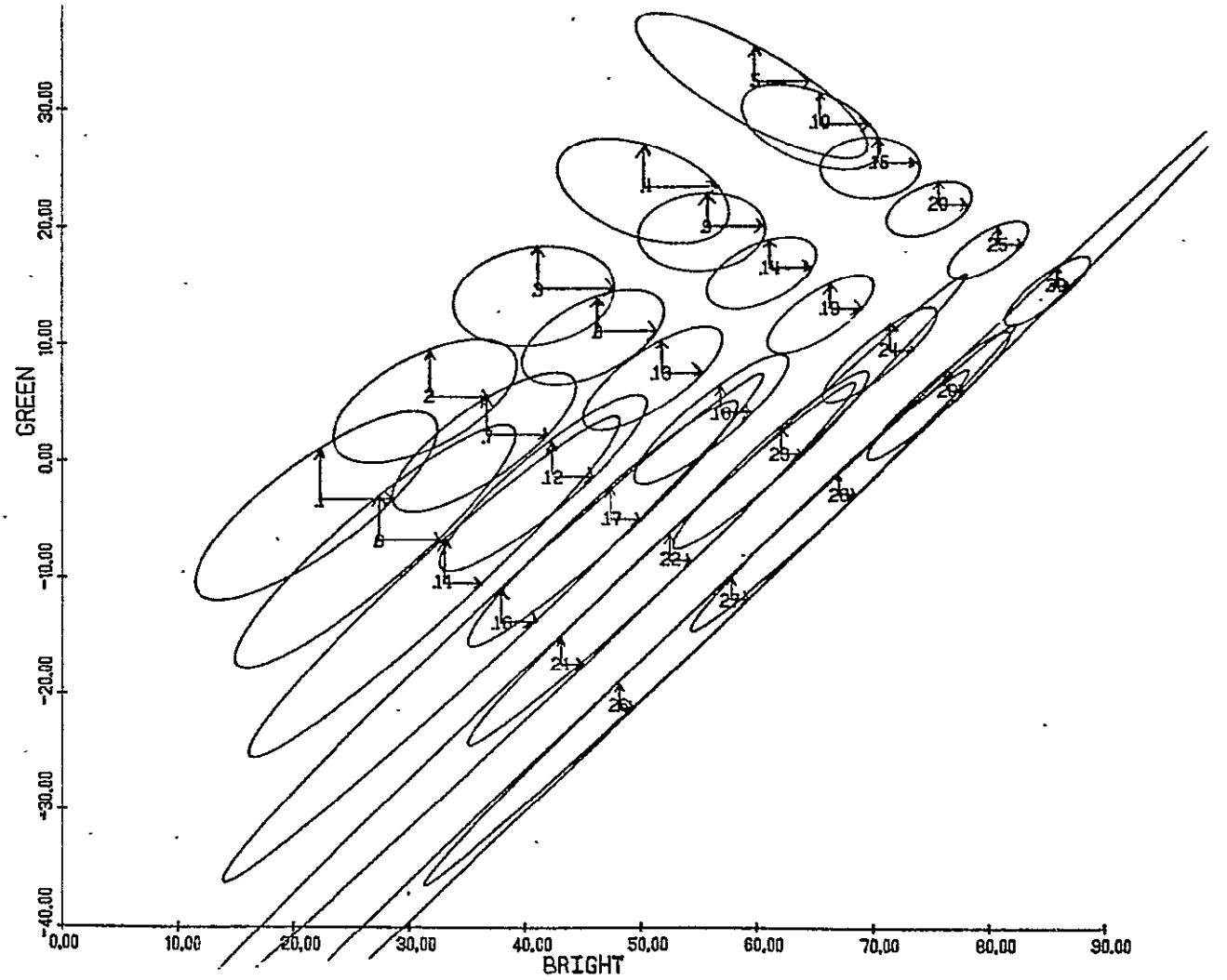

FIGURE 4. BRIGHTNESS AND GREENNESS DISPLACEMENT VECTORS WITHIN SENSITIVITY ELLIPSES

We can form iso-sensitivity lines by connecting points with roughly the same length vector in the Brightness or Greenness direction. Figure 5 shows the result for Brightness and Figure 6 for Greenness. Indicated alongside each iso-sensitivity line is the quantity $5/|\delta|$. Thus from the sensitivity ellipses we have derived rough equivalents to Brightness and Greenness sensitivity measures and iso-sensitivity lines.

We are now in a position to compare results. Comparing the derived results, Figures 5 and 6, with the calculated results of your example, Figures 1 and 2,we note a strong similarity in the pattern of the iso-lines. In the Brightness sensitivity plots the lines are nearly straight and cross parallel, lengthwise across the range. In the Greenness plot the lines bend. The actual magnitude of the sensitivity, $5/|\delta|$, agrees with the calculated $\Delta c/|\delta|$, at least as well as one would expect in this rough comparison. Note that the variation in sensitivity follows the same patterns in both sets of results. We conclude the two sets of results are consistent with each other.

3.0 COMMENT ON THE PATTERN OF SENSITIVITY ELLIPSE SHAPES

The pattern of sensitivity ellipses observed in Figure 3 may be elucidated by consideration of the nature of the transformation from data to perception space. This transformation involves two non-linear steps. If the transformation were entirely linear, the shapes of the ellipses would all be identical (not necessarily round though). The non-linearities cause the shapes to migrate in a characteristic way, as will be explained below.

The appropriate space to work in when attempting to understand the pattern of ellipses is what I have referred to as CH2' to CH4' space. The three dimensions CH1',CH2', CH4' are simply a rotation of CH1, CH2, CH4 space which is the data space used to produce Product One and Kraus imagery. The rotation was arranged so that CH2'and CH4'together span the plane which represents the projection of the Tasselled Cap hyperplane into the subspace of CH1,CH2, CH4 The transformation is as follows:

$$\begin{pmatrix} CH1' \\ CH2' \\ CH4' \end{pmatrix} = \begin{pmatrix} .88972 & -.4403 & -.10595 \\ .44655 & .89476 & 0 \\ .09480 & -.04731 & .99270 \end{pmatrix} \begin{pmatrix} CH1 \\ CH2 \\ CH4 \end{pmatrix}$$

The restriction was made that CH2' should be the intersection of the projected Tasselled Cap plane with the CH1, CH2 plane. Then CH4' was taken perpendicular to CH2' and in the projected Tasselled Cap plane. It turns out that CH2' lies at an angle of 26 1/2° from

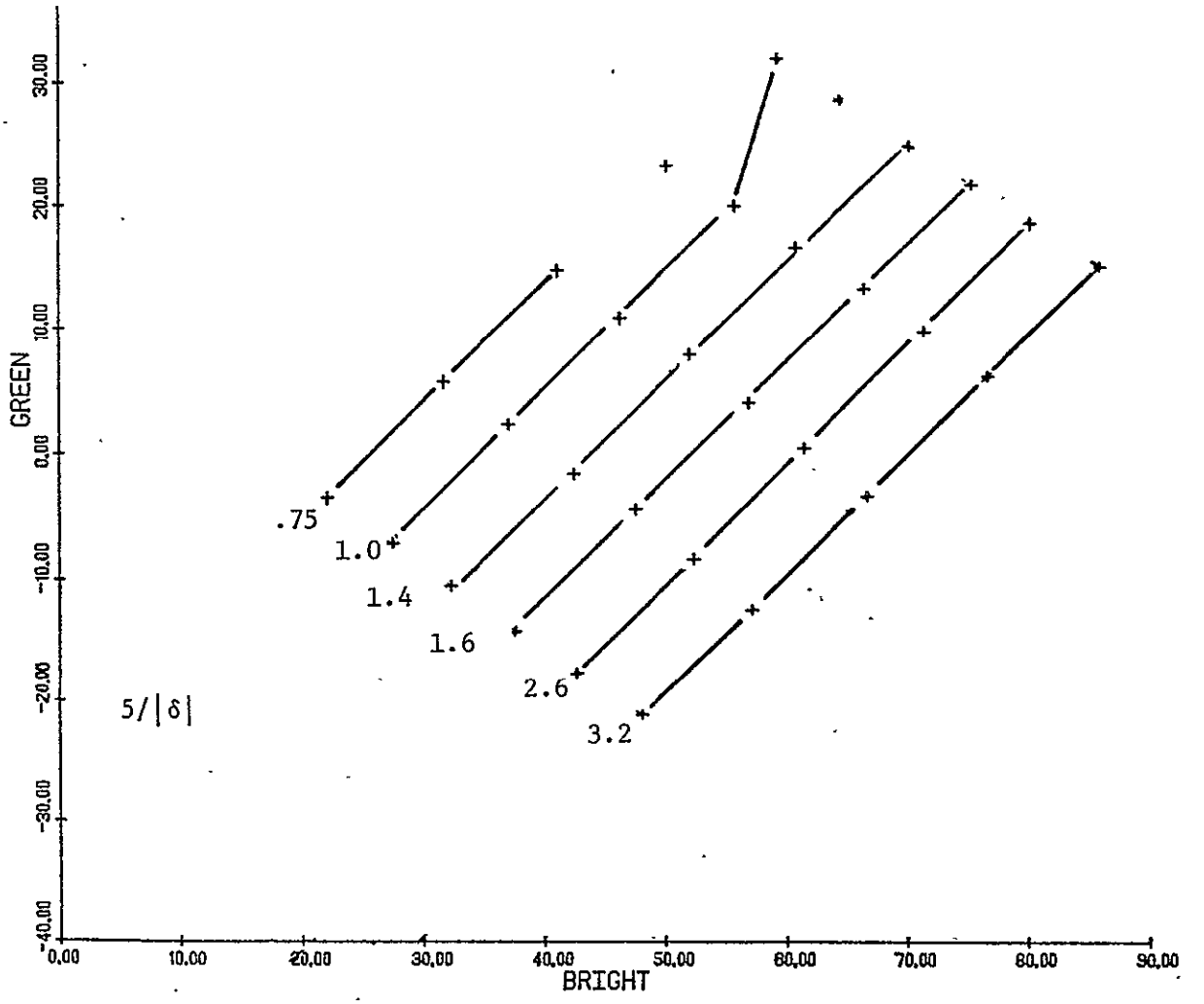

FIGURE 5. BRIGHTNESS ISO-SENSITIVITY LINES
DERIVED FROM SENSITIVITY ELLIPSES

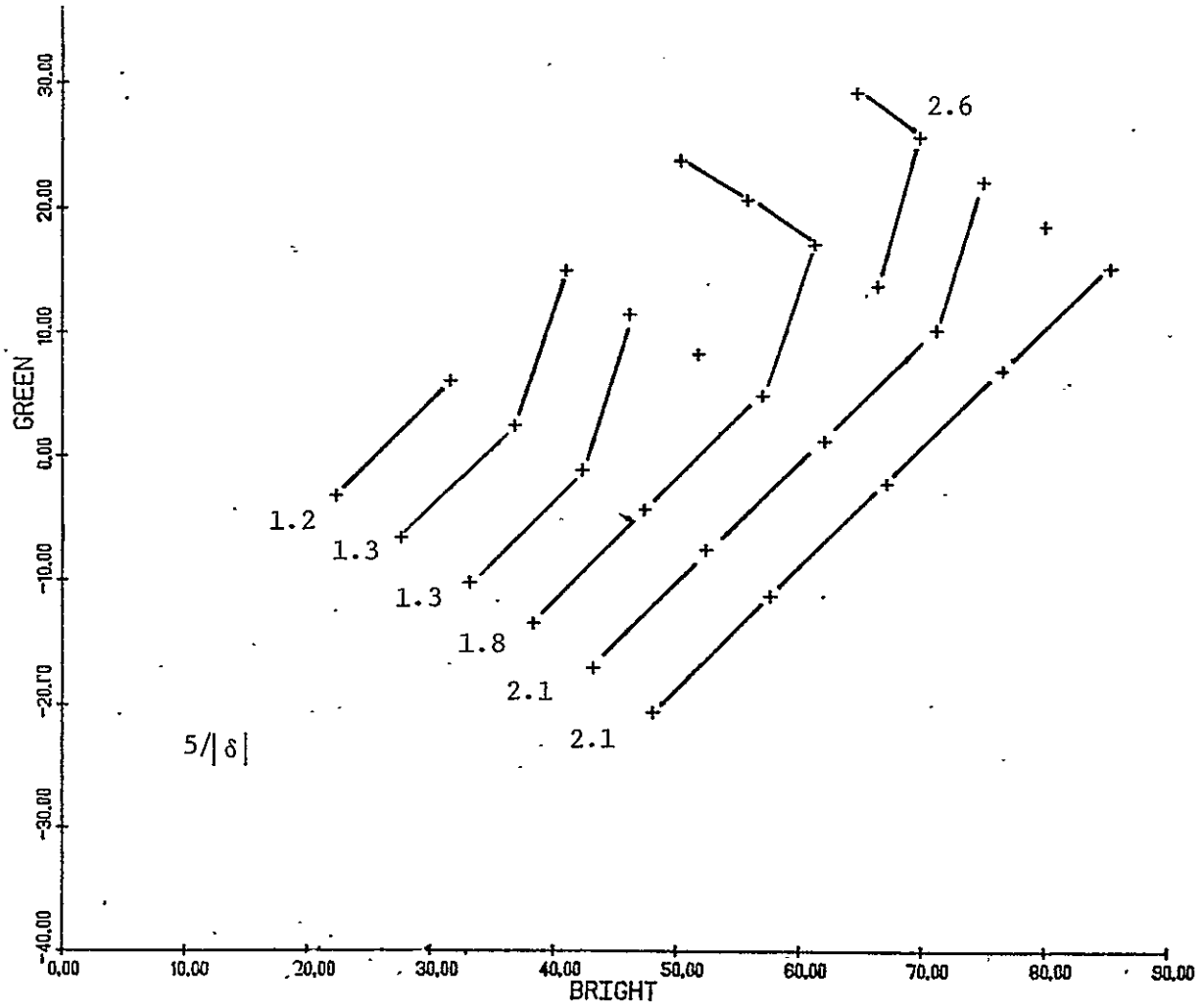

FIGURE 6. GREENNESS ISO-SENSITIVITY LINES
DERIVED FROM SENSITIVITY ELLIPSES

CH2, and CH4' is very nearly coincident with CH4. CH1' is perpendicular to the projected Tasselled Cap Plane. As you might guess, CH1' closely resembles the Kauth YELLOWNESS coordinate. In primed space we can look at the plane of data concentration while still seeing the channels which drive the primaries. CH4' drives the red primary while CH2' drives the other two.

Let us look at the pattern of sensitivity ellipses in primed space. Figure 7 shows a sensitivity plot in primed space for the set of Product One bias and scale values used in your example. Observe the pattern of ellipses along the bottom row only (CH4' = 6). They appear as follows:

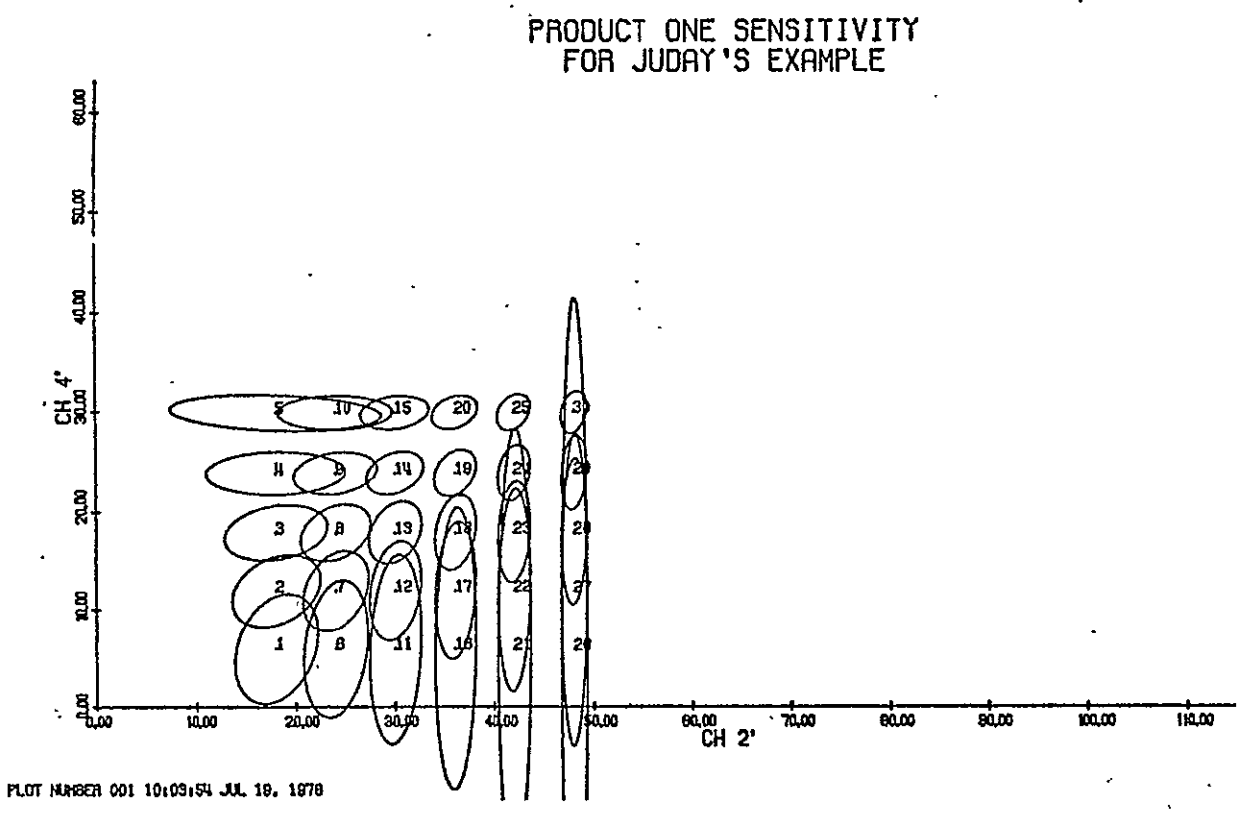

FIGURE 7. PRODUCT ONE SENSITIVITY IN CH2' TO CH4' PLANE FOR JUDAY'S EXAMPLE

The migration of shapes is due to the non-linearities of the data to perception space mapping. One non-linearity is in the transformation from input exposure control level (gun counts) to film transmission. The relationship is exponential. This emphasizes greatly points near the high end of the range. This is illustrated in Figure 7 by a narrowing of ellipses toward the upper range of CH2' values. This is the effect which you have termed chromaticity jamming in previous work.

The second non-linearity occurs in the transformation to Uniform Color Space. The UCS transformation involves cube roots. The effect, in terms of sensitivity, is counter to the exponential transformation. Sensitivity becomes greater near the low end of the scale of activation rather than the high end. We can illustrate this by removing the first non-linearity. We make an appropriate alteration of the mathematics of the model in order to simulate linear transmission control rather than exponential control. We can then see the effect of the UCS transformation in isolation. The resulting sensitivity ellipse plot is shown in Figure 9. This figure shows the eye's response to linear changes in stimulus. Note that sensitivity to change increases as the size of the stimulus decreases, i.e., as you move downward in CH2' and/or CH4'.

Referring back to the original model (Figure 8) this accounts for the growth of the ellipses in the CH4' direction as CH2' increases. The blue and green guns on the high part of the exponential curve swamp the red gun on the low part, making changes in CH4' invisible. Analogous reasoning applies to low CH2' values, i.e., the left-hand edge of Fig. 7. Here the effects are somewhat less pronounced because there are two primaries vieing for attention against the single red primary.

4.0 COMMENTS

Interpretation of sensitivity measurement values in the Brightness and Greeness directions can be misleading. Since the Tasselled Cap transformation rotates the CH2' to CH4' axes by about 45° the effects of the nonlinearites described above will be largely obscured. Examination of Figure 4 shows that sampling sensitivity in Brightness and Greenness does not give a complete picture of image sensitivity. Sensitivity ellipse plots of the kind used in this memo are readily produced. We would be happy to produce plots for any sets of bias and scale values you wish to examine.

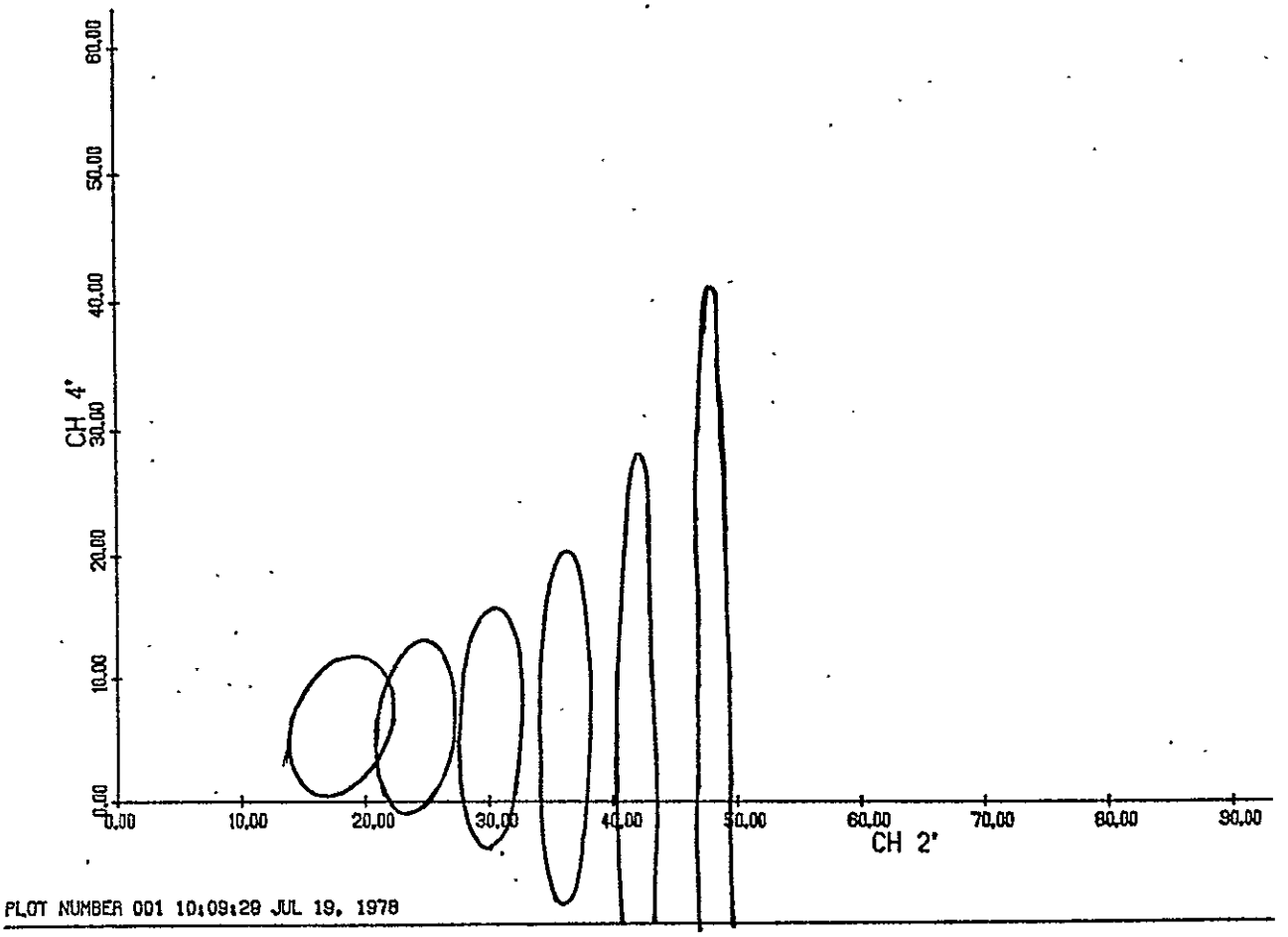

FIGURE 8. ELLIPSES AT LOW ACTIVATION OF RED PRIMARY

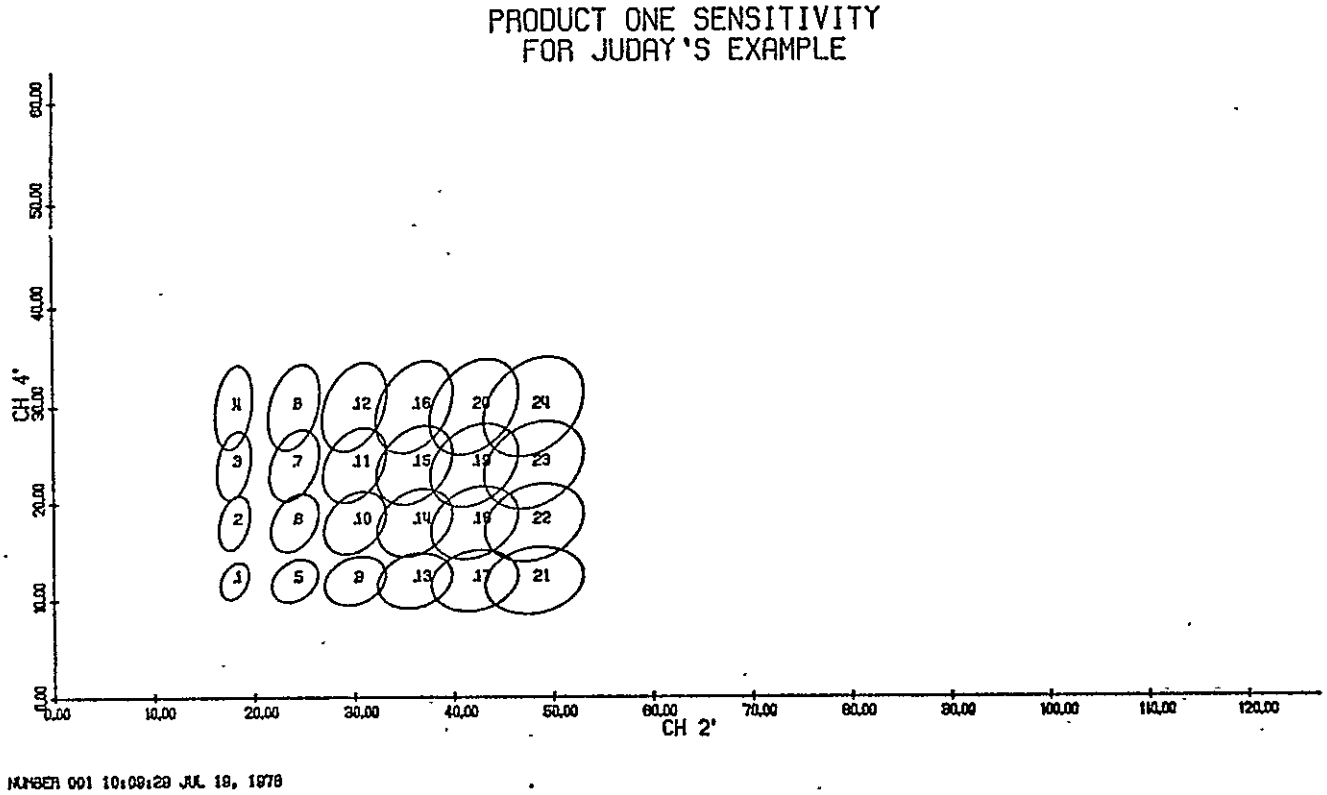

FIGURE 9. PRODUCT ONE SENSITIVITY WITH HYPOTHETICAL LINEAR CONTROL OF FILM TRANSMISSION

REFERENCES

1. Bizzell, R. M., et al, Results from The Crop Identification Technology Assessment for Remote Sensing (CITARS) Project, Proceeding of Tenth International Symposium on Remote Sensing of Environment, ERIM, U. of M. Extension Service, Ann Arbor, Mich., 1975.

2. MacDonald, R. B., R. B. Erb, F. G. Hall, "LACIE: A Look into the Future", Proceedings of Eleventh International Symposium on Remote Sensing of Environment, E.R.I.M. and U. of M. Extension Service, Ann Arbor, Mich., 1977.

3. Kaneko, Toyohisa and Sharon Tinkler, LACIE Film Study, Generation of Color Infrared Films, 78-FM-8, JSC-13847, NASA/JSC, Houston, Texas, February 1978.

4. Coberly, W. A., Jack Tubbs, and P. L. Odell, "The Influence of False Color Infrared Film on Training Errors in LACIE", University of Texas at Dallas Annual Report, June 1, 1975 - August 31, 1976.

5. Austin, W. W., "PFC Film Products for LACIE Segments", Memorandum to L. M. Flores, NASA, December 6, 1976.

6. Kaneko, T., "Analysis of Methods of Generating Bias and Scale Factors for PCC Guns", IBM Memo RES 20-53-134, August 12, 1976.

7. Kraus, G., "Another Method for Computing PFC Scaling Factors", NASA Memo TF3/76-630, September 9, 1976.

8. Hocutt, W. T., "An Improved Method of Calculating Scale Factors and Bias for Color Film Generation", LEC-8301, June 1976.

9. Juday, Richard D., Colorimetric Principles As Applied to Multichannel Imagery, Earth Observations Division, NASA/JSC, Revision B, 15 July 1978.

10. Juday, Richard D., "Color Formulation for Analysis in Image Space", NASA/JSC, SF5/78-175, Memo to M. C. Trichel, July 5, 1978.

11. Johnson Space Center, LACIE Transition Project, Transition Year Classification and Mensuration Subsystem (CAMS) Detailed Analysis Procedures, LACIE-00723, JSC-13735, Houston, Texas, March 1978.

12. Wyszecki, G., and W. S. Stiles, Color Science, John Wiley & Sons, New York, 1967.

REFERENCES (Cont'd)

13. Judd, D. B., G. Wyszecki, Color in Business Science and Industry, John Wiley & Sons, New York, 1975.

14. Evans, R. M., W. T. Hanson, Jr., and W. L. Brewer, Principles of Color Photography, John Wiley & Sons, New York, 1953.

15. Juday, Richard D., "Color Project Status 7-21-28", Correspondence received August 8, 1978.

16. Suits, Gwynn H., in consultation (private communication), ERIM, January 1978.

17. Land, Edwin H., "The Retinex Theory of Color Vision", Scientific American, December 1977, pp. 108-128.

18. MacAdam, David L., "Uniform Color Scales", Journal of the Optical Society of America, Vol. 64, No. 12, December 1974, pp. 1691-1702.

19. CIE 18^{e} Session, Compte Rendu, CIE N° 36, Bureau Central de la CIE, Paris.

20. Cicone, R. C., J. L. Stinson, and R. J. Balon, An Evaluation of the Signature Extension Approach to Large Area Crop Inventories Utilizing Space Image Data, ERIM 122700-33-F, Environmental Research Institute of Michigan, Ann Arbor, Michigan, November 1977.

21. Kaplan and Lewis, Advanced Calculus, John Wiley & Sons, New York.

22. Kauth, R. J. and G. S. Thomas, "The Tasselled Cap -- A Graphic Description of the Spectral-Temporal Development of Agricultural Crops as Seen by Landsat", Symposium Proceedings on Machine Processing of Remotely Sensed Data, Purdue University, W. Lafayette, Indiana, June 29 - July 1, 1976.

23. Lambeck, P. F., "Signature Extension Preprocessing for Landsat MSS Data", ERIM 122700-32-F, Environmental Research Institute of Michigan, Ann Arbor, Michigan, November 1977.

24. Malila, W. A. and J. M. Gleason, "Investigations of Spectral Separability of Small Grains, Early Season Wheat Detection, and Multicrop Inventory Planning", ERIM 122700-34-F, Environmental Research Institute of Michigan, Ann Arbor, Michigan, November 1977.

Technical and Final Report Distribution List

NASA Contract NAS9-15476

NAME	NUMBER OF COPIES
NASA/Johnson Space Center Earth Observations Division Houston, Texas 77058	
Attn: Dr. J. D. Erickson/SF3	(1)
Attn: Dr. R. P. Heydorn/SF3	(1)
Attn: Mr. M. C. Trichel/SF3	(1)
Attn: Mr. I. D. Browne/SF3	(2)
Attn: Research Data Facility/SF6	(2)
Attn: Mr. K. Baker/SF3	(1)
Attn: Mr. T. Pendleton/SF3	(1)
Attn: Mr. J. L. Dragg/SF4	(1)
Attn: Mr. Richard Juday	(1)
NASA/Johnson Space Center Space and Life Sciences Directorate Houston, Texas 77058	
Attn: Mr. R. B. MacDonald	(1)
Attn: Mr. W. E. Rice	(1)
NASA/Johnson Space Center Technical Library Branch Houston, Texas 77058	
Attn: Ms. Retha Shirkey/JM6	(4)
NASA/Johnson Space Center Technical Support Procurement Branch Houston, Texas 77058	
Attn: Mr. B. T. McGuire/BB6	(1)
Department of Mathematics Texas A&M University College Station, Texas 77843	
Attn: Dr. L. F. Guseman, Jr.	(1)

NAME	NUMBER OF COPIES
Department of Mathematics University of Houston 3801 Cullen Boulevard Houston, Texas 77004	
Attn: Dr. H. P. Decell, Jr.	(1)
University of California School of Forestry Berkeley, California 94720	
Attn: Dr. Robert Colwell	(1)
University of California 260 Space Sciences Laboratory Berkeley, California 94720	
Attn: Ms. Claire M. Hay	(1)
Purdue University Purdue Industrial Research Park 1220 Potter Drive West Lafayette, Indiana 47906	
Attn: Dr. Marvin Bauer	(1)
Texas A&M University Institute of Statistics College Station, Texas 77843	
Attn: Dr. H. O. Hartley	(1)
University of Tulsa Mathematics-Sciences Department 600 South College Tulsa, Oklahoma 74104	
Attn: Dr. W. A. Coberly	(1)


JUL 1979
RECEIVED
NASA STI FACILITY
ACCESS DEPT.